CHEMICAL CONSEQUENCES OF AIR QUALITY STANDARDS AND CONTROL IMPLEMENTATION PROGRAMS

Final Report

CONTRACT NO. A1-030-32

CALIFORNIA AIR RESOURCES BOARD

Principal Investigator
James N. Pitts, Jr.

Co-Principal Investigators
Roger Atkinson
William P. L. Carter

Program Manager
Arthur M. Winer

Research Staff
Ernesto C. Tuazon

UNIVERSITY OF CALIFORNIA
STATEWIDE AIR POLLUTION RESEARCH CENTER
RIVERSIDE, CA 92521

April 1983

ABSTRACT

Using our environmental chambers and spectroscopic and kinetic facilities, we have carried out studies concerning the atmospheric chemistry of long chain n-alkane and aromatic (i.e., benzene and toluene) hydrocarbons, two classes of organics which are major constituents of gasoline and other commercial fuels. In addition, we have concluded our CARB-sponsored investigations of environmental chamber effects. Specifically, we have:

- Investigated selected aspects of the atmospheric chemistry of the higher ($\geq C_4$) alkanes. This study involved the determination of alkyl nitrate yields during the NO_x-air photooxidations of the C_2-C_8 n-alkanes, and the kinetics of the reactions of the n-alkanes and of selected reaction products with the hydroxyl radical. In addition, a series of NO_x-air irradiations of n-hexane, n-heptane and n-octane were carried out. The data obtained show that alkyl nitrate formation is an important process for the higher n-alkanes ($\geq C_6$), especially since the formation of these organic nitrates is a sink for both NO_x and radical species. Consistent with these observations, the NO_x-air photooxidations of the C_6-C_8 n-alkanes show that these longer-chain alkanes are photochemically unreactive compared to the smaller n-alkanes such as n-butane.

- Investigated the atmospheric chemistry of benzene and toluene. We have determined the photolysis rates and the reaction rates with hydroxyl radicals of the α-dicarbonyls glyoxal and methylglyoxal, key photolabile intermediate species formed during the atmospheric photooxidation of these two aromatics. In addition, glyoxal and methylglyoxal yields from benzene and toluene were determined, and NO_x-air photooxidations of benzene were carried out. The photolysis rate of the α-dicarbonyl methylglyoxal, which has been postulated to be the major radical source in aromatic photooxidations, was determined to be lower by a factor of 2-7 than previously thought. Since benzene, which cannot form methylglyoxal, was observed to exhibit an unexpectedly high photochemical reactivity, these data show that the present NO_x-air photooxidation mechanisms of the aromatic hydrocarbons are incorrect in certain aspects and must be re-evaluated. This has significant implications for air pollution models currently in use by atmospheric scientists and regulatory agencies, including the CARB.

- Concluded our previous studies of chamber-dependent radical sources utilizing the SAPRC 5800-ℓ Teflon-coated evacuable chamber and the 6400-ℓ all-Teflon chamber. The data obtained confirm our previous conclusions that chamber-dependent radical sources are present in environmental chambers. Additionally, we have demonstrated experimentally that nitrous acid is present at part-per-billion concentrations at the commencement of irradiations. While this initial nitrous acid is mainly responsible for the observed radical fluxes in these chambers during the first 30-60 min of irradiation, a further chamber-dependent radical source is operative during and after this time period. These results remove one of the major ambiguities in using environmental chamber data to validate reaction mechanisms for photochemical air pollution.

The data from these three research elements are critical inputs into chemical kinetic computer models of the NO_x-air photooxidations of fuel constituents and will enhance the utility and reliability of such models in developing emission control strategies.

TABLE OF CONTENTS

ACKNOWLEDGMENTS

Stimulating discussion and valuable exchanges of technical information, for which we expresss our appreciation, took place at various times during this program with the following members of the California Air Resources Board: Drs. John R. Holmes, Alvin O. Gordon and Jack K. Suder. We gratefully acknowledge Ms. Sara M. Aschmann and Mr. William D. Long for carrying out this research, and Ms. I. M. Minnich in typing this report.

This report was submitted in fulfillment of Contract No. A1-030-32 by the Statewide Air Pollution Research Center, University of California, Riverside, under the partial sponsorship of the California Air Resources Board. Work was completed as of December 23, 1982.

The statements and conclusions in this report are those of the contractor and not necessarily those of the California Air Resources Board. The mention of commercial products, their source or their use in connection with material reported herein is not to be construed as either an actual or implied endorsement of such products.

LIST OF FIGURES

LIST OF FIGURES

LIST OF FIGURES

LIST OF FIGURES

LIST OF FIGURES

LIST OF TABLES

LIST OF TABLES

LIST OF TABLES

LIST OF TABLES

I. EXECUTIVE SUMMARY

This report presents results from several research topics of direct relevance to the development and implementation of air pollution control strategies by the California Air Resources Board. In two new areas of research, we have investigated the atmospheric chemistry of (a) a series of n-alkanes, which are major constituents of commercially utilized fuels (e.g., gasoline, diesel and aviation fuels) and (b) benzene and to a lesser extent toluene, selected members of the aromatic hydrocarbons a class which, along with the alkanes, constitutes a major fraction of commercial fuels. In addition, we have completed our investigation of chamber-dependent radical sources with an extensive study designed to validate the experimental techniques utilized. Among these techniques was the use of differential optical absorption spectroscopy to monitor nitrous acid in situ prior to and during irradiations of NO_x-air mixtures.

The work carried out on these three research elements, which is summarized in this section, has significantly advanced our knowledge and has generated data which are critical inputs into chemical computer models for airshed modeling studies. Sections II through IV provide a detailed report of the work carried out in the studies cited above, and Appendix A provides the detailed data sheets for the environmental chamber experiments dealing with the long-chain alkanes and benzene.

A. Investigation of the Atmospheric Chemistry of Selected Long-Chain Alkanes

The long-chain alkanes, exemplified by the $\geq C_6$ n-alkanes, are important constituents of gasoline, diesel fuel and aircraft fuels. In order to accurately assess the atmospheric impact of these fuels, a knowledge of the chemistry of the long-chain alkanes as it occurs under polluted atmospheric conditions is necessary. Although it has been established from basic laboratory investigations, supported by smog chamber modeling studies (Hendry et al. 1978, Whitten et al. 1979, 1980; Carter et al. 1979a) that under ambient atmospheric conditions the sole chemical loss process of the alkanes is via reaction with the OH radical, it has also been shown (Carter et al. 1976, Darnall et al. 1976, Baldwin et al. 1977) that the subsequent reactions may depend to a large extent on the size of

the molecule. For the smaller alkanes ($\lesssim C_4$), mechanisms involving formation of carbonyl compounds as intermediate products and efficient regeneration of OH radicals appear to fit the data reasonably well (Hendry et al. 1978, Whitten et al. 1979, 1980; Carter et al. 1979a). However, for the larger alkanes the formation of alkyl nitrates via the reaction of peroxy radicals with NO

$$RO_2 + NO \xrightarrow{M} RONO_2$$

and the isomerization of the long-chain alkoxy radicals via H-atom migration, e.g.

$$HCH_2CH_2CH_2CH_2O. \rightarrow .CH_2CH_2CH_2CH_2OH$$

becomes increasingly important and results in the formation of significantly different products.

In this program, the alkyl nitrate yields from the reaction of RO_2 radicals with NO have been determined for ethane through n-octane. This also necessitated the determination of the OH radical rate constants for these n-alkanes and for the alkyl nitrates formed, since reaction with OH radicals is the major loss process not only for the n-alkanes, but also for the alkyl nitrates under simulated atmospheric conditions. In addition, OH radical rate constants were determined for a series of ketones, which are also products of NO_x-air photooxidations of the n-alkanes. Finally, NO_x-air and methyl nitrite-air photooxidations of n-hexane, n-heptane and n-octane were carried out in order to establish a data base for the development of detailed chemical kinetic computer models for these long-chain alkanes. The data obtained are briefly summarized below.

Determination of Rate Constants for the Reaction of OH Radicals with a Series of Ketones, n-Alkanes and Alkyl Nitrates. Rate constants for the ketones 2-pentanone, 3-pentanone, 2-hexanone, 3-hexanone, 2,4,-dimethyl-3-pentanone, 4-methyl-2-pentanone and 2,6-dimethyl-4-heptanone, the n-alkanes propane through n-decane and the alkyl nitrates 2-propyl, 1-butyl, 2-butyl, 2-pentyl, 3-pentyl, 2-hexyl, 3-hexyl, 3-heptyl and 3-octyl nitrate were determined at ~299 ± 2 K, using a relative rate technique which has been described in detail in the literature (Atkinson

et al. 1981a, 1982a). The rate constants obtained are given in Tables I-1 for the ketones, I-2 for the n-alkanes and I-3 for the alkyl nitrates. These rate constants, which are generally in good agreement with the available literature data, provide a data base for the reaction of OH radicals with the three classes of organics. These data further allow the development of a priori predictive techniques for the estimation of OH radical rate constants and, since these reactions are the major atmospheric loss process for these organics, of atmospheric lifetimes (see Section II.B). In addition, the rate constants for the reactions of OH radicals with the n-alkanes and the alkyl nitrates are needed to correct for secondary reaction of the alkyl nitrates (formed from the reaction of alkyl peroxy radicals with NO) with OH radicals (Section II.C).

Alkyl Nitrate Yields from the NO_x-Air Photooxidations of C_2 through C_8 n-Alkanes. Alkyl nitrate yields have been determined for the NO_x-air photooxidations of the C_2 through C_8 n-alkane series, and the importance of the nitrate-forming reaction (1), relative to the competing radical chain-propagating and NO_x-conserving reaction of alkyl peroxy radicals with NO (reaction 2)

$$RO_2 + NO \rightarrow RONO_2 \qquad (1)$$

$$RO_2 + NO \rightarrow RO + NO_2 \qquad (2)$$

has been quantitatively determined, allowing its dependence on alkane chain length to be better understood.

The two chemical systems used to form RO_2 radicals in the presence of NO were the photolysis at $\lambda \geq 290$ nm of ppm levels of either methyl nitrite-NO-n-alkane mixtures or Cl_2-NO-n-alkane mixtures in ultra-zero air. The irradiations were carried out in ~75-ℓ FEP Teflon cylindrical reaction chambers surrounded by 24 GE F15T8-BL 15-W blacklights, and the light intensity corresponded to photolysis half-lives of ~30 min for methyl nitrite and ~20 min for Cl_2. All irradiations were carried out at 299 ± 2 K and ~735 torr total pressure.

Table I-1. Rate Constants k for the Reaction of OH Radicals with a Series of Ketones[a]

Ketone	10^{12} x k(cm^3 $molecule^{-1}$ sec^{-1})
2-Pentanone	4.74 ± 0.14
3-Pentanone	1.85 ± 0.34
2-Hexanone	9.16 ± 0.61
3-Hexanone	6.96 ± 0.29
2,4-Dimethyl-3-pentanone	5.43 ± 0.41
4-Methyl-2-pentanone	14.5 ± 0.7
2,6-Dimethyl-4-heptanone	27.7 ± 1.5

[a]At 299 ± 2 K. Placed on an absolute basis using a rate constant for the reaction of OH radicals with cyclohexane of 7.57 x 10^{-12} cm^3 $molecule^{-1}$ sec^{-1} (Atkinson et al. 1982a). The indicated errors are two standard deviations.

Table I-2. Room Temperature Rate Constants for the Reaction of OH Radicals with n-Alkanes

Alkane	10^{12} x k (cm^3 $molecule^{-1}$ sec^{-1})[a]
Propane	1.22 ± 0.05
n-Butane	2.58[b]
n-Pentane	4.13 ± 0.08
n-Hexane	5.70 ± 0.09
n-Heptane	7.30 ± 0.17
n-Octane	9.01 ± 0.19
n-Nonane	10.7 ± 0.4
n-Decane	11.4 ± 0.6

[a]At 299 ±2 K. Placed on an absolute basis using a rate constant for the reaction of OH radicals with n-butane of 2.58 x 10^{-12} cm^3 $molecule^{-1}$ sec^{-1}. The indicated errors are two standard deviations.

[b]Mean of absolute literature values of Greiner (1970), Stuhl (1973), Perry et al. (1976) and Paraskevopoulas and Nip (1980).

Table I-3. Rate Constants for the Reaction of OH Radicals with Alkyl Nitrates at 299 ± 2 K

Alkyl Nitrate	$10^{12} \times k_1$ (cm^3 $molecule^{-1}$ sec^{-1})[a]
2-Propyl	0.18 ± 0.05
1-Butyl	1.42 ± 0.11
2-Butyl	0.69 ± 0.10
2-Pentyl	1.87 ± 0.12
3-Pentyl	1.13 ± 0.20
2-Hexyl	3.19 ± 0.16
3-Hexyl	2.72 ± 0.22
3-Heptyl	3.72 ± 0.43
3-Octyl	3.91 ± 0.80

[a]Placed on an absolute basis using a rate constant for the reaction of OH radicals with cyclohexane of 7.57×10^{-12} cm^3 $molecule^{-1}$ sec^{-1} (Atkinson et al. 1982a). The indicated error limits are two standard deviations.

Alkyl nitrate formation was observed without any apparent induction period in all irradiations, and the amount of alkyl nitrate formed increased linearly with the amount of n-alkane consumed. One experiment was conducted with ~1 ppm of NO_2 in the initial reactant mixture, and it was observed to have no observable effect on the alkyl nitrate yields or their isomeric ratios. This is consistent with our analysis of the chemistry occurring in these systems, from which it is evident that the only important route to alkyl nitrate formation is via the reaction of RO_2 radicals with NO:

$$RO_2 + NO \rightarrow RONO_2 \qquad (1)$$

with the reaction of alkoxy radicals with NO_2

$$RO + NO_2 \rightarrow RONO_2 \qquad (3)$$

being of negligible importance, except for the case of ethane (as also indicated by the experimental data). Thus the major source of alkyl nitrates observed in the present experiments is from reaction (1), and the observed alkyl nitrate yields should reflect the rate constant ratio $k_1/(k_1 + k_2)$.

The total alkyl nitrate yields from the n-alkanes studied, corrected for secondary reactions of the alkyl nitrates, are given in Table I-4 and are plotted against carbon number in Figure I-1. The correction for secondary reactions utilized the rate constants for the reaction of OH radicals with organic nitrates measured in this program, and in all cases the correction was <20%. For propane through n-octane, the data given are from the CH_3ONO-n-alkane-air irradiations, but the corrected yield ratios for the observed alkyl nitrates in the Cl_2 photolysis experiments agreed with those in the CH_3ONO photolysis experiments to within ± 15% for n-butane through n-hexane, and to within ± 20% for propane. The Cl atom initiation system also enabled an upper limit to the alkyl nitrate yield to be obtained for the ethane system; this was not practical using CH_3ONO initiation since OH radicals react with ethane too slowly to yield an appreciable degree of reaction. This datum for ethane is, however, rigorously an upper limit since alkoxy radical combination with NO_2 could contribute a significant amount of the ethyl nitrate yields observed (for the other alkanes, this contribution is, as discussed above, minor).

It can be seen from Figure I-1 that the amount of alkyl nitrate formed from the RO_2 + NO reaction increases rapidly from ≤1% for ethane to ~30-33% for n-heptane and n-octane. The present data for propane through n-hexane, when compared with previous literature estimates for propane, n-butane, n-pentane and n-hexane (see Section II.C) are in reasonable agreement, especially so for propane and n-butane.

Since the formation of alkyl nitrates in hydrocarbon-NO_x-air irradiations is a sink for both oxides of nitrogen and radicals, the observed increase of the alkyl nitrate yields with the size of the n-alkane means that the potential for contributing to photochemical air pollution (or at least some aspects of it) may be less for the larger ($\geq C_6$) n-alkanes than for the smaller ones. This is supported by the results of our environmental chamber studies discussed below.

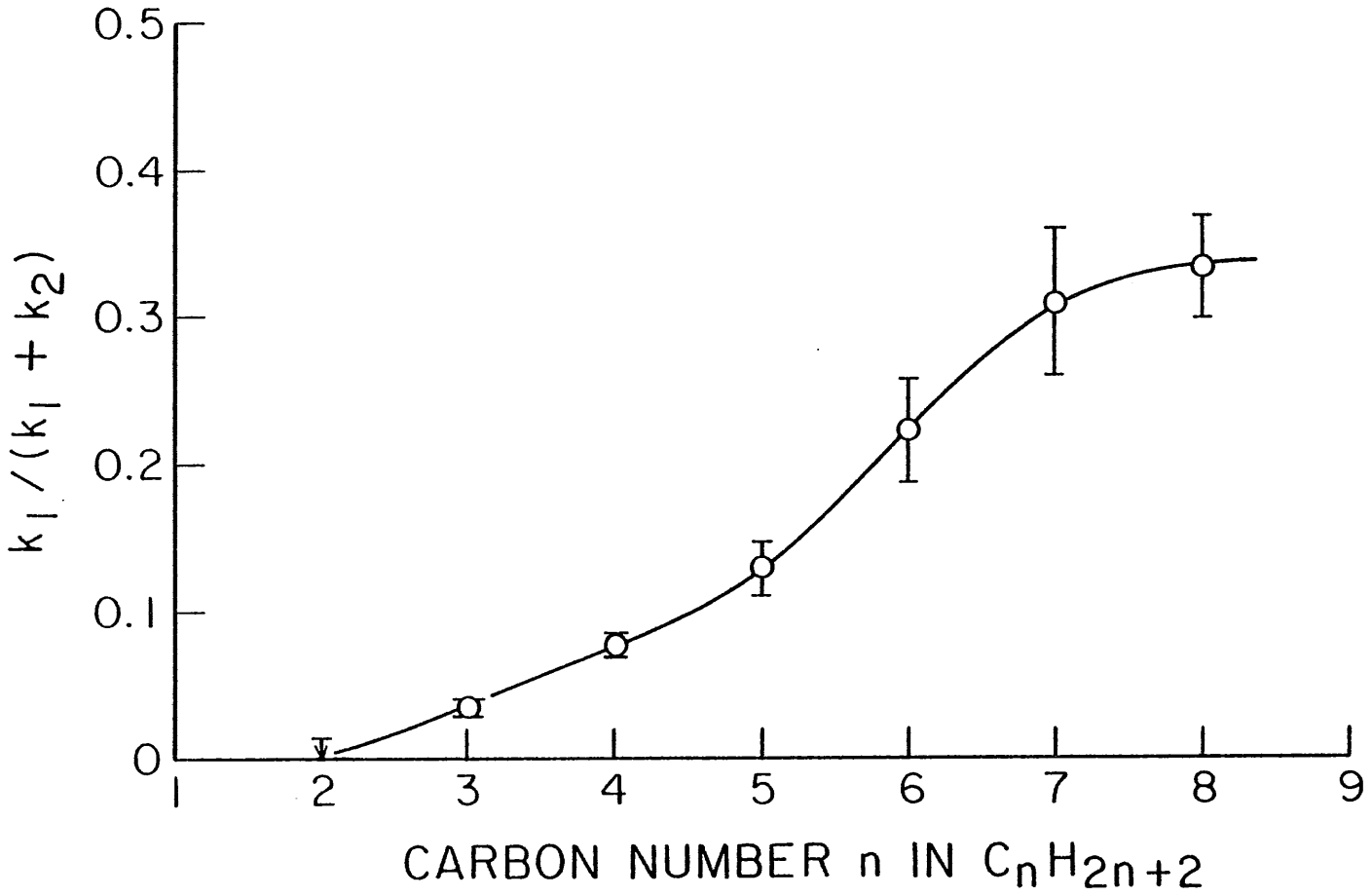

Figure I-1. Plot of $k_1/(k_1 + k_2)$ Against the n-Alkane Carbon Number. $k_1/(k_1 + k_2)$ is Set to be the Fractional Yield of Alkyl Nitrate Observed Under the Present Atmospheric Conditions. The Datum for Ethane is from the Cl_2-NO-Ethane-Air Irradiation and is an Upper Limit. The Other Data are from CH_3ONO-NO-n-Alkane-Air Irradiations.

Table I-4. Fractions of n-Alkanes Reacting to Form Alkyl Nitrates Via Reaction (1), i.e., the Rate Constant Ratio $k_1/(k_1 + k_2)$, Under Atmospheric Conditions

n-Alkane	$k_1/(k_1 + k_2)$
Ethane	≤ 0.014[a]
Propane	0.036 ± 0.005[b]
n-Butane	0.077 ± 0.009[b]
n-Pentane	0.129 ± 0.019[b]
n-Hexane	0.223 ± 0.035[b]
n-Heptane	0.309 ± 0.050[b]
n-Octane	0.332 ± 0.034[b]

[a]From the Cl_2-NO-ethane-air irradiation.

[b]From CH_3ONO-NO-n-alkane-air irradiations.

NO_x-Air Photooxidations of C_6-C_8 n-Alkanes. In order to assess the photochemical reactivity of the longer-chain n-alkanes and to provide a data base for the development of detailed chemical kinetic computer models for this important class of organics, a series of NO_x-air and CH_3ONO-air irradiations of n-hexane, n-heptane and n-octane were carried out in the SAPRC 6400-ℓ all-Teflon environmental chamber. For comparison purposes, several NO_x-air irradiations of n-butane were also carried out.

The results of these alkane-NO_x-air irradiations are summarized in Table I-5. The photochemical reactivity in these runs was extremely low, even when hydrocarbon/NO_x ratios as high as ~400 were employed. In no case was an ozone maximum obtained during 6 hr of irradiation, and only in the ~43 ppm n-heptane run was a possible O_3 maximum observed during the irradiation (0.36 ppm in 6.25 hr).

Although the fact that O_3 maxima were not obtained in most of these runs means that they cannot be used to compare maximum O_3 yields, they can be used to compare the efficiency of the alkanes in oxidizing NO. As is well known, ozone formation in hydrocarbon-NO_x-air irradiations is caused by the oxidation of NO by the peroxy radical intermediates formed in the hydrocarbon oxidation reactions, and if the overall alkane photooxidation mechanism is represented as follows:

Table I-5. Initial Concentrations and Selected Results of the Alkane-NO_x-Air Irradiations Conducted in the SAPRC Evacuable Chamber

Alkane	Inital Conc. (ppm)		6-Hour O_3 (ppm)	NO Conversion per Alkane Reacted[a]
	Alkane	NO_x		
n-Butane	3.75	0.09	0.15	1.7 ± 0.1
n-Butane	2.96	0.12	0.13	2.2 ± 0.2
n-Hexane	46.57	0.13	0.35	1.7 ± 0.2
n-Heptane	8.62	0.12	0.15	1.0 ± 0.2
	43.65	0.11	0.35	~0.7 - 1.4
n-Octane	53.60	0.13	0.32	0.8 ± 0.3

[a]NO conversion = $\Delta([O_3]-[NO])$ (see Section II.D); alkane reaction calculated from observed alkyl nitrate yields, using the yield ratios of the nitrates from these alkanes determined as discussed in Section II.C.

$$OH + \text{alkanes} \rightarrow -\alpha\ NO + \beta\ NO_2 + \gamma\ OH + \text{products}$$

then it can be shown that α, the efficiency of the alkane in oxidizing NO, can be approximated by

$$\alpha \simeq \frac{\Delta([O_3]-[NO])}{[\text{alkane reacted}]}$$

The estimated alkane oxidation efficiencies, α, derived from the results of these runs (where the amount of alkane reacted was calculated from the observed alkyl nitrate yields) are also summarized in Table I-5. The results of these experiments indicate that α, the efficiency of the alkanes in oxidizing NO and thus causing O_3 formation, is approximately 2.0, 1.7, 1.0 and 0.8 for n-butane, n-hexane, n-heptane and n-octane, respectively. This contrasts with estimates for α of 2.3, 2.4, 2.2 and 2.1, respectively, based on the currently assumed alkane-NO_x-air

photooxidation mechanisms discussed elsewhere in this report. This discrepancy could possibly be due in part to conversion of NO_2 back to NO by processes involved in the chamber radical source (see Section IV), and in part to increased alkyl nitrate formation efficiency from the reactions of oxygenated peroxy radical intermediates involved in these systems (see Section II). It is clear, however, that more direct data concerning the mechanism and the products formed following the isomerization of long-chain alkane radicals are required before this aspect of the alkane photooxidation mechanism is adequately understood.

It should be noted that the parameter α, derived as discussed above, reflects only the efficiency of the alkane in oxidizing NO, and does not directly reflect the tendency of the alkanes to remove both NO_x and radicals from the system, which influences both the maximum O_3 yields and the rate at which O_3 is formed. In order to obtain data under conditions where maximum O_3 yields could be determined, a series of n-hexane, n-heptane and n-octane air irradiations were carried out where both the radicals and the NO_x are produced by the rapid photolysis of methyl nitrite:

$$CH_3ONO + h\nu \xrightarrow{O_2} HCHO + NO_2 + OH$$

(See Section II.C for a discussion of the CH_3ONO photolysis system.) This system has the advantages that radical levels are sufficiently high that maximum O_3 yields can be reliably obtained in a reasonable amount of time, and also that the radicals are formed by a homogeneous and reproducible chemical process, as opposed to the chamber radical source (see Section IV) which is the dominant radical source in the alkane-NO_x-air irradiations.

The results of the CH_3ONO-alkane-air irradiations are summarized in Table I-6. It can be seen that the addition of 1-9 ppm of n-hexane, n-heptane or n-octane to a CH_3ONO (0.4-0.5 ppm)-air irradiation causes the final O_3 yield to increase from ~0.4 ppm to 1.0-1.3 ppm; but the final O_3 yields in these alkane-CH_3ONO-air irradiations appears to be remarkably insensitive to the amount of alkane present or even to the identity of the particular alkane added. However, the data do suggest that under similar

Table I-6. Initial Conditions and Observed and Calculated Maximum O_3 Yields and Alkane Consumed in the CH_3ONO-Air and the CH_3ONO-Alkane-Air Irradiations Carried Out in the SAPRC 6400-ℓ Indoor Teflon Chamber[a]

Alkane Studied	Initial Conc. (ppm)		O_3 Yield[c] (ppm)	Alkane Consumed[c] (ppm)
	Alkane	CH_3ONO[b]		
n-Hexane	0.92	0.48	1.4	0.33
	4.69	0.47	1.20	0.69
	9.25	0.42	1.15	0.81
n-Heptane	0.91	0.47	0.98	0.35
	4.29	0.46	1.11	0.61
	8.17	0.45	1.10	0.70
n-Octane	0.96	0.45	0.92	0.38
	4.75	0.46	0.99	1.18
	8.21	0.48	1.10	0.76
-	0	0.44	0.39	-
	0	0.49	0.33	-
	0	0.42	0.39	-

[a] $T = 301 \pm 1$ K, <5% RH, $k_1 = 0.32\ min^{-1}$.

[b] Initial CH_3ONO based on increase in total NO_x measurement after CH_3ONO injected, based on assuming 100% interference of alkyl nitrites on commercial chemiluminescence NO_x detector (Winer et al. 1974).

[c] After 240 min of irradiation.

conditions, n-hexane may form slightly more O_3 than n-heptane, which in turn may form slightly more O_3 than n-octane. This trend in reactivity is the opposite of what one would expect on the basis of their respective rate constants for reaction with an OH radical, but is consistent with the increasing NO_x and radical removal resulting from the increased alkyl nitrate yields for the higher alkanes (Section II.C), as well as the apparent reduction in the NO oxidation efficiency with size of the alkane as discussed above.

In order to determine if the O_3 yields and amounts of alkane consumed in these CH_3ONO-alkane irradiations were consistent with the currently assumed mechanisms, computer model simulations of these experiments were conducted. In general, excellent fits to the O_3 yields and to the O_3 concentration-time profiles were obtained in both the CH_3ONO-air and the CH_3ONO-alkane-air runs. However, the calculated amounts of alkane reacted were generally slightly overpredicted in the 1 ppm alkane runs and slightly underpredicted in 8-9 ppm alkane runs. This underprediction at higher alkane levels may be due to some loss of alkanes due to dilution or other non-chemical processes, but the overprediction at low alkane levels suggests a possible problem with the reaction mechanism. However, in general the fits of these calculations to the data were quite good, though this may reflect more the insensitivity of this experimental system to variations in reactivity parameters than the accuracy of the model. This latter likelihood is also indicated by the fact that this model did not correctly predict the observed NO oxidation efficiencies of these alkanes in the absence of CH_3ONO.

B. An Investigation of the Atmospheric Chemistry of Selected Aromatic Hydrocarbons and Aromatic Photooxidation Products

Significant advances have been made in recent years concerning the atmospheric chemistry of aromatic hydrocarbons which are constituents of unleaded gasoline and other fuels currently in use. From both laboratory and smog chamber studies, it has been known since the early 1970s that the only important chemical loss process for the aromatic hydrocarbons under atmospheric conditions is via reaction with the OH radical. Data are now available concerning both the overall OH radical rate constants and the relative amounts of OH radical addition and H-atom abstraction for most aromatics, including benzene (Atkinson et al. 1979). For substituted benzenes such as toluene, two reaction pathways occur (Atkinson et al. 1979), OH radical addition to the ring and H-atom abstraction from the substituent groups, with abstraction occurring ~8% of the time for toluene (Atkinson et al. 1983a), the most studied aromatic. The overall process and products (again for toluene) are believed to be (Atkinson et al. 1980):

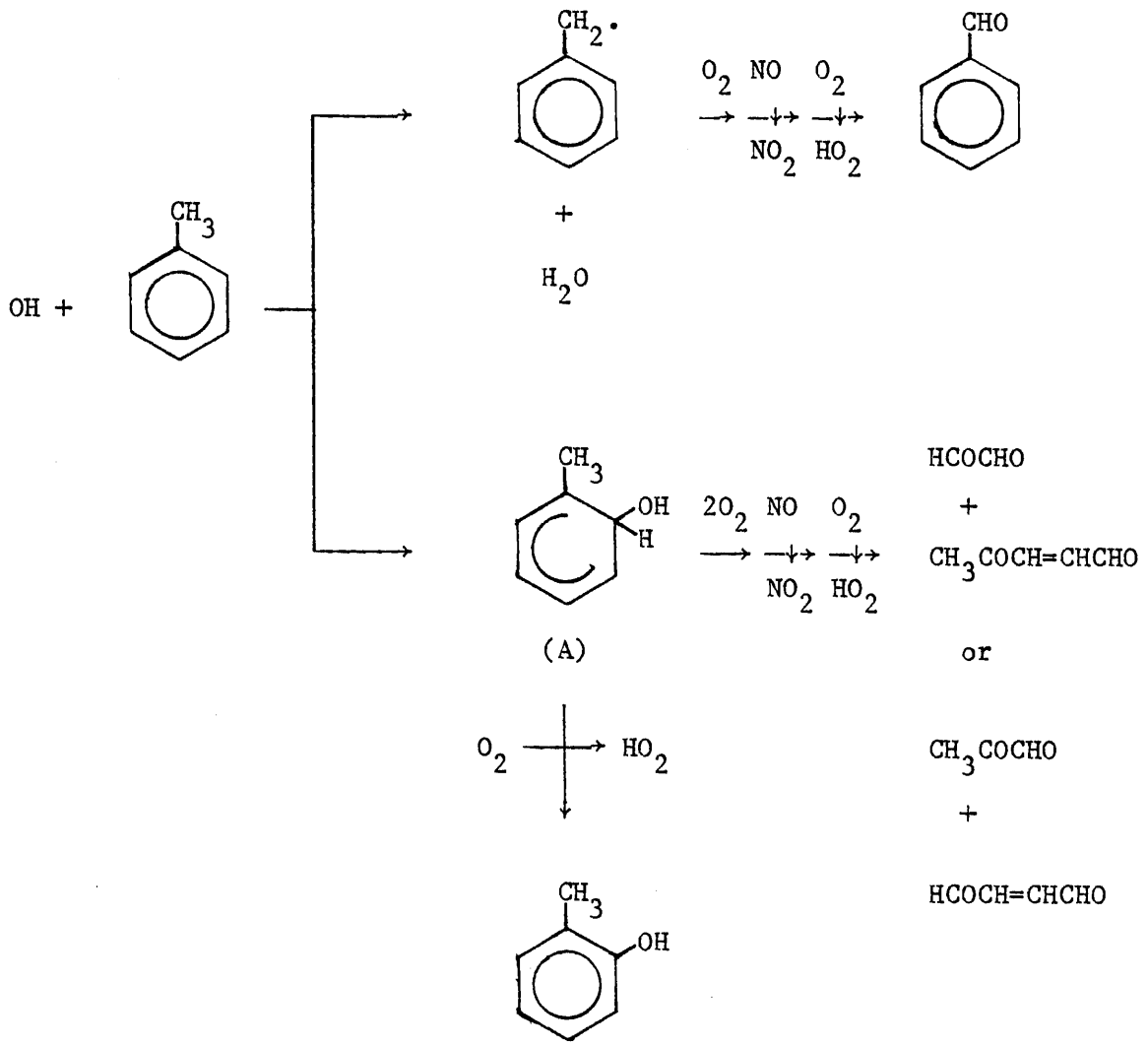

This mechanism is supported by the observation of formation of benzaldehyde and cresols from toluene (Atkinson et al. 1983a, and references therein), the prompt formation of biacetyl and other α-dicarbonyls in the NO_x photooxidation of o-xylene (Darnall et al. 1979, Takagi et al. 1980), and the formation of unsaturated 1,4-dicarbonyls from toluene (Besemer 1982) and 2,3,4-triethylbenzene (Takagi et al. 1982). The mechanism also gives reasonable fits of model calculations to toluene-NO_x-air (Atkinson et al. 1980, 1982b) and xylene-NO_x-air (Atkinson et al. 1982b) environmental chamber data. However, a number of potentially significant uncertainties still remain. In particular, the applicability

of this general mechanism to benzene, the simplest of the aromatics, has yet to be demonstrated, the yields of the α-dicarbonyls from representative aromatic systems are not quantitatively known, and information concerning the reaction rates and mechanisms of the α-dicarbonyls and of the unsaturated 1,4-dicarbonyls is presently highly limited.

Therefore, during this program, we have carried out the following exploratory studies dealing mainly with benzene and the α-dicarbonyls: (1) The yields of glyoxal from benzene and of glyoxal and methylglyoxal from toluene during their CH_3ONO-NO-air photooxidations have been determined using differential optical absorption spectroscopy. (2) The yield of phenol from benzene during these irradiations has been determined using gas chromatography. (3) The OH radical rate constants and the photolysis rates in the SAPRC 5800-ℓ evacuable chamber of the α-dicarbonyls glyoxal, methylglyoxal and biacetyl have been determined. (4) A series of NO_x-air photooxidations of benzene have been carried out in the 6400-ℓ all-Teflon chamber. The data obtained from these studies are summarized briefly below.

Atmospheric Reactions of α-Dicarbonyls: Upper Limit for Reaction with O_3. Upper limit rate constants for the reaction of O_3 with glyoxal and methylglyoxal were determined using a static technique developed and utilized in these laboratories (Atkinson et al. 1981b, 1982c). With this technique the rate constants are derived from the enhanced decay rates of O_3 in the presence of known concentrations of the reactive organic. For both glyoxal and methylglyoxal, these ozone decay rates in the presence of the α-dicarbonyls were indistinguishable from the background O_3 decay rates observed in the absence of reactants, thus allowing determination only of upper limits to the rate constants:

$$k(O_3 + \text{glyoxal}) < 3 \times 10^{-21} \text{ cm}^3 \text{ molecule}^{-1} \text{ sec}^{-1}$$

and

$$k(O_3 + \text{methylglyoxal}) < 6 \times 10^{-21} \text{ cm}^3 \text{ molecule}^{-1} \text{ sec}^{-1}$$

Thus it can be concluded that, as expected, the reactions of O_3 with these α-dicarbonyls are totally negligible under atmospheric conditions.

Atmospheric Reactions of α-Dicarbonyls: Reaction with OH Radicals. Rate constants for the reactions of OH radicals with glyoxal and methylglyoxal were determined at 298 ± 2 K, using a relative rate technique. The photolysis of methyl nitrite in air was used as the source of OH radicals, and cyclohexane, a compound with an accurately known OH radical rate constant (Atkinson et al. 1982a), was used as the reference organic. The α-dicarbonyls were monitored by differential optical absorption spectroscopy, and cyclohexane was monitored by gas chromatography.

The relative rate constants obtained in this study, placed on an absolute basis using k(OH + cyclohexane) = (7.57 ± 0.05) x 10^{-12} cm^3 $molecule^{-1}$ sec^{-1} (Atkinson et al. 1982a), were:

$$k(OH + glyoxal) = (1.15 \pm 0.04) \times 10^{-14} \text{ cm}^3 \text{ molecule}^{-1} \text{ sec}^{-1}$$

$$k(OH + methylglyoxal) = (1.73 \pm 0.13) \times 10^{-11} \text{ cm}^3 \text{ molecule}^{-1} \text{ sec}^{-1}$$

These values are very close to what one might expect based on the analogous reactions of OH radicals with formaldehyde and acetaldehyde (Atkinson et al. 1979). The presence of an α-carbonyl group apparently does not significantly affect the rate of OH radicals with aldehydes.

Atmospheric Reactions of α-Dicarbonyls: Rates of Photolysis, Effective Quantum Yields and Atmospheric Lifetimes. The rates of photolysis of glyoxal, methylglyoxal and biacetyl have been measured in the SAPRC 5800-ℓ evacuable chamber using the 25 KW xenon arc solar simulator as the light source. The radiation from this solar simulator, which approximates that of the deep space solar spectrum in the ultraviolet and visible regions (Winer et al. 1980), was filtered through a 0.64-cm Pyrex pane in order to eliminate radiation below ~300 nm. The resulting spectral distribution approximated that of the lower tropospheric solar spectrum, and the light intensity employed in these determinations corresponded to a measured NO_2 photolysis rate, k_{NO_2}, of 1.4 x 10^{-3} sec^{-1}.

The photolysis rates observed in our experiments were (1.1 ± 0.07) x 10^{-5} sec^{-1} for glyoxal (2.7 ± 0.7) x 10^{-5} sec^{-1} for methylglyoxal and (5.0 ± 0.3) x 10^{-5} sec^{-1} for biacetyl. While these rates are only strictly applicable for the light intensity and spectral distribution employed in these irradiations, these data can be normalized for differences in the

light intensity by dividing the observed α-dicarbonyl photolysis rates by the observed NO_2 photodissociation rate constant, and these resulting photolysis rate ratios are given in Table I-7. Also given in Table I-7 are the maximum photolysis rate ratios calculated from the spectral distribution and absorption cross-sections of the α-dicarbonyls assuming a photodissociation quantum yield of unity. It can be seen from Table I-7 that the observed photolysis rate ratios are significantly less than the calculated maximum values, and the "effective" quantum yields for the photodissociation of the α-dicarbonyls studied here, obtained by dividing the observed photolysis rate ratios by those calculated assuming a unit quantum yield, are also given in Table I-7. Since, in general, it is expected that ϕ_λ will vary with wavelength, these "effective" quantum yields are valid only for the particular spectral distribution used in this study. However, since the spectral distribution of the filtered solar simulator used is similar to that of sunlight in the lower troposphere (Winer et al. 1980), then the photolysis rate ratios k^{phot}/k_{NO_2} observed here can be used with the NO_2 photodissociation rate constants k_{NO_2} to estimate the atmospheric α-dicarbonyl photolysis rates k^{phot}.

These estimated atmospheric photodecomposition lifetimes for glyoxal, methylglyoxal and biacetyl are compared in Table I-8 with the estimated lifetimes for removal by reaction with OH radicals and with O_3. It can be seen that, despite the relatively low "effective" photodissociation quantum yields, the photodissociation lifetimes are appreciably shorter than the lifetimes due to reaction with OH radicals or O_3 (the latter reaction being essentially negligible). Photolysis of these α-dicarbonyls is thus clearly their major tropospheric loss process.

These data are important and necessary inputs to chemical kinetic computer modeling studies of the aromatic hydrocarbons and of isoprene. In particular, this work indicates that the photolysis rate of methylglyoxal, a critical parameter in chemical computer models for NO_x-air photooxidation of toluene and other aromatics, is significantly lower than has been previously assumed. (Compare the present photolysis rate ratio of $k^{phot}/k_{NO_2} = 0.019 \pm 0.005$ with the previously assumed ratios of ~0.045 [Killus and Whitten 1982] and 0.15 [Atkinson et al. 1980]). Thus, it is obvious that all present chemical computer models of the aromatic-NO_x-air systems need to be re-evaluated in the light of these present data.

Table I-7. Observed and Calculated Photolysis Rate Ratios k^{phot}/k_{NO_2} for Glyoxal, Methylglyoxal and Biacetyl, and Calculated α-Dicarbonyls Effective Quantum Yields

a-Dicarbonyl	k^{phot}/k_{NO_2} Obs[a]	k^{phot}/k_{NO_2} Calculated $\phi_\lambda = 1$	Effective Quantum Yield ϕ[b]
Glyoxal	0.008 ± 0.005	0.29	0.029 ± 0.018
Methylglyoxal	0.019 ± 0.005	0.18	0.107 ± 0.030
Biacetyl	0.036 ± 0.004	0.23	0.158 ± 0.024

[a]The indicated error limits include two standard deviations of the α-dicarbonyl photolysis rates together with a 10% uncertainty in k_{NO_2}.

[b]Effective quantum yield = $[k^{phot}/k_{NO_2}(obs)]/[k^{phot}/k_{NO_2}(calc, \phi_\lambda = 1)]$.

Table I-8. Atmospheric Lifetimes of Glyoxal, Methylglyoxal and Biacetyl Due to Photolysis, Reaction with OH Radicals and Reaction with O_3

α-Dicarbonyl	$\tau_{Photolysis}$[a] (hrs)	τ_{OH}[b] (hrs)	τ_{O_3}[c] (hrs)
Glyoxal	5	24	$>9 \times 10^4$
Methylglyoxal	2	16	$>4 \times 10^4$
Biacetyl	1	>900	$\gtrsim 4 \times 10^4$[d]

[a]At a zenith angle of 0°.

[b]At an OH radical concentration of 1×10^6 cm^{-3}.

[c]At an O_3 concentration of 1×10^{12} cm^{-3} (40 ppb).

[d]Estimated by analogy with glyoxal and methylglyoxal.

Determination of Product Yields from the NO_x Photooxidation of Benzene and Toluene. The yields of selected products (glyoxal and phenol from benzene, and glyoxal and methylglyoxal from toluene) were determined during irradiations of CH_3ONO-NO-aromatics-air mixtures carried out in the 5800-ℓ evacuable chamber. The α-dicarbonyls glyoxal and methylglyoxal were monitored in situ by long path differential optical absorption spectroscopy, while the aromatic hydrocarbons and phenol were analyzed by gas chromatography.

Since phenol, glyoxal and methylglyoxal react with OH radicals more rapidly than do benzene or toluene, corrections, using the rate constants for glyoxal and methylglyoxal determined in this program and a literature value for phenol (Zetzch 1982), had to be made for these secondary reactions in order to derive the fraction of the OH radical reaction with the aromatics yielding phenol, glyoxal and methylglyoxal.

For benzene the sole observed glyoxal concentration corresponds to an ~25% yield of glyoxal. It should be noted that because benzene reacts so slowly with OH radicals (with a rate constant of 1.2×10^{-12} cm^3 $molecule^{-1}$ sec^{-1} [Atkinson et al. 1979]) it was difficult to achieve a high enough conversion of benzene to detect glyoxal using the DOAS system. The observed phenol yields, corrected for secondary reactions, indicate that the reaction of OH radicals with benzene yields phenol ~28 ± 8% of the time; the scatter in the data may be due, at least partially, to the difficulty of analyzing phenol and to uncertainties in the OH radical rate constant for phenol. Obviously, further work is necessary before the yields of these and other products can be known with a greater degree of confidence.

For toluene, the glyoxal yield, after correction for secondary reactions, is 29 ± 3%, where the indicated error is two least squares standard deviation. The methylglyoxal data correspond to an ~64% yield. Since the benzaldehyde and o-cresol yields have been determined (Atkinson et al. 1983a) to be 7.3 ± 2.2% and 13.1 ± 7.2%, respectively, the major expected reaction pathways thus give a reasonable (though somewhat high) overall balance,

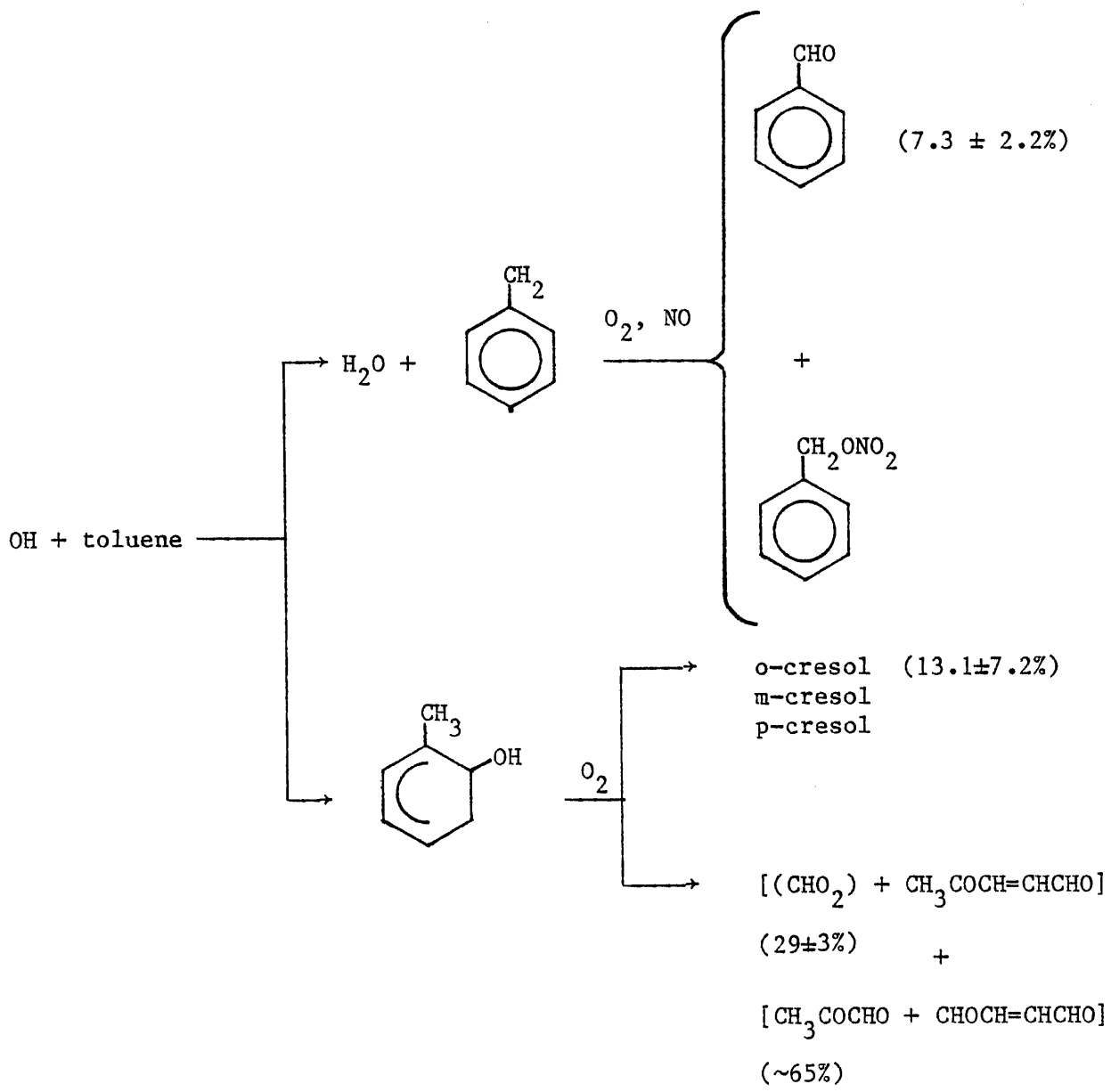

since the benzyl nitrate and the m- and p-cresol yields are expected (Atkinson et al. 1983a) to be minor (<5% combined). This scheme gives an overall product yield of ~115-120% (uncertain to at least ±20%), indicating that the major reaction pathways have indeed been monitored.

NO_x-Air Photooxidation of Benzene. In order to investigate the photochemical reactivity of benzene and to provide a data base for the development of detailed chemical computer models for this aromatic hydrocarbon, a series of benzene-NO_x-air photooxidations were carried out in

the ~6400-ℓ all-Teflon chamber. A summary of the initial concentrations and selected results are given in Table I-9.

In all cases, an O_3 maximum was obtained, and it is apparent from these results that benzene is much more photoreactive than the $\geq C_6$ n-alkanes, despite the fact that it has a much lower rate constant for reaction with OH radicals. As in the case of toluene (see, for example, Atkinson et al. 1980), this is believed to be due to secondary reactions of the products and not to reactions of benzene itself, and it should be noted that an apparent induction period in the decay of both total NO_x and of benzene was observed. This induction period indicates that radical initiation and NO_x removal processes occur at much more rapid rates later in the irradiation than initially.

In order to assess to what extent current aromatic photooxidation mechanisms are consistent with these data, a limited computer modeling study was carried out. It was observed that our current aromatic photooxidation mechanism, when adapted to benzene, did not satisfactorily predict the high reactivity of benzene. This is because the major radical initiation assumed in the current mechanisms for toluene and the xylenes is photolysis of methylglyoxal and (for o-xylene) biacetyl, neither of which can be formed in the benzene system. On the other hand, a much better fit to the O_3 and NO_x profiles (though not those for benzene itself) in the benzene-NO_x-air irradiations is obtained if 2-butene-1,4-dial is assumed to photolyze rapidly to produce radicals, and this may be a significant radical source in the photooxidations of other aromatics as well. However, the atmospheric reactions of the unsaturated 1,4-dicarbonyls are presently completely unknown, and clearly more information concerning these species is required before the aromatic photooxidation mechanisms can be adequately understood.

C. An Experimental Investigation of Chamber Dependent Radical Sources

An important aspect of the development of reliable computer models for the formation of photochemical smog is their validation against smog chamber data. This requires not only a complete understanding of the kinetics and mechanisms of the chemical reactions which occur during the photooxidations of part-per-million (ppm) concentrations of NO_x and organics in air, but also an adequate and quantitative understanding of major chamber

Table I-9. Initial Conditions and Selected Results of the Benzene-NO_x-Air Irradiations Carried Out in the SAPRC ~6400-ℓ All-Teflon Chamber[a]

Initial Conc. (ppm)			Maximum NO_2		Maximum O_3	
Benzene	NO	NO_2	(ppm)	(hours)	(ppm)	(hours)
55.38	0.079	0.037	0.078	0.5	0.323	1.5
13.19	0.082	0.032	0.084	0.5	0.273	1.75
13.96	0.434	0.125	0.373	2.75	0.412	4.75

[a] $T = 301 \pm 1$ K, ~50% RH, $k_1 = 0.32$ min^{-1}.

effects. Recent computer modeling studies have shown that the presence of an as yet unknown source of radicals is necessary in order to match computer-predicted time-concentration profiles with the results of smog chamber experiments (Hendry et al. 1978, Falls and Seinfeld 1978, Carter et al. 1979a, Whitten et al. 1979, 1980; Atkinson et al. 1980). Modelers have differed on how best to represent this radical source in their mechanisms, although it is generally assumed to be chamber-dependent. Since aspects of the photochemical mechanisms relating to radical initiation and termination processes cannot be unambiguously validated using smog chamber data until this radical source is characterized, this causes serious problems in validating computer models for photochemical smog formation.

During the past two years, we have developed an approach allowing a systematic investigation of these effects. This involves the irradiation of NO_x-air mixtures, with trace levels of organics present to monitor OH radical concentrations. While we have reported much of these data in our final report for ARB Contract No. A8-145-31 (Pitts et al. 1981), we have carried out numerous further experiments to (a) validate the experimental technique, (b) obtain more detailed data for the SAPRC ~6400-ℓ indoor Teflon chamber and (c) obtain direct measurements of HONO levels both prior to and during these irradiations. In addition, we have carried out a re-analysis of our earlier data and, while this re-analysis does not change our conclusions, minor changes in the data have occurred. Thus we report in Section IV our total data base concerning this important topic.

Results of Tracer-NO_x-Air Irradiations. Tracer-NO_x-air irradiations were carried out in four different environmental chambers, whose major characteristics are summarized in Table I-10. Initial NO concentrations ranged from ~0-3.6 ppm and and initial NO_2 from ~0.04-4.9 ppm. Approximately 10 ppb each of either propene and propane, propene and n-butane, or (for a few runs) n-butane and neopentane were included in the reaction mixture to monitor OH radicals from their relative rates of consumption. This technique for monitoring OH radical levels was validated by experiments conducted during the period covered by this report as described in Section IV. The results of most of these experiments were discussed in our last report (and are discussed in detail in Section IV), and thus are only briefly summarized here.

The hydroxyl radical levels derived from the results of these runs were in all cases significantly higher (e.g., by at least one order of magnitude) than expected based on the known homogeneous reactions of the NO_x-air system. The data could be fit by model calculations only if it was assumed that there was both initially present HONO (which supplies radicals from its rapid photolysis in the early stages of the irradiation) and also a continuous radical source, the latter being the far more important factor after the first ~30 min of irradiation. This is shown for a representative run in Figure I-2, where the observed OH levels are compared to results of model calculations with and without a continuous radical source and initial HONO.

The hydroxyl radical levels observed in the latter stages of these NO_x-air irradiations thus reflect predominantly the continuous radical source. These levels, and thus the continuous radical source, were found to be proportional to light intensity, to depend on the chamber employed (even after the dependence of light intensity is removed), to increase with increasing NO_2 but to be independent of NO, and to increase with both temperature and humidity. The dependence of the OH radical levels on the chambers employed (normalized to the NO_2 photolysis rate to account for differences in light intensity) is shown in Table I-11. Table I-12 shows the dependence of the OH radical levels on the temperature and humidity in the evacuable chamber. The dependence of the normalized radical source (i.e., the radical input rate divided by the light intensity as measured

Table I-10. Physical Characteristics of the Four Chambers Used

	Evacuable Chamber	Indoor Teflon Chamber	Outdoor Teflon Chamber	Teflon Bag
Location	Indoors	Indoors	Outdoors	Indoors
Volume (liters)	5800	~6400	~40,000	~100
Surface Material	Teflon (TFE)-coated aluminum	FEP Teflon	FEP Teflon	FEP Teflon
Irradiation Source	Xenon arc	Florescent blacklights	Sunlight	Fluorescent blacklights
NO_2 Photolysis Rate (k_1)	0.49 min^{-1}[a]	~0.45 min^{-1}[a]	~0.3 min^{-1}	~0.27 min^{-1}
Intensity Profile	Constant	Constant	Diurnal	Constant
NO_x Injection Technique	Vacuum	Syringe	Syringe	Syringe

[a]Typical value. Other values of k_1 used.

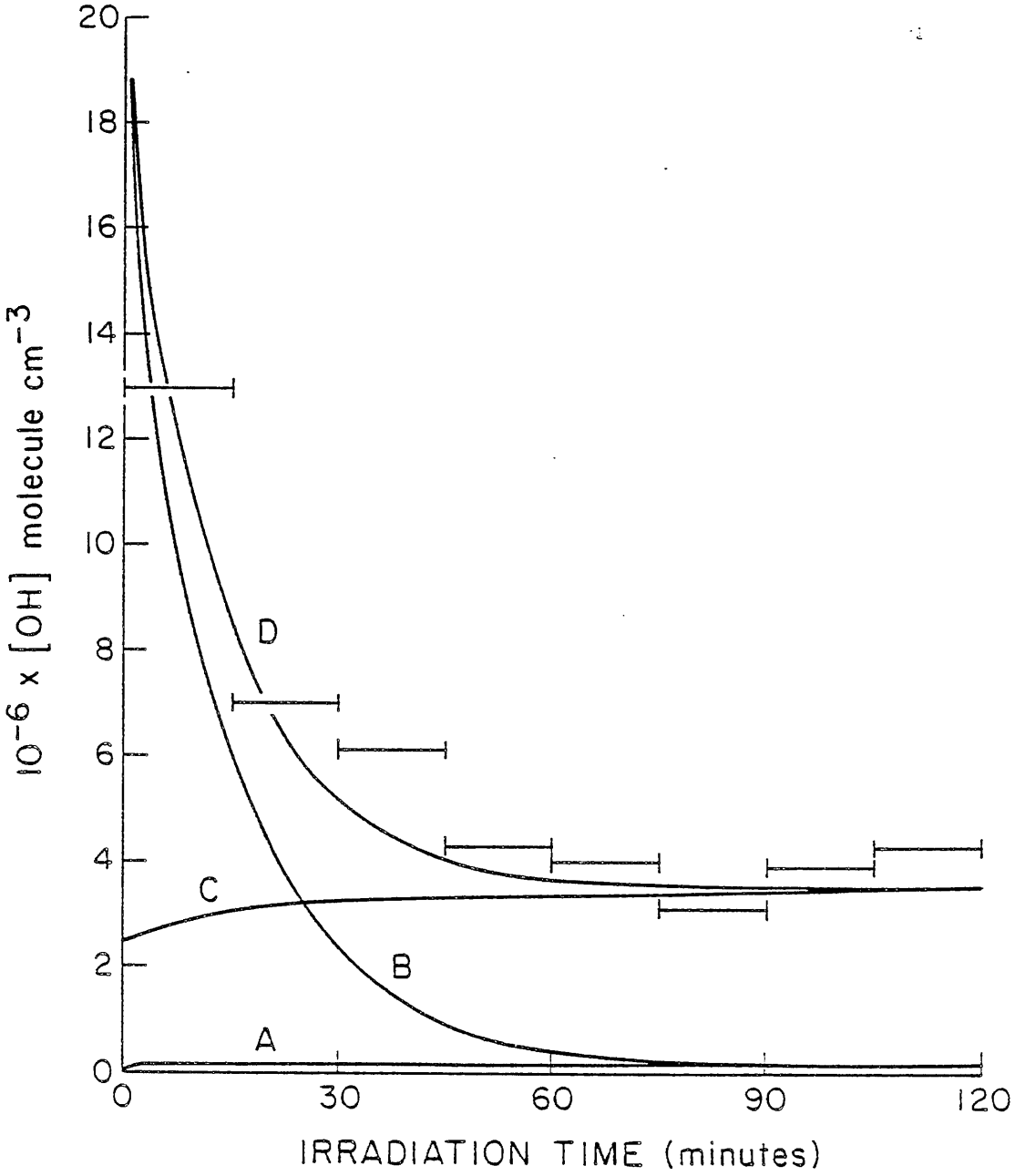

Figure I-2. Hydroxyl Radical Concentrations as a Function of Irradiation Time. ——— Experimental Data for EC-442 [Uncorrected for Minor Consumption of Propene by Reaction with O_3 or $O(^3P)$; A - Model Calculations with the Homogeneous Gas Phase Chemistry; B - Model Calculations with $[HONO]_{initial}$ = 0.050 ppm; C - Model Calculations with a Constant OH Radical Flux of 0.61 ppb min^{-1}; D - Model Calculations with $[HONO]_{initial}$ = 0.050 ppm and a Constant OH Radical Flux of 0.61 ppb min^{-1}.

Table I-11. Dependence on Chamber Employed of OH Radical Levels Observed in Comparable[a] NO_x-Air Irradiations

Chamber	k_1[b] (min^{-1})	[OH] (10^6 cm^{-3})	[OH]/k_1 (Normalized)[c]
Small Teflon Bag No. 4	0.27	4.4 ± 0.7	3.2 ± 0.5
Small Teflon Bag No. 5	0.27	1.4	1.0
Evacuable	0.49	2.5 ± 0.2	1.0
Indoor Teflon	0.45	0.65 ± 0.15	0.3 ± 0.1
Outdoor Teflon	~0.3 ± 0.05[d]	0.9 ± 0.3	0.6 ± 0.2

[a]Initial [NO] ≅ 0.1 ppm; RH <10%, T = 303-308 K.

[b]k_1 = NO_2 photolysis rate.

[c]Normalized to ratio observed in the evacuable chamber runs.

[d]Estimated from radiometer readings using the empirical relationship derived by Zafonte et al. (1977).

Table I-12. Dependence on Temperature and Relative Humidity (RH) of OH Radical Levels Observed in Standard[a] NO_x-Air Irradiations

		10^{-6} x [OH] radical cm^{-3}			
Chamber	T(K)	<10% RH	50% RH	80% RH	100% RH
	284	1.6	2.1	-	4.7
Evacuable	303	2.5	4.4	16 → 11[b]	20 → 12[b]
	323	5.7	18 → 9[b]	-	50 → 8[b]
Indoor Teflon	303	0.6	1.9	-	-

[a]Initial [NO] ≅ 0.4 ppm; [NO_2] ≅ 0.1 ppm; NO_2 photolysis rate k_1 = 0.49 min^{-1} (evacuable chamber), 0.45 (indoor Teflon chamber).

[b]OH radical concentrations changed throughout the run; initial and final values given.

by the NO_2 photolysis rate) is shown in Figure I-3 for the evacuable chamber, and in Figure I-4 for the indoor Teflon chamber. The NO_2 dependence data for the indoor Teflon chamber was obtained during this year of our program, allowing this chamber effect to be assessed for photochemical smog simulation experiments conducted in that chamber as well as in the evacuable chamber.

Measurements of HONO Levels in the SAPRC Evacuable Chamber. During the period covered by this report, a number of experiments were conducted in which differential optical absorption spectroscopy was employed with an *in situ* multi-pass optical system to monitor HONO with a sensitivity of ~2-3 ppb in the evacuable chamber in order to elucidate the role of HONO in the chamber radical source.

As indicated in the previous sections, the results of model calculations on the tracer-NO_x-air irradiations indicate the presence of both initial HONO and a continuous radical source. In order to verify the prediction of initially present HONO, HONO was monitored immediately prior to several of these irradiations. The initial concentrations and the observed initial HONO levels for these runs are compared with initial HONO levels required for model calculations to fit the experimental OH radical profiles and are listed in Table I-13. It can be seen that the observed and calculated HONO concentrations are in good agreement, thus verifying the model predictions.

The experimental conditions and HONO and OH radical concentrations observed in the experiments where HONO was monitored during the irradiations are given in Table I-14. During these experiments, HONO concentrations were observed to rise from those initially present to a constant level within 2-3 hr after the start of irradiation, at which time the OH radical concentrations also had leveled off. In some of the experiments, the system was perturbed at, or after, this time by (a) adding O_3 to change the NO/NO_2 ratio without affecting the NO_x concentration, (b) adding NO_2 or (c) changing the light intensity. In each case, the OH radical and HONO concentrations were monitored until a new equilibrium was reached.

The experiments in which HONO was monitored during the irradiation can give some information as to whether HONO is the immediate radical

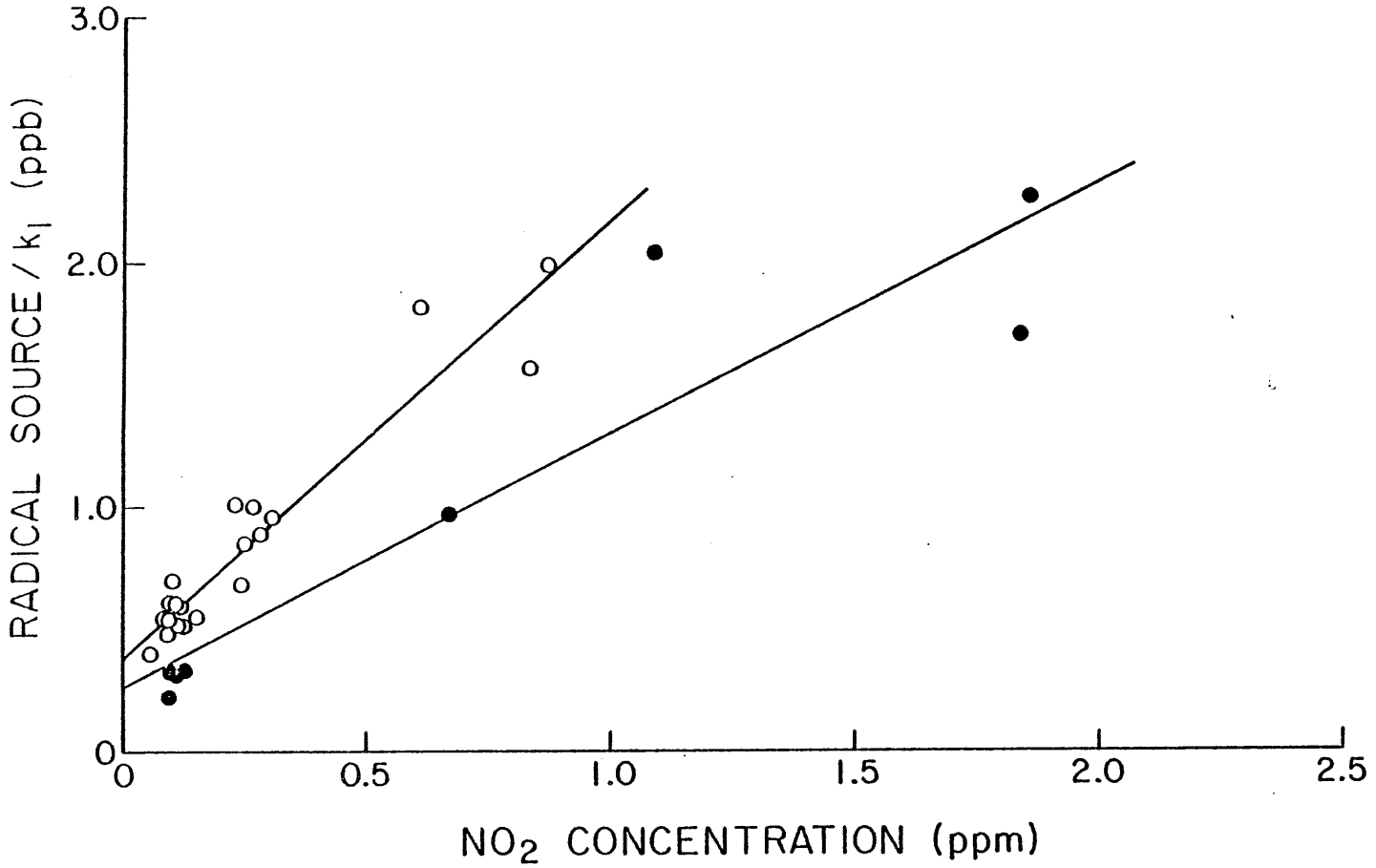

Figure I-3. Plot of (Radical Source/k_1) Against the Average NO_2 Concentration for t > 60 Min in Evacuable Chamber Irradiations at 303 K. ● - ~0% Relative Humidity, O - ~50% Relative Humidity.

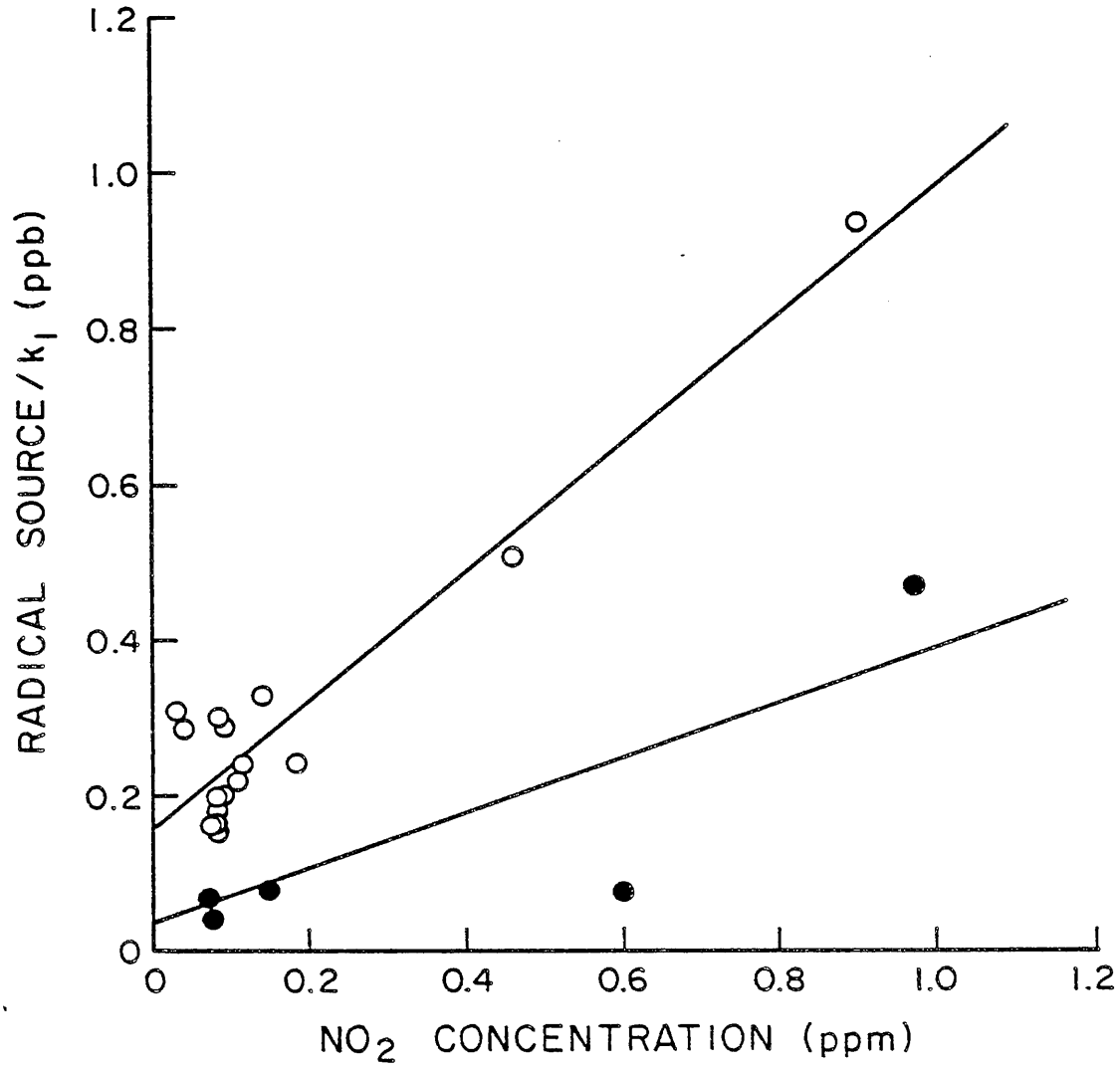

Figure I-4. Plot of (Radical Source/k_1) Against Average NO_2 Concentration for ≥60 Min for the Indoor Teflon Chamber Irradiations. ● - ~0% Relative Humidity, O - ~50% Relative Humidity.

Table I-13. Initial Concentrations and Observed and Calculated[a] Initial HONO Levels for Tracer-NO_x-Air Irradiations in the SAPRC Evacuable[b] Chamber in which HONO was Monitored Prior to the Irradiation

EC Run No.	Initial		Initial HONO (ppb)	
	NO (ppm)	NO_2 (ppm)	Obs.	Calc.
539	0.107	0.356	26	25
540	0.083	0.288	27	25
541	0.378	0.324	13	12
542	0.029	0.131	4	11

[a]Calculated HONO = initial HONO level required for model simulations to fit the observed concentration-time profiles for hydroxyl radical levels.
[b]T = 304 ± 1 K, RH ≅ 50%, $k_{NO_2} \cong 0.4\ min^{-1}$.

precursor in the continuous radical source (i.e., whether the continuous radical involves the continuous formation of HONO as the rate determining step, followed by its rapid photolysis), or whether photolysis of some other species is forming these radicals. Since HONO undergoes rapid photolysis during these irradiations, it can be assumed to be in photostationary state, with its concentration being proportional to its rate of formation. Thus, as discussed in Section IV, if the continuous radical source involves HONO formation, stationary state levels would be higher than if there were no HONO formation mechanism other than the known reaction of OH + NO. The HONO photostationary state levels can be calculated for a given experiment assuming HONO is or is not the continuous radical precursor (see Section IV for a discussion of how these are calculated), and these calculated HONO levels are compared with the experimental HONO levels in Table I-14.

It can be seen from Table I-14 that the data are somewhat ambiguous, in that HONO levels for some runs are better predicted by assuming HONO is not the radical precursor, while those for others are better fit by assuming it is. However, some of this ambiguity can be resolved since it is observed that these experiments fall into two classes: (1) those runs where the OH radical levels were within the range generally observed in

Table I-14. Experimental Conditions and HONO and OH Radical Data for NO_x-Air Irradiations in which HONO was Measured by DOAS

Run No.	k_1 (min^{-1})	NO (ppm)	NO_2 (ppm)	10^{-6}x[OH] (cm)[B]	[HONO] (ppb) Observed	Calculated[a] (A)	(B)
567	0.31	1.45	0.467	2.77	21.0	24.4	38.0
568	0.31	1.032	0.772	2.01	12.0	12.6	29.0
569A	0.39	1.058	0.100	3.33	>25.0	17.0	19.8
569B	0.39	0.668	0.450	3.00	15.0	9.7	21.0
570A	0.36	2.464	0.370	1.96	29.0	25.3	31.9
570B	0.36	1.724	0.840	2.07	17.0	18.7	34.5
626	0.32	0.385	0.103	1.37	5.1	3.1	4.5
630A	0.32	2.322	0.824	1.02	21.7	13.9	22.5
630B	0.15	2.163	0.838	0.53	28.6	14.4	24.1
631A	0.14	1.936	1.053	0.31	16.6	8.1	15.7
631B	0.31	1.950	0.898	0.41	11.8	4.9	8.7
632A	0.32	2.198	0.794	0.81	19.4	10.5	17.1
633B	0.32	2.189	0.806	0.87	14.6	11.2	18.4

[a]A - Calculated as described in Section IV, assuming HONO is not the precursor in the continuous radical source.

B - Calculated as described in Section IV, assuming HONO is the precursor of the continuous radical source.

NO_x-air irradiations performed previously in the SAPRC evacuable chamber and (2) those runs (specifically EC-567 through 570) where the OH radical levels were significantly higher than expected, indicating possible contamination effects. It can be seen that, within the experimental uncertainties, the observed HONO levels in the "normal" experiments agreed reasonably well with the values calculated assuming HONO is the radical precursor, while in the runs with unusually high radical levels, the observed HONO values were much closer to HONO levels calculated assuming contaminant(s) other than HONO are causing the higher radical levels in those experiments. Obviously, additional experiments are required to more adequately resolve this apparent ambiguity.

Summary. The results of the experiments reported here show conclusively that radical input from unknown sources is an important process in smog chamber systems, and that, in terms of the total number of radicals produced in a typical smog simulation irradiation of ≥6-hr duration, photolysis of initial HONO is at most a minor contributor to this process. Thus, it is clear that photochemical smog models validated against chamber data assuming only initial HONO as the radical source must be re-evaluated. However, it is also clear that assuming only a constant radical flux during an irradiation is also an oversimplification, particularly in view of the fact that this assumption generally leads to an underprediction of radical levels in the initial stages of the irradiation, especially for mixtures with high NO_2/NO ratios. Furthermore, the assumption of a constant radical source does not take into account the dependence of the radical flux on NO_2 levels, which in general vary during typical smog chamber irradiations.

Radical input from unknown sources is strongly influenced by both temperature and relative humidity and is highly dependent on the chamber employed. This fact should be taken into account when using smog chamber data to assess the effects of various parameters on photochemical smog formation. Thus, the radical source must be considered to be another chamber effect which (like O_3 wall destruction) must be measured periodically by appropriate control experiments in order for the data obtained during experimental runs to be adequately characterized. In particular, the apparent strong dependence of smog forming potential on temperature previously reported from these laboratories (Carter et al. 1979b) and by Countess et al. (1979) may be wholly or partially a result of this radical source effect. Clearly, extrapolation of environmental chamber data to ambient atmospheric conditions must be carried out with caution, especially until it can be established whether or not such radical sources are present in the atmosphere.

Although the results of experiments reported here are not adequate to establish the exact mechanism causing this effect, they have given some indication as to its nature and allowed a number of possibilities to be ruled out. In particular, the available data suggest that this effect is due, at least in part, to a heterogeneous reaction and is not a result of contamination.

II. INVESTIGATION OF THE ATMOSPHERIC CHEMISTRY OF SELECTED LONG-CHAIN ALKANES

A. Introduction and Background

The long-chain alkanes, exemplified by the $\geq C_6$ n-alkanes, are important constituents of gasoline, diesel fuel and aircraft fuels. In order to accurately assess the atmospheric impact of these fuels, a knowledge of the chemistry of the long-chain alkanes, as it occurs under polluted atmospheric conditions, is necessary. Although it has been established from basic laboratory investigations and supported by smog chamber modeling studies (Hendry et al. 1978, Whitten et al. 1979, 1980; Carter et al. 1979a) that under ambient atmospheric conditions the sole chemical loss process of the alkanes is via reaction with the OH radical,

$$OH + RH \rightarrow H_2O + R$$

followed by rapid addition of O_2 to the alkyl radical to form peroxy radicals,

$$R + O_2 \xrightarrow{M} RO_2$$

it has been shown (Carter et al. 1976, Darnall et al. 1976, Baldwin et al. 1977) that the subsequent reactions may depend to a large extent on the size of the molecule. For the smaller alkanes ($\lesssim C_4$), the following scheme, involving formation of carbonyl compounds as intermediate products and efficient regeneration of OH radicals, appears to fit the data reasonably well (Hendry et al. 1978, Whitten et al. 1979, 1980; Carter et al. 1979a):

$$RO_2 + NO \rightarrow RO. + NO_2$$

$$RO. = \left\{ \begin{array}{c} R_1CH_2O. \\ \text{or} \\ R_1R_2CHO. \end{array} \right\} + O_2 \rightarrow \left\{ \begin{array}{c} R_1CHO \\ \text{or} \\ R_1COR_2 \end{array} \right\} + HO_2$$

$$R_1R_2CHO. \rightarrow R_1. + R_2CHO$$

$$R_1 \xrightarrow{O_2} \xrightarrow{NO} \left\{ \begin{array}{c} HCHO \\ \text{or} \\ R'CHO \\ \text{or} \\ R'COR'' \end{array} \right\} + HO_2$$

$$HO_2 + NO \rightarrow OH + NO_2$$

However, for the larger alkanes, formation of alkyl nitrates via the alternate route in the reaction of peroxy radicals with NO

$$RO_2 + NO \xrightarrow{M} RONO_2$$

and isomerization of longer-chain alkoxy radicals via H-atom migration, e.g.

$$HCH_2CH_2CH_2CH_2O. \rightarrow .CH_2CH_2CH_2CH_2OH$$

becomes increasingly important, resulting in the formation of significantly different products.

The isomerization of alkoxy radicals was first proposed to be important in room temperature NO_x photooxidations by Carter et al. (1976), and subsequently by Baldwin et al. (1977). Thermochemical calculations by both groups (Carter et al. 1976, Pitts et al. 1976, Baldwin et al. 1977) have shown that under ambient atmospheric conditions the 1,4-H shifts of alkoxy radicals (via six-membered ring transition states) can compete significantly with their reaction with O_2 and unimolecular decomposition. For n-butane, the isomerization pathway only affects ~15% of the total reaction pathway with the OH radical, since the initial radicals are ~15% n-butyl (which can undergo isomerization) and ~85% sec-butyl (which cannot) (Carter et al. 1979a, Atkinson et al. 1979). However, for n-pentane, of the total number of alkoxy radicals formed, ~70% can undergo

isomerization and for the higher n-alkanes, 100% of the alkoxy radicals initially formed can undergo isomerization. Thus, alkoxy radical isomerization is clearly an important process to consider in the photooxidation of the long-chain alkanes.

Until recently, the reactions subsequent to the first isomerization were a matter of conjecture. However, it has been shown (Niki et al. 1978, Carter et al. 1979c, Radford 1980, Washida 1981, Ohta et al. 1982) that α-hydroxy radicals react with O_2 to form the corresponding carbonyl and HO_2

$$RR_1\dot{C}OH + O_2 \rightarrow RCOR_1 + HO_2$$

and so terminate the isomerization sequence after a total of two isomerizations. This is illustrated below for the 2-pentoxy radical which forms a δ-hydroxy carbonyl

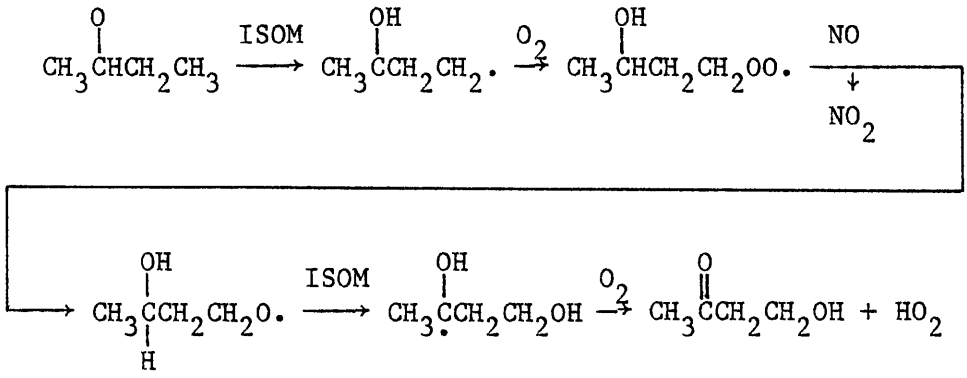

Thus, formation of bifunctional products and enhanced conversion of NO to NO_2 is expected to result from alkoxy radical isomerization.

In addition to formation of bifunctional products, evidence from smog chamber data indicates that alkyl nitrate formation becomes increasingly important for the higher alkanes (Darnall et al. 1976). The following mechanism was proposed to account for the observations:

$$RO_2 + NO \rightarrow RO + NO_2$$

$$RO_2 + NO \rightarrow RO_2NO^*$$

$$RO_2NO^* \rightarrow RONO_2^*$$

$$RONO_2^* \rightarrow RO + NO_2 \quad \text{decomposition}$$

$$RONO_2^* \xrightarrow{M} RONO_2 \quad \text{stabilization}$$

This effect of the size of the n-alkane on the alkyl nitrate yield was rationalized in terms of quantum statistical effects, since the rate of decomposition of the vibrationally excited $RONO_2^*$ or $ROONO^*$ adducts is inversely related to their number of internal degrees of freedom.

However, additional data are required to more completely test this proposed mechanism and to obtain more accurate alkyl nitrate yields from the NO_x photooxidation of the n-alkanes. In particular, the smog chamber data for the C_6 alkanes (Darnall et al. 1976) were highly uncertain because authentic samples of the C_6 alkyl nitrates were unavailable, and it was not known whether alkyl nitrate formation would approach 100% as the size of the molecule increases, or indeed whether alkyl nitrate formation would exhibit the pressure dependences predicted by this mechanism.

A more detailed understanding of alkyl nitrate formation in atmospheric systems is of importance for several reasons. First, alkyl nitrate formation from RO_2 + NO is unaffected by the alkoxy radical isomerization discussed above since peroxy radical formation precedes alkoxy radical formation in the alkane photooxidation mechanism. Second, model calculations (Carter et al. 1979a, Carter et al. 1981) have shown that this reaction has a greater effect on predicted O_3 yields and other measurements of photochemical reactivity than does alkoxy radical isomerization. This is at least partly because formation of alkyl nitrates amounts to an effective sink for NO_x, without which ozone formation and many radical propagation reactions cannot occur. Furthermore, alkyl nitrate formation is a radical termination process, so if it plays a major role in the atmospheric degradation of long chain alkanes, those compounds could indeed act as radical inhibitors in atmospheric systems.

In this program, we have investigated these and other selected aspects of the atmospheric chemistry of the n-alkanes. The alkyl nitrate yields from the reaction of RO_2 radicals with NO have been determined for ethane through n-octane. This also necessitated the determination of the

OH radical rate constants for these n-alkanes and for the alkyl nitrates formed, since reaction with OH radicals are the major loss processes of both the n-alkanes and the alkyl nitrates under simulated atmospheric conditions. In addition, OH radical rate constants were determined for a series of ketones, these also being products of the NO_x-air photooxidations of the alkanes, and NO_x-air and methyl nitrite-air photooxidations of n-hexane, n-heptane and n-octane were carried out in order to establish a data base for the development of detailed chemical kinetic computer models for these long-chain alkanes. These studies are described in detail below.

B. Determination of Rate Constants for the Reaction of OH Radicals with a Series of Ketones, n-Alkanes and Alkyl Nitrates

Rate constants for the ketones 2-pentanone, 3-pentanone, 2-hexanone, 3-hexanone, 2,4-dimethyl-3-pentanone, 4-methyl-2-pentanone and 2,6-dimethyl-4-heptanone, the n-alkanes propane through n-decane and the alkyl nitrates 2-propyl, 1-butyl, 2-butyl, 2-pentyl, 3-pentyl, 2-hexyl, 3-hexyl, 3-heptyl and 3-octyl nitrate were determined using a relative rate technique at ~299 ± 2 K.

Experimental

Hydroxyl radicals were generated by the photolysis ($\lambda \gtrsim 290$ nm) of methyl nitrite (CH_3ONO) in air at part-per-million (1 ppm = 2.38×10^{13} molecule cm^{-3} at 298 K and 735 torr total pressure) concentrations:

$$CH_3ONO + h\nu \rightarrow CH_3O + NO$$

$$CH_3O + O_2 \rightarrow HCHO + HO_2$$

$$HO_2 + NO \rightarrow OH + NO_2$$

In order to minimize the formation of O_3 during these irradiations, NO was added to the reaction mixtures, which had initial concentrations of CH_3ONO, 4-30 ppm; NO, ~5 ppm, and 0.5-1.0 ppm each of the reference organic and the reactant organic(s). Ultra-zero air (Liquid Carbonic, < 0.1 ppm hydrocarbons) was used as the diluent gas.

Irradiations were carried out in an ~75-ℓ FEP Teflon cylindrical reaction bag surrounded by 24 GE F15T8-BL 15-W blacklights. By switching off sets of lamps, light intensities of ~1/3 and 2/3 of the maximum could be obtained. With all the lamps on, the light intensity, determined as the photolysis rate of NO_2 in N_2, was 0.27 min^{-1}, and corresponded to a methyl nitrite half-life of ~10 min. In order to avoid any significant temperature rise on irradiation, a stream of air was blown between the lamp assemblies and the Teflon reaction bag, and for all irradiations the air temperature immediately outside the reaction bag was 299 ± 2 K. Prior to irradiation, the reaction bag/lamp assembly was covered with an opaque cover to avoid any photolysis of the reactants.

Methyl nitrite was prepared (Taylor et al. 1980) by the dropwise addition of 50% H_2SO_4 to methanol saturated with sodium nitrite. The CH_3ONO produced was swept out of the reaction flask by a stream of ultra-high purity nitrogen, passed through a trap containing saturated NaOH solution to remove any H_2SO_4, dried by passage through a trap containing anhydrous $CaCl_2$, and collected in a trap at 196 K. The CH_3ONO was then degassed and vacuum-distilled on a greaseless high-vacuum system and stored under vacuum at 77 K in the dark. Known amounts of the CH_3ONO, NO and the reference and reactant organics were flushed from Pyrex bulbs by a stream of ultra-zero air into the Teflon reaction bag, which was then filled with ultra-zero air.

The reactants were quantitatively monitored prior to and during the irradiations by gas chromatography with flame ionization detection. The columns used for the various reactants were as follows. The ketones, the $\leq C_6$ alkyl nitrates, n-hexane, n-nonane and n-decane were analyzed using a 10-ft x 1/8-in stainless steel (SS) column of 10% Carbowax 600 on C-22 Firebrick (100/110 mesh), operated at 348 K; the 3-heptyl and 3-octyl nitrates were analyzed using a 5-ft x 1/8-in SS column of 5% Carbowax 600 on C-22 Firebrick (100/110 mesh), operated at 348 K; cyclohexane, CH_3ONO, and the $\geq C_6$ alkanes using a 20-ft x 1/8-in SS column with 5% DC703/C20M on 100/120 mesh AW, DMCS Chromosorb G, operated at 333 K; and propane, n-butane and n-pentane using a 36-ft x 1/8-in SS column of 10% 2,4-dimethylsulfolane (DMS) on C-22 Firebrick (60/80), operated at 273 K.

The alkyl nitrates were obtained as follows: 2-propyl, Eastman Kodak; 1-butyl, Matheson, Coleman and Bell; 2-butyl, 2-pentyl, 2-hexyl,

3-heptyl and 3-octyl, Fluorochem Inc. The 2-pentyl- and 2-hexyl nitrates had significant levels (~15-30%) of the 3-isomers, allowing rate constant data to be obtained for these isomers as well. The alkanes and ketones were obtained commercially and were used without further purification.

Analysis of the Data

In the presence of added organics and a reference organic (n-hexane or cyclohexane in this study), the OH radicals generated from the photolysis of CH_3ONO in air can, besides reacting with CH_3ONO, NO and NO_2 and the organic reaction products, react with these organics:

$$OH + \text{organic} \rightarrow \text{products} \quad (1)$$

$$OH + \text{reference organic} \rightarrow \text{products} \quad (2)$$

Additionally, the organics may also photolyze

$$\text{organic} + h\nu \rightarrow \text{products} \quad (3)$$

and the possibility of first order wall decay must also be considered:

$$\text{organic} \xrightarrow{\text{wall}} \text{loss of organic} \quad (4)$$

(No evidence for first-order decay of cyclohexane or n-hexane was observed in this study.) Under the experimental conditions employed, reactions of the reference organics and the organic reactants with $O(^3P)$ atoms and O_3 were negligible, and, since dilution due to sampling was avoided by use of a collapsible Teflon reaction bag, then:

$$d[\text{organic}]/dt = k_1[OH][\text{organic}] + (k_3 + k_4)[\text{organic}] \quad (I)$$

$$d[\text{reference organic}]/dt = k_2[OH][\text{reference organic}] \quad (II)$$

and hence

$$\ln([\text{organic}]_{t_o}/[\text{organic}]_t) = k_1 \int_{t_o}^{t} [OH]dt + (k_3 + k_4)(t-t_o) \quad (III)$$

and

$$\ln([\text{reference organic}]_{t_o}/[\text{reference organic}]_t) = k_2 \int_{t_o}^{t} [OH]dt \qquad \text{(IV)}$$

where k_1, k_2, k_3 and k_4 are the rate constants for reactions (1), (2), (3) and (4), respectively, $[\text{organic}]_{t_o}$, and $[\text{reference organic}]_{t_o}$ are the concentrations of the organic and reference organic, respectively, at time t_o, and $[\text{organic}]_t$ and $[\text{reference organic}]_t$ are the corresponding concentrations at time t. Eliminating the OH radical concentrations from equations (III) and (IV) yields:

$$\frac{1}{(t-t_o)} \ln\left\{\frac{[\text{organic}]_{t_o}}{[\text{organic}]_t}\right\} = (k_3 + k_4) + \frac{k_1}{k_2(t-t_o)} \ln\left\{\frac{[\text{reference organic}]_{t_o}}{[\text{reference organic}]_t}\right\} \qquad \text{(V)}$$

Hence plots of $(t-t_o)^{-1} \ln ([\text{organic}]_{t_o}/[\text{organic}]_{t_o})$ against $(t-t_o)^{-1} \ln ([\text{reference organic}]_{t_o}/[\text{reference organic}]_t)$ should yield straight lines of slope k_1/k_2 and intecept $(k_3 + k_4)$. If photolysis and/or wall loss processes of the organics are absent [i.e., $(k_3 + k_4) = 0$], as was the case for the n-alkane series, then the simplified expression

$$\ln\left\{\frac{[\text{organic}]_{t_o}}{[\text{organic}]_t}\right\} = \frac{k_1}{k_2} \ln\left\{\frac{[\text{reference organic}]_{t_o}}{[\text{reference organic}]_t}\right\} \qquad \text{(VI)}$$

is applicable. In this case, plots of $\ln([\text{organic}]_{t_o}/[\text{organic}]_t)$ against $\ln([\text{reference organic}]_{t_o}/[\text{reference organic}]_t)$ should yield straight lines with a zero intercept and a slope of k_1/k_2.

Results and Discussion

Ketones. Irradiations of CH_3ONO-NO-cyclohexane-ketone-air mixtures were carried out at 299 ± 2 K with cyclohexane acting as the reference organic. Five different ketone mixtures, chosen to avoid interferences in the gas chromatographic analyses, were irradiated: 2-pentanone, 3-pentanone, 2-hexanone, 3-hexanone and 3-pentanone + 4-methyl-2-pentanone + 2,4-

dimethyl-3-pentanone + 2,6-dimethyl-4-heptanone. Irradiations of CH_3ONO-NO-cyclohexane-2-butanone-air mixtures were also carried out, but methyl nitrate, a product of these irradiations, had the same retention time as 2-butanone on the gas chromatographic column employed, thus precluding obtaining any accurate rate constant data. Irradiations of CH_3ONO-NO-cyclohexane-air mixtures showed no other gas chromatographic product peaks in the region where the other ketones appeared.

In order to vary the OH radical concentrations, and thus the relative importance of OH radical reaction versus photolysis, duplicate irradiations were carried out with differing initial concentrations of CH_3ONO. For the irradiations involving the four ketones together, and those with 3-pentanone singly, one-third light intensity was used to extend the duration of the irradiations and thus allow two or three data points to be obtained per irradiation. For the irradiations with 2-pentanone, 2-hexanone and 3-hexanone, higher light intensities were used since the gas chromatographic retention times for these ketones allowed more frequent sampling.

During these irradiations, CH_3ONO and the organics were observed to disappear, accompanied by NO to NO_2 conversion and the appearance of expected products (e.g., methyl nitrate). Ozone concentrations at the end of the irradiations were $\leq$0.15 ppm, and since the alkanes and saturated carbonyls react very slowly with O_3 (Herron et al. 1979, Hendry and Kenley 1979, Atkinson et al. 1979, 1981b), reaction with O_3 was calculated to be negligible under these conditions at the OH radical concentrations observed [$(0.1\text{-}1.3) \times 10^8$ cm^{-3}]. Similarly, reaction with $O(^3P)$ atoms (Herron and Huie 1973) was calculated from the NO_2 concentrations observed and the light intensity to contribute $\leq$1% of the overall cyclohexane and ketone loss rates.

Plots of equation (V) are shown in Figures II-1 and II-2, and the rate constant ratios k_1/k_2 and the intercepts $(k_3 + k_4)$ obtained by least squares analyses of these plots are given in Table II-1. The cyclohexane data obtained on each of the two different gas chromatographic columns for the irradiations which involved 2-pentanone and 3-pentanone, when plotted against each other in the form of equation (V), yielded a zero intercept (0.00001 $\pm$ 0.00069) and a slope of 0.998 $\pm$ 0.029 (where the errors are two

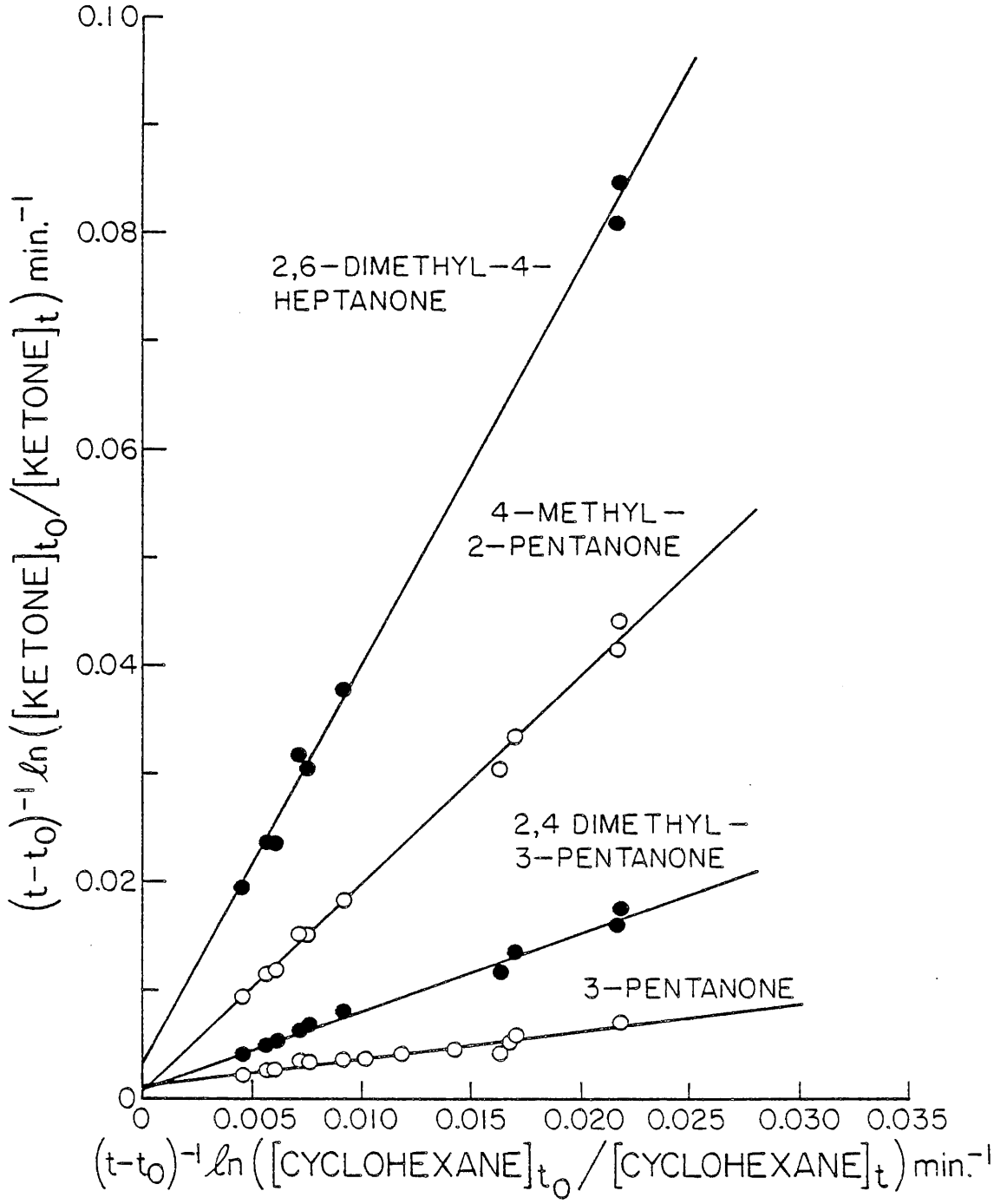

Figure II-1. Plots of Equation (V) for the Ketones 3-Pentanone, 2,4-Dimethyl-3-Pentanone, 4-Methyl-2-Pentanone and 2,6-Dimethyl-4-Heptanone.

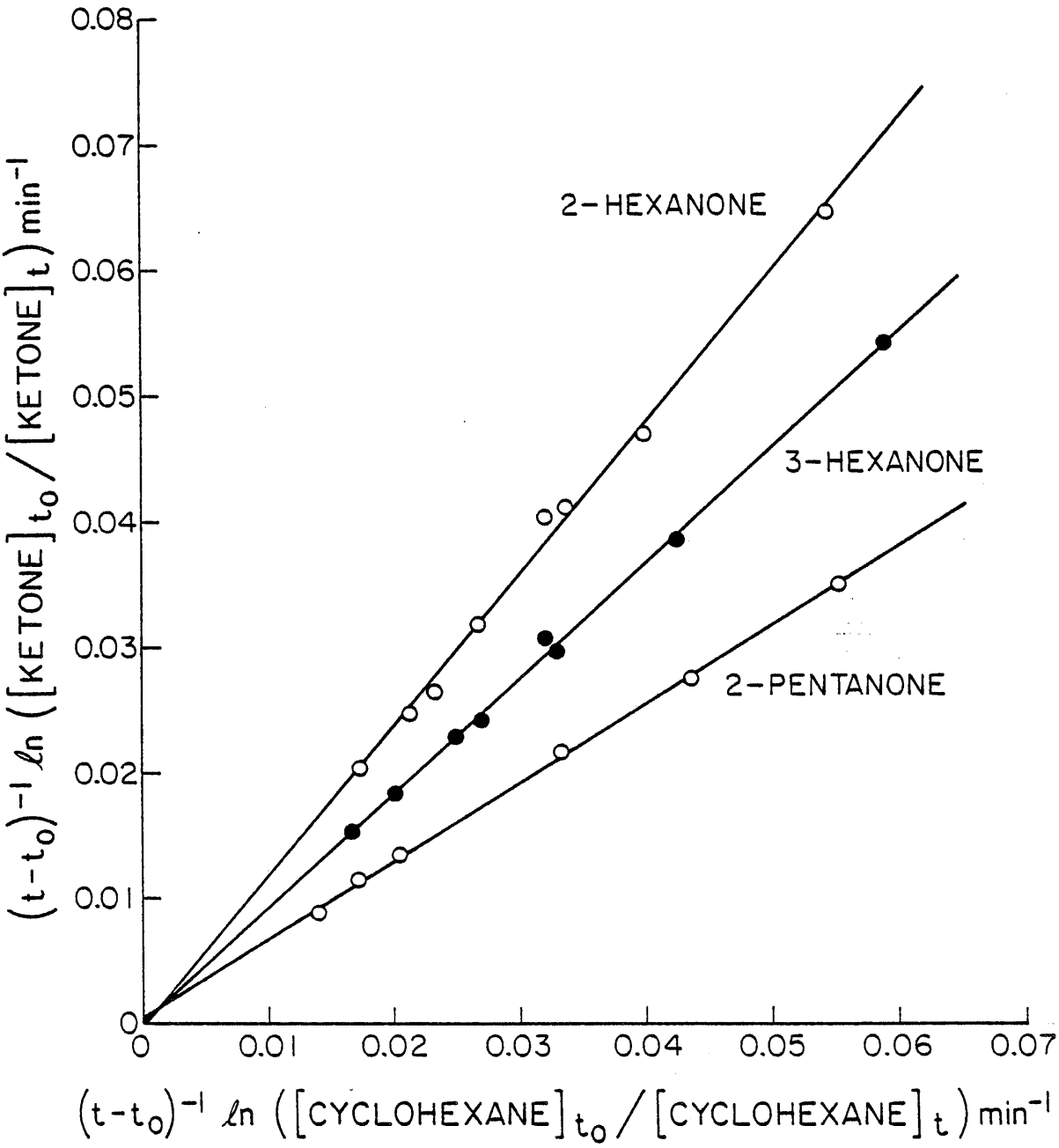

Figure II-2. Plot of Equation (V) for the Ketones 2-Pentanone, 2-Hexanone and 3-Hexanone.

Table II-1. Rate Constant Ratios k_1/k_2 and Intercepts $(k_3 + k_4)$ at 299 ± 2 K

Ketone	k_1/k_2[a]	$10^5 \times (k_3 + k_4)(sec^{-1})$[a]
2-Pentanone	0.626 ± 0.018	0.8 ± 1.0[b]
3-Pentanone	0.245 ± 0.044	2.1 ± 0.9[c]
2-Hexanone	1.21 ± 0.08	-0.6 ± 4.0[d]
3-Hexanone	0.919 ± 0.038	0.0 ± 2.2[d]
2,4-Dimethyl-3-pentanone	0.717 ± 0.054	1.5 ± 1.2[c]
4-Methyl-2-pentanone	1.91 ± 0.09	1.3 ± 1.9[c]
2,6-Dimethyl-4-heptanone	3.66 ± 0.19	5.5 ± 3.8[c]

[a]Indicated errors are two standard deviations of the least squares analysis of the plots shown in Figures II-1 and II-2.

[b]Two-thirds maximum light intensity.

[c]One-third maximum light intensity.

[d]Maximum light intensity.

standard deviations), indicating no gas chromatographic problems for the cyclohexane analyses.

It can be seen from Figures II-1 and II-2 that the experimental data are in good accord with equation (V), with the variable intercepts suggesting that first-order wall loss and, to a lesser extent, photolysis of the ketones was occurring in this system along with OH radical reaction, though these first-order loss processes were relatively unimportant except for the case of 3-pentanone.

The rate constants k_1 can be placed on an absolute basis using a rate constant for the reaction of OH radicals with cyclohexane of $k_2 = 7.57 \times 10^{-12}$ cm^3 $molecule^{-1}$ sec^{-1} determined recently with this technique (Atkinson et al. 1982a) (which in turn is based on a rate constant for the reaction of OH radicals with n-butane of 2.58×10^{-12} cm^3 $molecule^{-1}$ sec^{-1} at 299 ± 2 K (Atkinson et al. 1982a). These rate constants, k_1, are given in Table II-2, along with other reported literature data. It can be seen that the present rate constants for 4-methyl-2-pentanone and 2,6-dimethyl-4-heptanone are in good agreement with the literature data. It should

also be noted that the present data are consistent with the lower rate constant for 2-butanone recently obtained by Cox et al. (1981), since OH radicals should react more slowly with 2-butanone than with 3-pentanone, and the higher 2-butanone rate constants (Winer et al. 1976, Cox et al. 1980) are higher than our present value for 3-pentanone.

Comparison of the rate constants k_1 with those calculated (Atkinson et al. 1979) for alkanes with the same number of primary, secondary and tertiary C-H bonds is of interest from the viewpoint of structure-reactivity predictive schemes. As shown in Table II-2, with respect to the analogous alkanes, 3-pentanone is less reactive, 2,4-dimethyl-3-pentanone is of comparable reactivity, and the other five ketones studied in this work are more reactive. Of particular interest are the observations that 2-pentanone reacts with OH radicals a factor of ~2.6 faster than does 3-pentanone, and that 2-hexanone also reacts more rapidly than does 3-hexanone. These data can be explained if it is assumed that the carbonyl group decreases the reactivity of secondary C-H bonds at the α-position towards attack by the OH radical, relative to those in the analogous alkane, but increases the reactivity of the secondary C-H bonds at the β-position. This effect is somewhat unexpected, since the available thermochemical data (Kerr et al. 1975) for the primary C-H bond strengths in 2-propanone and the secondary C-H bonds in 2-butanone do not indicate any increase in C-H bond strength on the α-carbon. In fact for 2-butanone the reverse is true (Solly et al. 1970, Kerr et al. 1975), as noted by Cox et al. (1981).

n-Alkanes. Irradiations of a series of CH_3ONO-NO-alkane-air mixtures were carried out at 299 ± 2 K. In order to optimize the gas chromatographic analyses and to obtain, as much as possible, similar alkane conversion rates during the experiments, irradiations of CH_3ONO-NO-propane-n-butane-air, CH_3ONO-NO-n-pentane-n-hexane-n-heptane-n-octane-air, CH_3ONO-NO-n-hexane-n-nonane-air and CH_3ONO-NO-n-hexane-n-decane-air were carried out, with n-butane or n-hexane being used as the reference alkane. For these mixtures, duplicate irradiations were carried out with differing initial concentrations of CH_3ONO.

Plots of equation (VI) are shown in Figures II-3 through II-5, and the rate constant ratios k_1/k_2 obtained from these plots by least squares analyses are given in Table II-3.

Table II-2. Rate Constants k_1 for the Reaction of OH Radicals with a Series of Ketones

Ketone	$10^{12} \times k_1$ cm^3 molecule^{-1} sec^{-1}		
	This Work[a]	Literature	Analogous Alkane[b]
2-Butanone		4.5 ± 1.0[c] 2.8[d,e] 0.94 ± 0.09[e,f]	1.55
2-Pentanone	4.74 ± 0.14		2.7
3-Pentanone	1.85 ± 0.34		2.7
2-Hexanone	9.16 ± 0.61		3.9
3-Hexanone	6.96 ± 0.29		3.9
2,4-Dimethyl-3-pentanone	5.43 ± 0.41		5.0
4-Methyl-2-pentanone	14.5 ± 0.7	14 ± 4[c] 13.2[d,e] 13.7 ± 0.4[e,f]	3.9
2,6-Dimethyl-4-heptanone	27.7 ± 1.5	24 ± 7[c]	7.3

[a] At 299 ± 2 K. Placed on an absolute basis using $k_2 = 7.57 \times 10^{-12}$ cm^3 molecule^{-1} sec^{-1} (Atkinson et al. 1982a), which in turn is based on k(OH + n-butane) = 2.58×10^{-12} cm^3 molecule^{-1} sec^{-1} (Atkinson et al. 1982a). Error limits are two standard deviations of the k_1/k_2 ratio, and do not take into account any error associated with k_2.

[b] Calculated from the literature formula (Atkinson et al. 1979) for the same number of primary, secondary and tertiary C-H bonds as in each ketone (i.e., $k_{total_1} = (6.5 \times 10^{-14} N_1 + 5.8 \times 10^{-13} N_2 + 2.1 \times 10^{-12} N_3)$ cm^3 molecule^{-1} sec^{-1}) where N_1, N_2 and N_3 are the number of primary, secondary and tertiary C-H bonds, respectively.

[c] Winer et al. (1976), as re-evaluated by Atkinson et al. (1979).

[d] Cox et al. (1980).

[e] Relative to the rate constant for the reaction of OH radicals with ethene. A rate constant of 8.5×10^{-12} cm^3 molecule^{-1} sec^{-1} (Atkinson et al. 1982a) has been used here.

[f] Cox et al. (1981).

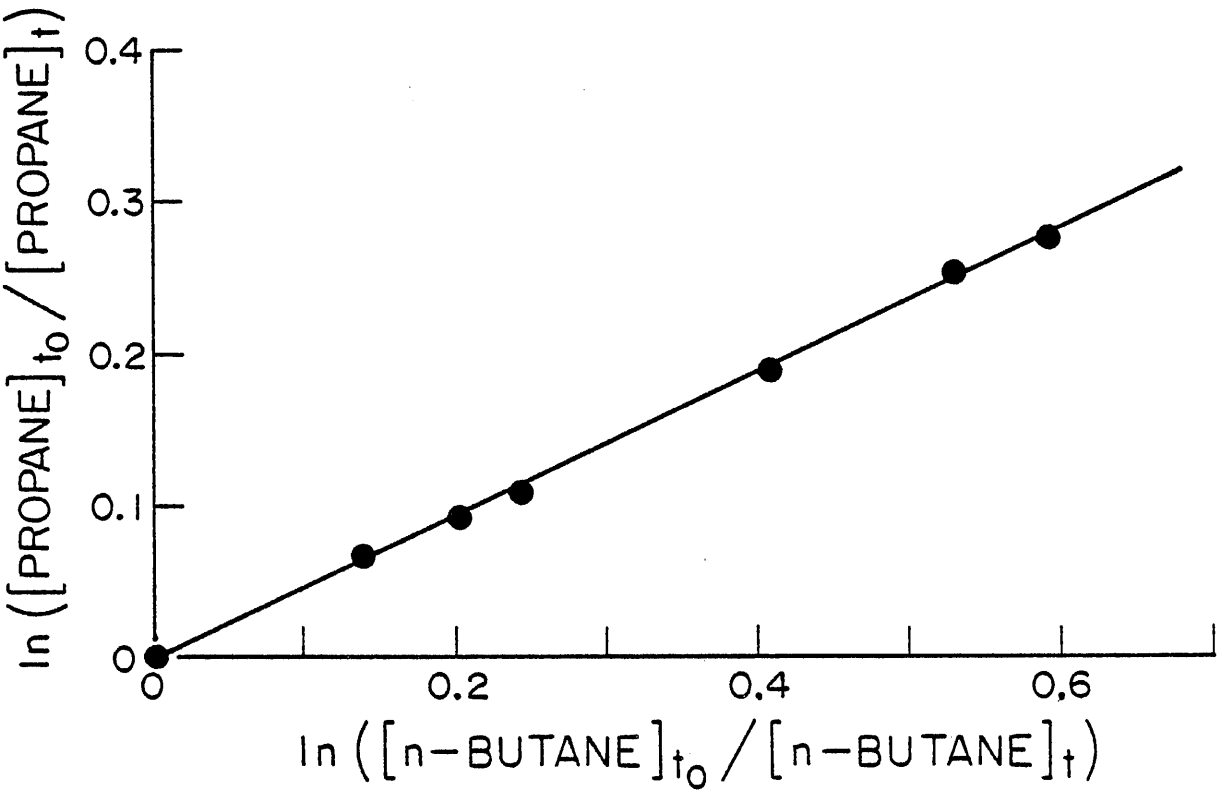

Figure II-3. Plot of $\ln([\text{propane}]_{t_o}/[\text{propane}]_t)$ Against $\ln([\text{n-butane}]_{t_o}/[\text{n-butane}]_t)$.

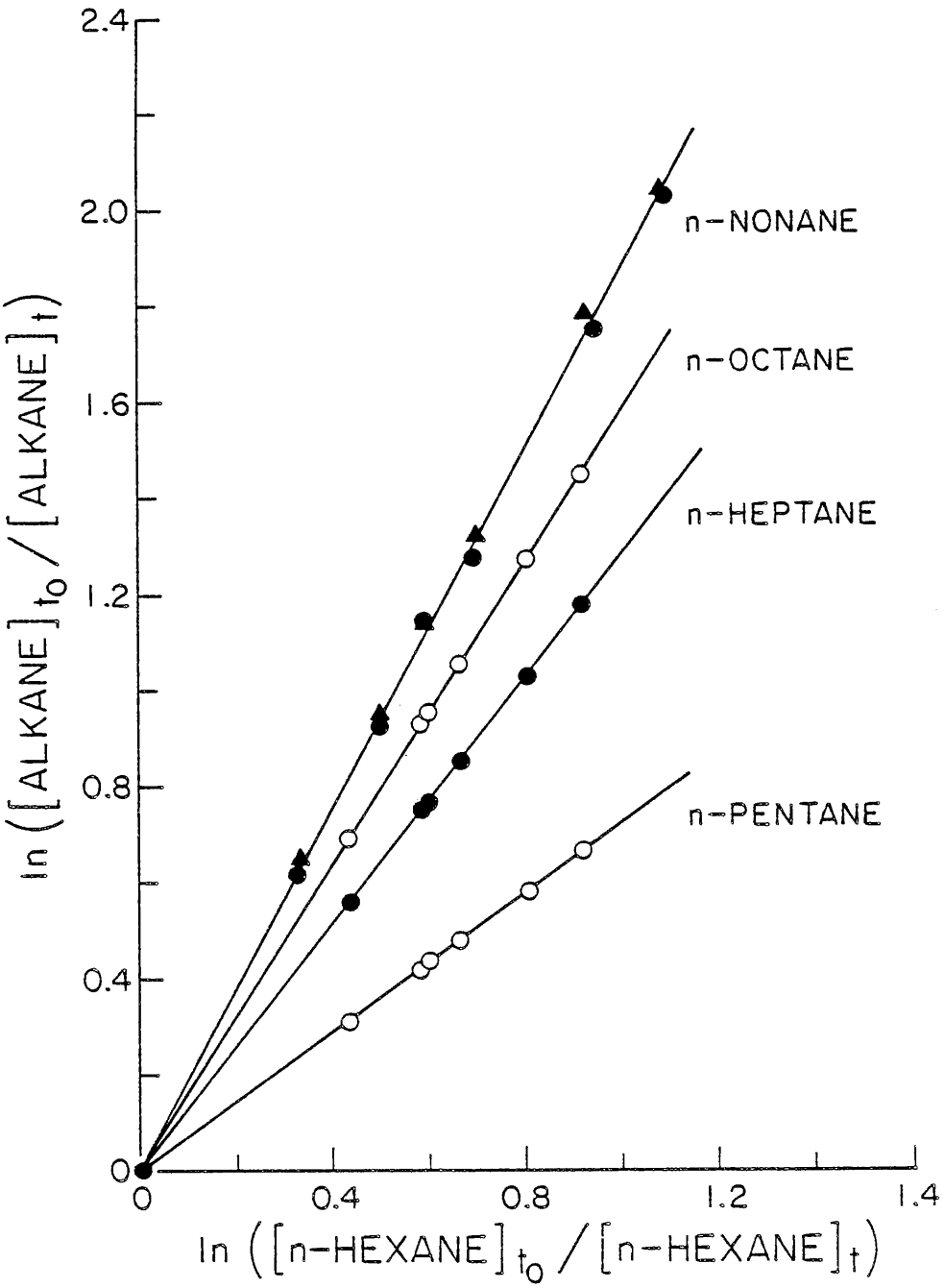

Figure II-4. Plots of $\ln([\text{alkane}]_{t_o}/[\text{alkane}]_t)$ Against $\ln([\text{n-hexane}]_{t_o}/[\text{n-hexane}]_t)$ for n-Pentane, n-Heptane, n-Octane and n-Nonane. The Different Symbols for n-Nonane Refer to the Two Independent Gas Chromatographic Analyses.

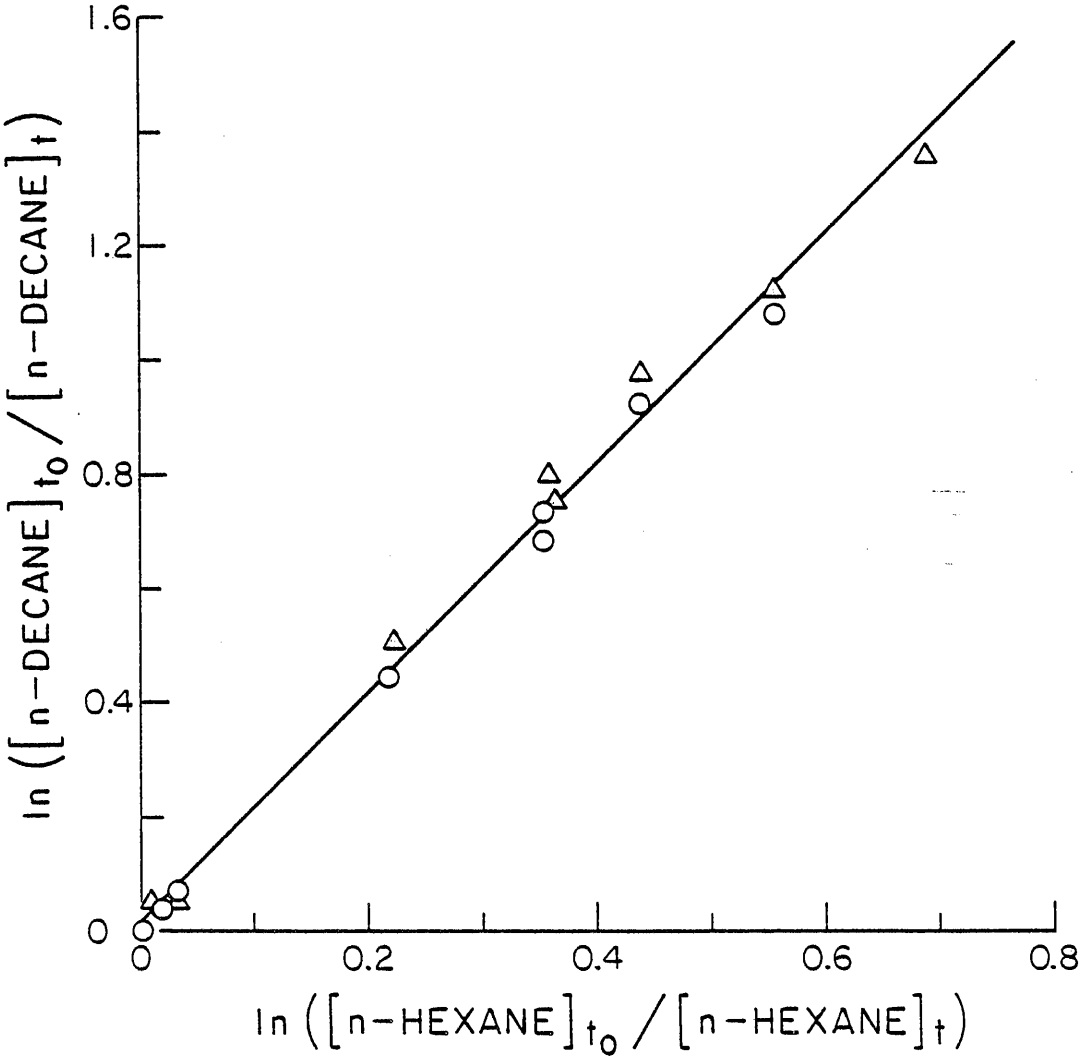

Figure II-5. Plot of $\ln([\text{n-decane}]_{t_o}/[\text{n-decane}]_t)$ Against $\ln([\text{n-hexane}]_{t_o})$. The Different Symbols Refer to the Two Independent Gas Chromatographic Analyses.

Table II-3. Relative Rate Constant Ratios k_1/k_2 at 299 ± 2 K

Alkane	k_1/k_2[a]	
Propane	0.473 ± 0.016	
n-Butane	1.00	0.453 ± 0.007[b]
n-Pentane		0.724 ± 0.008
n-Hexane		1.00
n-Heptane		1.28 ± 0.02
n-Octane		1.58 ± 0.02
n-Nonane		1.87 ± 0.05
n-Decane		2.00 ± 0.09

[a]Indicated errors are two standard deviations of the slopes of plots of equation (VI) shown in Figures II-3 through II-5.

[b]From Atkinson et al. (1982a).

As noted in the Experimental section above, for the irradiations involving n-nonane and n-decane, gas chromatographic analyses of the alkanes were carried out on two different columns, with, as shown in Figure II-4 and II-5, the data from the two analyses being in excellent (n-nonane) or good (n-decane) agreement. For the irradiated CH_3ONO-NO-n-hexane-n-decane-air system, the agreement between replicate irradiations was not as good as for the other alkane systems, probably due to wall adsorption/desorption problems. Hence for n-decane the rate constant ratio k_1/k_2 is of somewhat lower precision than for the other alkanes studied here.

In Table II-4, the rate constants k_1 have been placed on an absolute basis using the mean of the literature absolute rate constants for n-butane (Greiner 1970, Stuhl 1973, Perry et al. 1976, Paraskevopoulos and Nip 1980) (k_2 = 2.58 x 10^{-12} cm^3 $molecule^{-1}$ sec^{-1}), and are compared with the available literature rate constant data. No previous data have been reported for n-heptane, n-nonane or n-decane. For the remaining alkanes investigated, it can be seen that the present data are in excellent agreement with the absolute rate constants obtained by Greiner (1970) for

Table II-4. Room Temperature Rate Constants for the Reaction of OH Radicals with n-Alkanes

Alkane	10^{12} x k (cm^3 $molecule^{-1}$ sec^{-1})		
	This Work[a]	Absolute Literature Values	Relative Literature Values[b]
Ethane		0.283,[c] 0.264 ± 0.017,[d] 0.290 ± 0.060,[e] 0.26 ± 0.04[f]	
Propane	1.22 ± 0.05	1.20,[c] 0.83 ± 0.17,[g] 2.02 ± 0.10,[d]	1.51 ± 0.21,[k] 2.2 ± 0.6[l]
n-Butane	2.58[p]	2.57,[c] 2.35 ± 0.35,[h] 2.72 ± 0.27,[i] 2.67 ± 0.22[j]	
n-Pentane	4.13 ± 0.08		6.2,[m] 3.55 ± 0.13[k]
n-Hexane	5.70 ± 0.09[q]		5.6 ± 1.2,[n] 5.7,[m] 5.8[o]
n-Heptane	7.30 ± 0.17		
n-Octane	9.01 ± 0.19	8.42 ± 1.25[c]	
n-Nonane	10.7 ± 0.4		
n-Decane	11.4 ± 0.6		

[a] At 299 ± 2 K. Indicated errors are two standard deviations.
[b] Taken from Atkinson et al. (1979), which should be consulted for details. The data of Campbell et al. (1976), Lloyd et al. (1976) and Darnall et al. (1978), which are relative to n-butane, have been adjusted to be consistent with the presently used OH + n-butane rate constant.
[c] Greiner (1970).
[d] Overend et al. (1975).
[e] Howard and Evenson (1976).
[f] Leu (1979).
[g] Bradley et al. (1973).
[h] Stuhl (1973).
[i] Perry et al. (1976).
[j] Paraskevopoulos and Nip (1980).
[k] Darnall et al. (1978).
[l] Gorse and Volman (1974).
[m] Wu et al. (1976).
[n] Lloyd et al. (1976).
[o] Campbell et al. (1976).
[p] Mean of absolute literature values.
[q] From Atkinson et al. (1982a).

propane and n-octane, and are in general agreement with the previous relative rate data reported for propane, n-pentane and n-hexane.

Figure II-6 gives a plot of the rate constants obtained in this work against carbon number. While the rate constants increase monotonically with the carbon number of the n-alkane, reflecting the fact that the major reaction pathway is via H-atom abstraction from the secondary C-H bonds (Atkinson et al. 1979), it can be seen that the plot has significant curvature at the lower carbon numbers, and that the higher alkanes react significantly more rapidly than predicted by the updated (Darnall et al. 1978, Atkinson et al. 1979) formula of Greiner (1970) (Figure II-6). Hence, contrary to previous structure-reactivity relationships (Greiner 1970, Darnall et al. 1978, Atkinson et al. 1979, Hendry and Kenley 1979, Heicklen 1981), the rate constant per secondary C-H bond is not constant.

These data show that a further level of sophistication is necessary to account more fully for the observed trend in the rate constants. A possible approach is analogous to the group additivity techniques used by Benson (1976) (i.e., to assume that the OH radical rate constant per $-CH_2-$ group depends on the neighboring groups). The OH radical rate constant per CH_3- group at room temperature can be derived only from the data for ethane, neopentane and 2,2,3,3-tetramethylbutane. While the rate constant per CH_3- group varies from ~1.4 x 10^{-13} cm^3 $molecule^{-1}$ sec^{-1} for ethane (Table II-4) to ~1.9 x 10^{-13} cm^3 $molecule^{-1}$ sec^{-1} for neopentane and 2,2,3,3-tetramethylbutane (Greiner 1970, Atkinson et al. 1982a), at the magnitude of the overall rate constants measured in this work, even a 50% change in this CH_3- group rate constant along the series of n-alkanes studied will have only a small effect on the $-CH_2-$ group rate constants derived below.

Thus for the n-alkanes, the overall rate constants k are given by:

$$\text{propane:}\quad k = 2k_a + k_b \qquad \text{(VII)}$$

$$\text{n-butane through n-decane:}\quad k = 2k_a + 2k_c + (n-4)k_d \qquad \text{(VIII)}$$

where k_a is the rate constant per CH_3- group, k_b, k_c and k_d are the rate constants per $-CH_2-$ group bonded to two CH_3- groups, to one $-CH_2-$ and one $-CH_3$ group, and to two $-CH_2-$ groups, respectively, and n is the number of

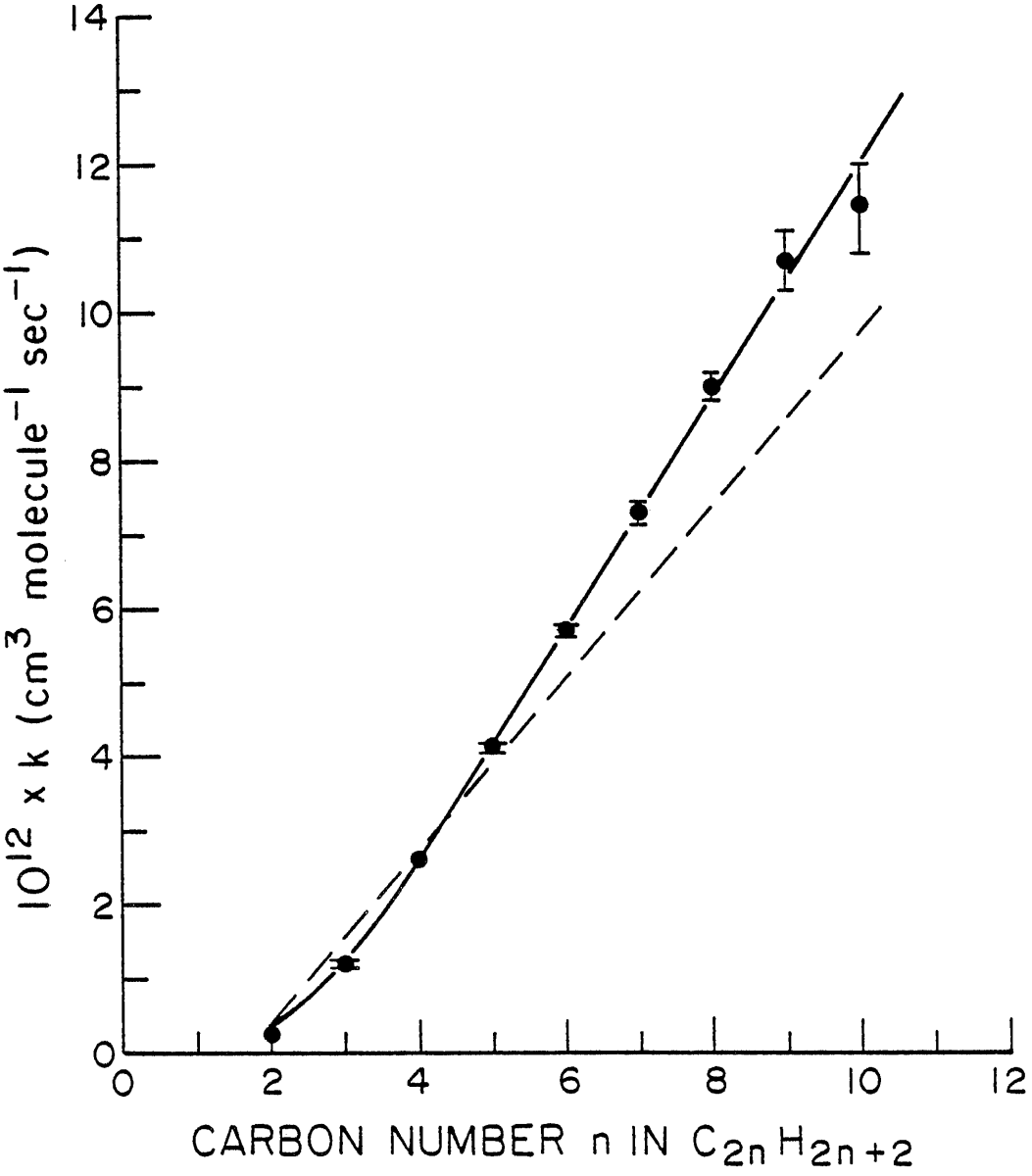

Figure II-6. Plot of the Rate Constant k Against the Carbon Number n in C_nH_{2n} + 2. --- Calculated from the Formula of Greiner (1970) as Updated (Darnall et al. 1978, Atkinson et al. 1979); —— Calculated from Equations (VII) and (VIII) with (x 10^{12} cm^3 $molecule^{-1}$ sec^{-1}): k_a = 0.19, k_b = 0.84, k_c = 1.10 and k_d = 1.57 (See Text).

carbon atoms in the n-alkane. Using k_a = 1.9 x 10^{-13} cm^3 $molecule^{-1}$ sec^{-1} at 299 ± 2 K, the present data for propane and n-butane yield k_b = 8.4 x 10^{-13} cm^3 $molecule^{-1}$ sec^{-1} and k_c = 1.10 x 10^{-12} cm^3 $molecule^{-1}$ sec^{-1}. With these values of k_a and k_c, the rate constants for n-pentane through n-decane then yield values of k_d (x 10^{12} cm^3 $molecule^{-1}$ sec^{-1}) of: 1.55 ± 0.08 for n-pentane, 1.56 ± 0.05 for n-hexane, 1.57 ± 0.06 for n-heptane, 1.61 ± 0.05 for n-octane, 1.62 ± 0.08 for n-nonane and 1.47 ± 0.10 for n-decane. Hence for this series of n-alkanes, k_d is, within the experimental error limits, reasonably constant, with a weighted average value of 1.57 x 10^{-12} cm^3 $molecule^{-1}$ sec^{-1}.

As shown in Figure II-6, the present approach yields a much better fit to the data than does the previous formula derived by Greiner (1970) as updated by Darnall et al. (1978) and Atkinson et al. (1979). However, the extra detail involved necessitates a much larger and more accurate data base than presently exists, or is likely to exist in the near future, before this approach can be extended to -CH< groups or to different substituents.

Alkyl Nitrates. Irradiations of CH_3ONO-NO-cyclohexane-alkyl nitrate-air mixtures were carried out at 299 ± 2 K. Four different alkyl nitrate mixtures, chosen to avoid interferences in the gas chromatographic analyses, were irradiated: 2-propyl nitrate, 2-butyl + 2-pentyl + 3-pentyl nitrates, 1-butyl + 2-hexyl + 3-hexyl nitrates and 3-heptyl + 3-octyl nitrates. In order to vary the OH radical concentration, duplicate irradiations were carried out with varying initial CH_3ONO concentrations.

Plots of equation (V) are shown in Figures II-7 through II-9, and the rate constant ratios k_1/k_2 and intercepts (k_3 + k_4) obtained by least squares analyses of these plots are given in Table II-5. As can be seen from these plots, the data for 3-octyl nitrate show a significant amount of scatter. This is almost certainly due to the increasing difficulty of precisely analyzing high molecular weight organic nitrates, and/or wall adsorption of this nitrate. The larger scatter in the data for the 3-pentyl and 3-hexyl nitrates relative to the 2-isomers is due to the fact that these nitrates occurred as impurities (~15-30%) in the 2-isomers, their lower concentrations giving rise to greater uncertainties in the disappearance rates.

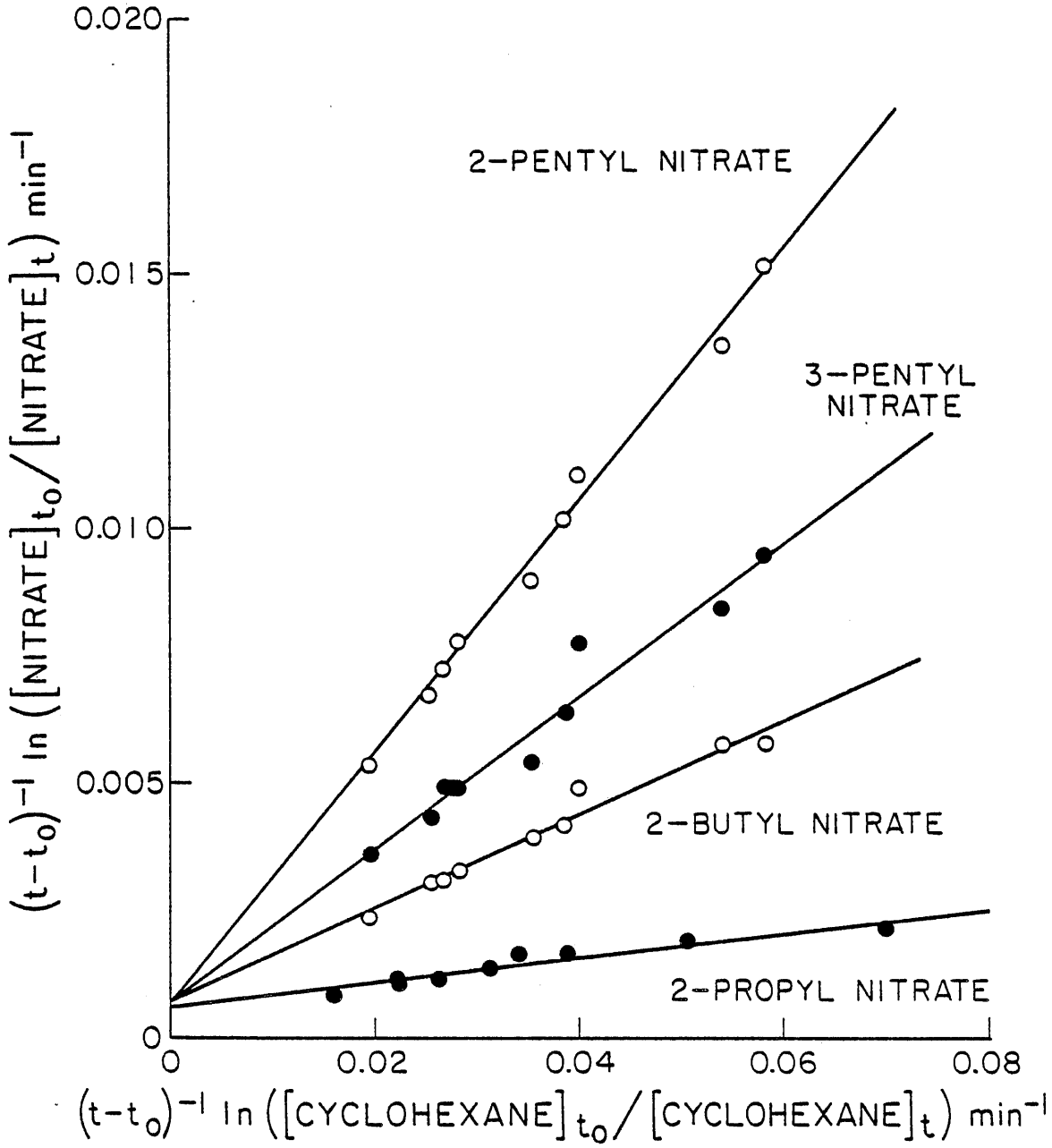

Figure II-7. Plots of Equation (V) for 2-Propyl, 2-Butyl, 2-Pentyl and 3-Pentyl Nitrates.

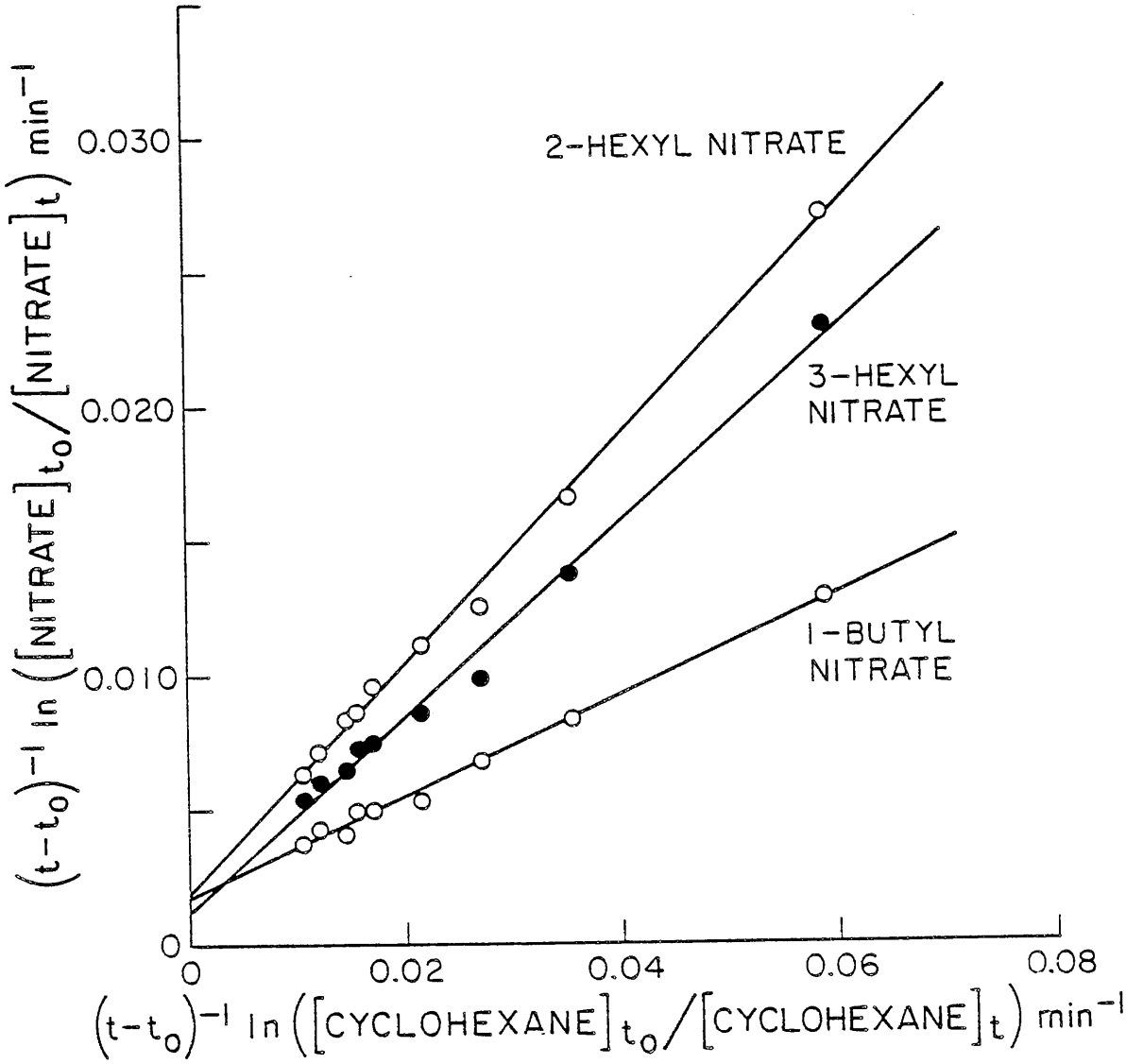

Figure II-8. Plots of Equation (V) for 1-Butyl, 2-Hexyl and 3-Hexyl Nitrates.

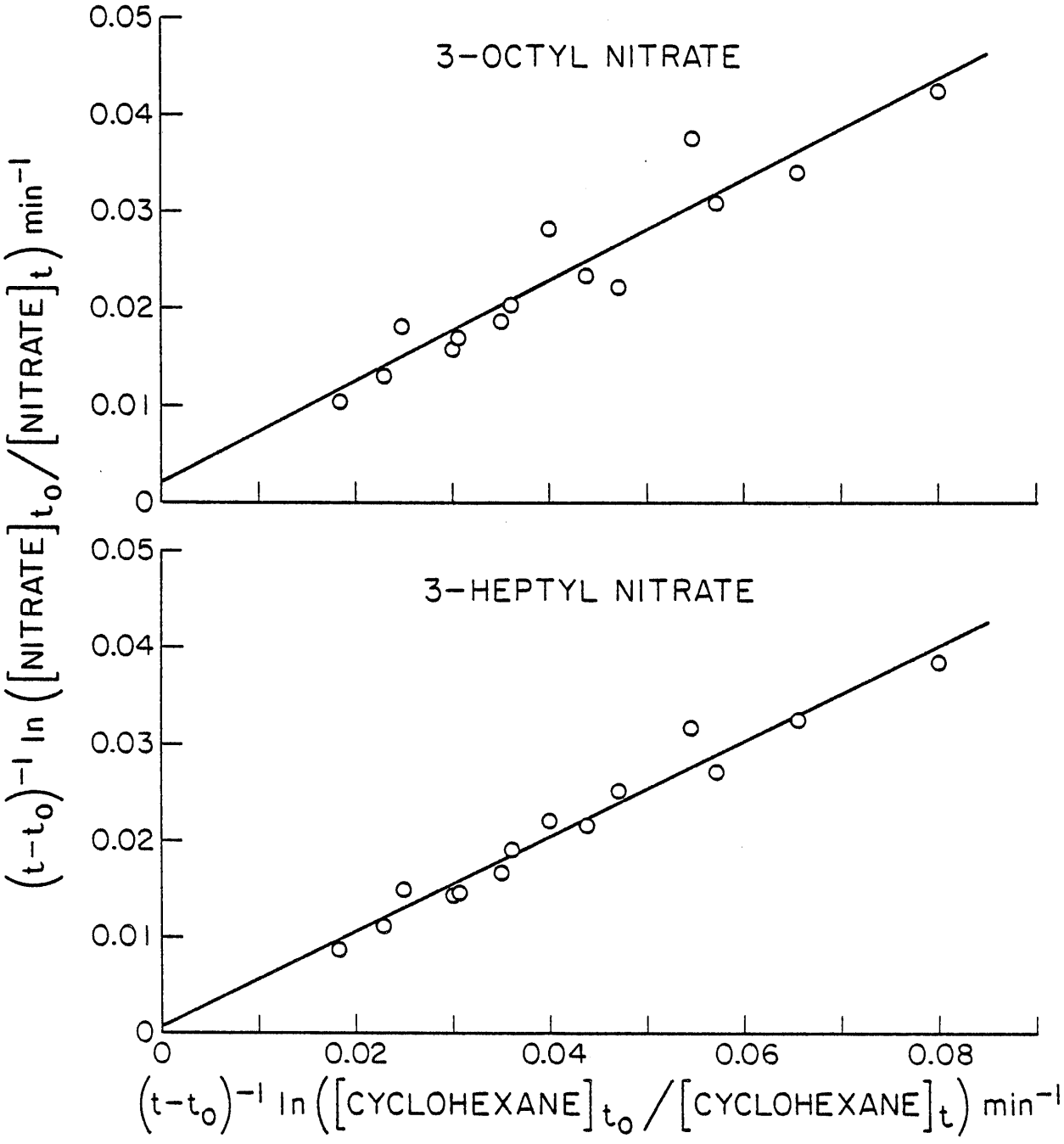

Figure II-9. Plots of Equation (V) for 3-Heptyl and 3-Octyl Nitrates.

Table II-5. Rate Constant Ratios k_1/k_2 and Intercepts k_3

Alkyl Nitrate	k_1/k_2[a]	$10^5 \times (k_3 + k_4)(sec^{-1})$[a]
2-Propyl	0.024 ± 0.006	1.0 ± 0.4
1-Butyl	0.187 ± 0.014	2.9 ± 0.7[b]
2-Butyl	0.091 ± 0.013	1.3 ± 0.8
2-Pentyl	0.247 ± 0.016	1.0 ± 1.0
3-Pentyl	0.149 ± 0.026	1.2 ± 1.7
2-Hexyl	0.422 ± 0.020	3.3 ± 0.9[b]
3-Hexyl	0.359 ± 0.028	2.1 ± 1.3[b]
3-Heptyl	0.491 ± 0.057	1.4 ± 4.3
3-Octyl	0.516 ± 0.105	3.6 ± 7.9

[a]Indicated errors are two standard deviations of the least squares analyses of the plots of equation (V) shown in Figures II-7 through II-9.

[b]One-third light intensity.

Figures II-7 through II-9 show that the data are, within the experimental scatter, in accord with equation (V). It can be seen that these plots have non-zero intercepts ($k_3 + k_4$), which indicates that photolysis and/or wall loss was occurring as well as OH radical reaction. The observation of larger intercepts at lower light intensities for the 1-butyl and 2- and 3-hexyl nitrates relative to the intercepts for the other nitrates makes it probable that this first-order loss rate was not primarily photolysis. Further experiments showed that these intercepts were affected if the Teflon reaction bag was changed, although the rate constant ratios k_1/k_2 remained constant within the experimental errors. This indicates that the first-order loss of nitrate was probably wall related. However, except for 2-propyl nitrate, this effect was small.

The rate constants k_1 were placed on an absolute basis using the value of $k_2 = 7.57 \times 10^{-12}$ cm^3 $molecule^{-1}$ sec^{-1} determined (Atkinson et al. 1982a) for the reaction of OH radicals with cyclohexane (which in turn is based on a rate constant for the reaction of OH radicals with n-butane of 2.58×10^{-12} cm^3 $molecule^{-1}$ sec^{-1} at 299 ± 2 K (Atkinson et al. 1982a), and are given in Table II-6. There are no other reported values for these

Table II-6. Rate Constants k_1 for the Reaction of OH Radicals with Alkyl Nitrates at 299 ± 2 K

Alkyl Nitrate	$10^{12} \times k_1$ (cm^3 $molecule^{-1}$ sec^{-1})		
	Observed[a]	Calculated[b]	Parent Alkane[c]
2-Propyl	0.18 ± 0.05[d]	0.18	1.22
1-Butyl	1.42 ± 0.11[e]	1.42	2.58
2-Butyl	0.69 ± 0.10[f]	0.67	2.58
2-Pentyl	1.87 ± 0.12[g]	1.77	4.13
3-Pentyl	1.13 ± 0.20[f]	1.16	4.13
2-Hexyl	3.19 ± 0.16	3.34	5.70
3-Hexyl	2.72 ± 0.22[g]	2.26	5.70
3-Heptyl	3.72 ± 0.43[g]	3.83	7.30
3-Octyl	3.91 ± 0.80	5.40	9.01

[a]Placed on an absolute basis using $k_2 = 7.57 \times 10^{-12}$ cm^3 $molecule^{-1}$ sec^{-1} (Atkinson et al. 1982a). The indicated error limits are two standard deviations.

[b]See text.

[c]From Table II-3.

[d]Used exclusively to derive the partial rate constant for $CH_3(CHONO_2)$.

[e]Used exclusively to derive the partial rate constant for $CH_2(CH_2)(CH_2ONO_2)$.

[f]Used in part to derive the partial rate constant for $CH_2(CH_3)(CHONO_2)$.

[g]Used in part to derive the partial rate constant for $CH_2(CH_2)(CHONO_2)$.

rate constants, and the corresponding OH radical rate constants for the parent alkanes are also shown in Table II-6 for comparison. It can be seen that the presence of the nitrate group decreases the overall OH radical rate constant by factors ranging from ~1.8 to >6, indicating that the nitrate group decreases the reactivity of neighboring C-H bonds towards reaction with the OH radical.

In the study of the kinetics of OH radical reactions with a series of n-alkanes, we have shown that the overall rate constants can be estimated from the number of $-CH_3$ and $-CH_2-$ groups, but that the rate constant per $-CH_2-$ group depends on the neighboring groups. As detailed above for the

C_3 through C_{10} n-alkanes, the following group rate constants (in units of 10^{-12} cm^3 $molecule^{-1}$ sec^{-1}) were derived: $CH_3(CH_2)$, 0.19; $CH_2(CH_3)_2$, 0.84; $CH_2(CH_2)(CH_3)$, 1.10 and $CH_2(CH_3)_2$, 1.57 (where, for example, the notation $CH_2(CH_2)(CH_3)$ refers to a $-CH_2-$ group bonded to one $-CH_3$ and one $-CH_2-$ group). This approach can in principle be extended to the alkyl nitrates by also considering the effects of $-ONO_2$, $-CH_2ONO_2$ and $-CHONO_2-$ neighboring groups.

Although the present data base is inadequate to unambiguously derive rate constants for all of the groups present in the alkyl nitrates studied, some estimations of these can be made. The fact that the rate constant for 2-propyl nitrate is approximately half that predicted on the basis of the $CH_3(CH_2)$ group rate constants alone suggests that the hydrogen atom bonded to the same carbon as the nitrate group has a very low reactivity towards OH radical reaction. If this is assumed to be the case (i.e., that $k[OH + CHONO_2(CH_3)_2]$ is negligible), then from the data for 2-propyl nitrate,

$$k[OH + CH_3(CHONO_2)] = 0.09 \times 10^{-12} \text{ cm}^3 \text{ molecule}^{-1} \text{ sec}^{-1}$$

which can be compared to a value of 0.19×10^{-12} cm^3 $molecule^{-1}$ sec^{-1} for the $CH_3(CH_2)$ group rate constant in the n-alkanes. Using this $CH_3(CHONO_2)$ value and the rate constant data for the 2-butyl and 2-pentyl nitrates, and assuming that the $CH_3(CH_2)$ and $CH_2(CH_2)(CH_3)$ group rate constants are the same as in the n-alkanes, then

$$k[OH + CH_2(CH_3)(CHONO_2)] = (0.39 \pm 0.01) \times 10^{-12} \text{ cm}^3 \text{ molecule}^{-1} \text{ sec}^{-1}$$

where the error reflects the difference between the values derived from 2-butyl or 3-pentyl nitrate. In an analogous manner, assuming that the $CHONO_2(CH_2)(CH_3)$ and $CHONO_2(CH_2)_2$ group rate constants are, as for the $CHONO_2(CH_3)_2$ group, also negligible, a rate constant for the $CH_2(CH_2)(CHONO_2)$ group can be derived from the rate constant data for the 2-pentyl, 3-hexyl, 3-heptyl and 3-octyl nitrates. In this case, the values of $k[OH + CH_2(CHONO_2)]$ are more variable, but indicate that

$$k[OH + CH_2(CH_2)(CHONO_2)] = k[OH + CH_2(CH_3)(CHONO_2)]$$

to within the uncertainties of the data. Finally, from the above group of rate constants and the 1-butyl nitrate OH radical rate constant, the value $k[OH + CH_2(CH_2)(CH_2ONO_2)] \approx 0.13 \times 10^{-12}$ cm^3 molecule^{-1} sec^{-1} can be derived.

Table II also gives the calculated overall OH radical rate constants k_1 using these group rate constants. It can be seen that, except for 3-octyl nitrate, for which the measured rate constant is significantly lower than that calculated, the derived partial rate constants and the overall rate constants are consistent, to within the experimental uncertainties. The discrepancy for 3-octyl nitrate may be due to experimental problems associated with gas phase studies of less volatile, higher molecular weight compounds.

Thus the present data allow a priori estimates to be made of the OH radical reaction rate constants for other simple primary and secondary alkyl nitrates, which are formed from the NO_x-air photooxidations of n-alkanes. These estimates are used to correct the observed alkyl nitrate yields in Section II.C below for secondary reactions.

C. Alkyl Nitrate Yields from the NO_x-Air Photooxidations of C_2 through C_8 n-Alkanes

Alkyl nitrate yields have been determined for the NO_x-air photooxidations of the C_2 through C_8 n-alkane series, and the importance of the nitrate-forming reaction (5), relative to the competing radical chain propagating and NO_x-conserving reaction of alkyl peroxy radicals with NO (reaction 6)

$$RO_2 + NO \rightarrow RONO_2 \qquad (5)$$

$$RO_2 + NO \rightarrow RO + NO_2 \qquad (6)$$

has been quantitatively determined, allowing its dependence on alkane chain length to be better understood.

Experimental

Two chemical systems were used to form RO_2 radicals in the presence of NO. The first consisted of photolysis at $\geq$290 nm of methyl nitrite-NO-

n-alkane mixtures in ultra-zero air, with typical initial reactant concentrations being CH_3ONO ~0.7-1.7 ppm, NO ~0.5-1.7 ppm and n-alkane ~1.0 ppm. One irradiation of this system was also carried out with ~1 ppm of NO_2 included in the reaction mixture. The other chemical system used consisted of the photolysis of Cl_2-NO-n-alkane mixtures in ultra-zero air, with typical initial reactant concentrations being Cl_2 ~1.0 ppm, NO ~0.6 ppm and n-alkane ~1.0 ppm.

The irradiations were carried out in ~75-ℓ FEP Teflon cylindrical reaction chambers surrounded by 24 GE F15T8-BL 15-W blacklights. For the irradiations carried out in this study, one-third of the maximum light intensity was employed, corresponding to photolysis half-lives of ~30 min for methyl nitrite and ~20 min for Cl_2. All irradiations were carried out at 299 ± 2 K and ~735 torr total pressure.

Nitric oxide, total NO_x, the n-alkane reactants and the alkyl nitrate products were quantitatively monitored prior to and during the irradiations. Nitric oxide and NO_x were monitored using a Columbia Industries, Inc., Model 1600 chemiluminescence analyzer and the organics were analyzed by gas chromatography with flame ionization detection (GC-FID). The alkanes n-butane through n-octane were analyzed using a 20-ft x 1/8-in stainless steel (SS) column with 5% DC703/C20M on 100/120 mesh AW, DMCS Chromosorb G, operated at 333 K, while propane was analyzed using a 36-ft x 1/8-in SS column of 10% 2,4-dimethylsulfolane (DMS) on C-22 Firebrick (60/80 mesh) operated at 273 K. No sample preconcentration was required for the analyses of these n-alkanes. The alkyl nitrates were analyzed using a 10-ft x 1/8-in SS column of 10% Carbowax 600 on C-22 Firebrick (100/110 mesh), operated at 348 K, for the propyl, butyl and pentyl nitrates, and a 5-ft x 1/8-in SS column of 5% Carbowax 600 on C-22 Firebrick (100/110 mesh) operated at 348 K for the hexyl, heptyl and octyl nitrates. For these analyses, 100 cm^3 of gas sample was preconcentrated in a ~1 cm^3 SS loop at liquid argon temperature prior to injection onto the column.

Gas chromatographic (GC) calibrations and retention times were determined for all of the individual n-alkanes studied and for 1-propyl, 2-propyl, 1-butyl, 2-butyl, 2-pentyl, 3-pentyl, 2-hexyl, 3-hexyl, 3-heptyl and 3-octyl nitrates. For the 2-heptyl, 4-heptyl, 2-octyl and 4-octyl nitrates, the retention times were determined from the GC positions of

peaks due to minor levels of these isomers in the authentic 3-heptyl and 3-octyl nitrate samples. The GC calibration factors were derived for these isomers by assuming that the GC-FID response was constant for all the heptyl nitrates, and similarly for the octyl nitrates. The alkyl nitrates were obtained as described above in Section II.B. Methyl nitrite was prepared and purified as also described above. For the other reactants, commercial samples (>98% stated purity level) were used without further purification.

For the experiments involving methyl nitrite photolysis, the irradiations were of ~30- to 60-min duration. For experiments involving Cl_2, which were more of a confirmatory nature (see below), because of the higher photolysis rate of Cl_2 (yielding two Cl atoms per Cl_2 photolyzed, and hence of production of alkyl peroxy radicals), several 1-, 2- or 5-min irradiations of the same mixture were carried out during each experiment, with GC analyses being conducted at the end of each irradiation period.

Results

The initial reactant concentrations and the observed amounts of n-alkane consumed and alkyl nitrate formed, as measured at various times during the irradiations, are given in Tables II-7 through II-12 for the CH_3ONO-NO-alkane-air irradiations and in Table II-13 for the Cl_2-NO-alkane-air runs. It can be seen from these tables that alkyl nitrate formation was observed without any apparent induction period and that it increased linearly with the amount of n-alkane consumed. One CH_3ONO-NO-n-butane-n-octane-air irradiation was carried out with 1 ppm of NO_2 also initially present. The results showed that the presence of NO_2 had no significant effect on the alkyl nitrate yields or isomeric ratios (see Tables II-8 and II-12, run 9-10).

The isomeric distribution of the 2- and 3-alkyl nitrates formed in the Cl_2-NO-n-alkane-air photolysis system were not significantly different from those in the methyl nitrite photolysis system for the n-pentane and n-hexane systems, but for propane and n-butane the observed ratios of [1-alkyl nitrate]/[2-alkyl nitrate] were significantly higher than those observed in the methyl nitrite system. These results are discussed in more detail in the following section.

Table II-7. Experimental Data for CH_3ONO-NO-Propane-Air Irradiations[a]

Run Number	Initial Concentration (ppb)			-Δ[Propane] (ppb)	Nitrate Yields (ppb)		
	CH_3ONO	NO	Propane		1-Propyl	2-Propyl	Total
9-11A	1400	664	959	123	0.6	3.6	4.2
				140	1.3	4.2	5.5
				166	0.8	4.6	5.4
9-11B	1400	555	1037	78	0.5	2.4	2.9
			137	1.0	4.0	5.0	
			159	1.1	4.8	5.9	
			185	1.1	5.6	6.7	

[a]Corrections for secondary reactions of propyl nitrates with OH radicals are negligible ($\lesssim$0.1 ppb) at the propyl nitrate concentrations observed.

Table II-8. Experimental Data from CH_3ONO-NO-n-Butane-Air Irradiations

Run Number	Initial Concentration (ppb)			Δ[n-Butane]	Nitrate Yields (ppb)				
					1-Butyl		2-Butyl		Total
	CH_3ONO	NO	n-Butane (ppb)	Obs	Obs	Corr[a]	Obs	Corr[a]	Corr[a]
9-8A	900	685	1012	129	0.8	0.8	10.3	10.5	11.3
				186	0.0	0.0	14.0	14.4	14.4
				223	0.8	0.0	15.5	16.0	16.0
9-8B	900	720	1034	134	0.0	0.0	10.0	10.2	10.2
				193	1.6	1.7	14.0	14.4	16.1
				236	0.0	0.0	16.7	17.3	17.3
9-9	700	680	1004	111	0.0	0.0	7.0	7.1	7.1
				160	0.3	0.3	10.4	10.7	11.0
				191	1.1	1.2	12.8	13.2	14.4
9-10[b]	900	875	889	36	0.0	0.0	2.0	2.0	2.0
				67	0.8	0.8	3.8	3.8	4.6
				87	1.4	1.4	4.2	4.3	5.6

[a]Corrected for subsequent reactions of alkyl nitrates with OH radicals (see text).

[b]1 ppm NO_2 also initially present.

Table II-9. Experimental Data for the CH_3ONO-NO-n-Pentane-Air Irradiations

Run Number	Initial Concentration (ppb)			Δ[n-Pentane]	Nitrate Yields (ppb)				
					2-Pentyl		3-Pentyl		Total
	CH_3ONO	NO	n-Pentane (ppb)	Obs	Obs	Corr[a]	Obs	Corr[a]	Corr[a]
9-6A	1100	1510	1358	178	12.1	12.5	8.1	8.2	20.7
				263	15.4	16.2	12.0	12.4	28.6
				318	22.2	23.6	15.1	15.7	39.3
9-7A	1000	648	1378	193	12.8	13.2	8.6	8.8	22.0
				276	18.0	19.0	12.4	12.8	31.8
				332	21.9	23.4	13.5	14.0	37.4
7-7B	1100	680	1218	141	9.0	9.3	5.8	5.9	15.2
				202	11.2	11.7	7.8	8.0	19.7
				234	14.0	14.7	9.6	9.9	24.6

[a]Corrected for reactions of the alkyl nitrates with OH radicals (see text).

Table II-10. Experimental Data for CH_3ONO-NO-n-Hexane-Air Irradiations

Run Number	Initial Concentration (ppb)			Δ[n-Hexane]	Nitrate Yields (ppb)				
					2-Hexyl		3-Hexyl		Total
	CH_3ONO	NO	n-Hexane (ppb)	Obs	Obs	Corr[a]	Obs	Corr[a]	Corr[a]
9-5A	900	1450	1133	118	9.5	9.8	12.6	12.9	22.7
				183	16.6	17.4	21.8	22.7	40.1
				229	17.5	18.7	22.7	23.9	42.6
				262	24.0	25.8	33.3	35.4	61.2
9-5B	900	830	1065	137	11.6	12.1	14.9	15.4	27.5
				203	16.5	17.5	22.2	23.3	40.8
				251	18.5	20.0	25.9	27.6	47.6
				284	21.4	23.4	30.7	33.1	56.5
9-7B	1100	680	1043	153	16.1	16.9	-[b]	-	-
				217	17.8	19.0	25.7	27.1	46.1
				252	21.0	22.7	27.8	29.7	52.4

[a]Corrected for reactions of the alkyl nitrates with OH radicals (see text).

[b]Peak offscale on gas chromatograph, not quantified.

Table II-11. Experimental Data for CH_3ONO-NO-n-Heptane-Air Irradiations

Run No.	Initial Conc (ppb)			Δ[n-Heptane] (ppb)	Nitrate Yields (ppb)						Total (Corr)[a]
					2-Heptyl		3-Heptyl		4-Heptyl		
	CH_3ONO	NO	n-Heptane		Obs	Corr[a]	Obs	Corr[a]	Obs	Corr[a]	
9-1A	1200	~1700	1313	175	15.6	16.3	20.4	21.2	9.4	9.7	47.2
				261	27.2	29.4	36.8	39.2	17.0	17.9	86.5
				280	28.5	30.9	37.0	39.6	16.0	16.9	87.4
				360	30.1	33.6	44.5	48.7	19.9	21.5	103.8
9-1B	1250	~1700	1335	114	8.8	9.1	11.5	11.8	5.3	5.4	26.3
				206	18.6	19.7	27.4	28.7	12.8	13.3	61.7
				273	25.3	27.3	32.5	34.6	14.4	15.2	77.1
				324	26.0	28.6	34.6	37.4	20.3	21.7	87.7
9-3A	1650	1730	1230	185	15.2	16.1	19.6	20.5	9.5	9.8	46.4
				261	22.2	24.1	31.8	34.0	14.4	15.2	73.3
				323	23.4	26.0	32.3	35.2	14.9	16.0	77.2
9-3B	1200	802	1361	120	8.0	8.3	10.8	11.1	5.1	5.2	24.6
				201	14.3	15.1	19.8	20.8	9.2	9.5	45.4
				255	19.7	21.2	30.1	32.0	12.7	13.3	66.5

[a]Corrected for reactions of alkyl nitrates with OH radicals (see text).

Table II-12. Experimental Data for CH_3ONO-NO-n-Octane-Air Irradiations

Run No.	Initial Conc (ppb)			Δ[n-Octane] (ppb)	Nitrate Yields (ppb)						
					2-Octyl		3-Octyl		4-Octyl		Total (Corr)[a]
	CH_3ONO	NO	n-Octane		Obs	Corr[a]	Obs	Corr[a]	Obs	Corr[a]	
9-2A	1200	~1700	1361	282	20.6	22.5	30.7	33.0	28.9	30.9	86.4
				406	29.7	34.0	42.5	47.5	39.2	43.4	124.9
				476	35.4	41.7	50.6	57.9	47.1	53.4	153.0
9-2B	1000	~1700	1320	136	11.5	12.0	17.2	17.8	15.8	16.3	46.1
				284	21.9	24.0	33.9	36.6	32.0	34.4	95.0
				355	25.6	28.8	37.2	41.0	35.6	38.9	108.7
				412	30.4	35.0	45.2	50.8	42.8	47.6	133.4
9-3A	1650	1730	1321	236	18.9	20.3	27.3	29.0	27.9	29.5	78.8
				337	25.4	28.4	35.4	38.8	35.0	38.2	105.4
				395	31.4	35.9	43.1	48.2	41.2	45.6	129.7
9-3B	1200	802	1385	152	11.7	12.2	15.8	16.4	14.0	14.5	43.1
				253	17.8	19.2	23.0	24.4	21.8	23.1	66.7
				317	20.6	22.7	30.0	32.5	30.2	32.6	87.8
9-10[b]	900	875	1001	119	10.0	10.5	15.1	15.7	14.0	14.5	40.7
				196	14.4	15.7	21.3	22.8	18.9	20.2	58.7
				249	16.5	18.4	22.2	24.3	19.3	21.0	63.7

[a]Corrected for reactions of alkyl nitrates with OH radicals (see text).
[b]~1 ppm NO_2 initially added to mixture.

Table II-13. Experimental Data for Cl_2-NO-n-Alkane-Air Irradiations

Run No.	n-Alkane	Initial Conc (ppb)			-Δ[n-Alkane] (ppb)	Nitrate Yields (ppb)				
		Cl_2	NO	n-Alkane		1-Alkyl	2-Alkyl	3-Alkyl	Total Obs	Total Corr[a]
9-15	Ethane	~1000	690	1244	32	0.4			0.4	0.4
					101	1.3			1.3	1.4
					184	1.9			1.9	2.1
9-15	Propane	~1000	690	997	70	0.5	1.5		2.0	2.1
					195	1.5	3.9		5.4	6.0
					292	1.8	5.0		6.8	8.2
9-13B	n-Butane	~1000	640	836	85	0.4	5.4		5.8	6.1
					146	1.5	9.3		10.8	11.9
					194	2.4	12.1		14.5	16.5
9-13A	n-Pentane	~1000	610	968	41		3.4	2.1	5.5	5.6
					120		9.1	5.6	14.7	15.7
					164		12.1	7.8	19.9	21.9
9-16A	n-Hexane	~1000	621	968	125		9.8	11.7	21.5	23.1
					201		14.7	17.0	31.7	35.9
9-16B	n-Hexane	~1000	640	946	57		3.5	3.7	7.2	7.4
					148		10.3	11.0	21.7	23.7
					179		15.8	17.8	33.6	37.3

[a]Corrected assuming that alkyl nitrates react as fast with Cl atoms as do the parent alkanes (see text).

Discussion

Methyl Nitrite Photolysis System. The major reactions occurring in the CH_3ONO-NO-n-alkane-air photolysis system can be represented as follows (Atkinson and Lloyd 1983)

$$CH_3ONO + h\nu \rightarrow CH_3O + NO \quad (7)$$

$$CH_3O + O_2 \rightarrow HCHO + HO_2 \quad (8)$$

$$HO_2 + NO \rightarrow OH + NO_2 \quad (9)$$

$$OH + RH \rightarrow R + H_2O \quad (10)$$

$$R + O_2 \xrightarrow{M} RO_2 \quad (11)$$

$$RO_2 + NO \xrightarrow{M} RONO_2 \quad (5)$$

$$RO_2 + NO \rightarrow RO + NO_2 \quad (6)$$

$$RO + NO_2 \xrightarrow{M} RONO_2 \quad (12)$$

$$RO \xrightarrow{\substack{O_2 \\ NO \\ NO_2}} OH + \text{oxygenated products} \quad (13)$$

$$RONO_2 + OH \rightarrow \text{products} \quad (14)$$

In this system, the n-alkane and the alkyl nitrates are consumed essentially solely by reaction with OH radicals (reactions 10 and 14). Reaction with NO, forming either the corresponding alkyl nitrate (reaction 5) or the alkoxy radical (reaction 6), is the only significant sink for the alkyl peroxy radicals formed from the reaction of OH radicals with the n-alkanes, since the reactions of alkyl peroxy radicals with NO_2 forming alkyl peroxy nitrates

$$RO_2 + NO_2 \underset{(-15)}{\overset{(15)}{\rightleftharpoons}} RO_2NO_2 \quad (15)$$

are insignificant due to the rapid back-decomposition of the alkyl peroxy nitrates (Carter et al. 1979a, Edney et al. 1979, Hendry and Kenley 1979, Bahta et al. 1982).

In this system the formation of alkyl nitrates can occur either from the reaction of alkyl peroxy radicals with NO (reaction 5) or from the reaction of alkoxy radicals with NO_2 (reaction 12). However, since alkoxy radicals can also react with O_2 (Barker et al. 1977, Baldwin et al. 1977, Batt 1979, 1980; Batt and Robinson 1979, Golden 1979, Cox et al. 1980, Gutman et al. 1982, Atkinson and Lloyd 1983), decompose (Baldwin et al. 1977, Batt 1979, 1980; Choo and Benson 1981, Atkinson and Lloyd 1983) or isomerize (Baldwin et al. 1977, Carter et al. 1976, Baldwin and Golden 1978, Niki et al. 1981, Atkinson and Lloyd 1983) to ultimately give rise to products other than alkyl nitrates [shown overall as reaction (13), above], a number of other reactions compete with alkyl nitrate formation from alkoxy radicals.

Upper limits for the contribution of reaction (12) to the observed alkyl nitrate yields for these experiments can be estimated from the rate constants for the reactions of alkoxy radicals with NO_2 and O_2, and the NO_2 and O_2 concentrations. Alkoxy radicals react with NO_2 with a rate constant of $k_1 \simeq 1.5 \times 10^{-11}$ cm^3 $molecule^{-1}$ sec^{-1} at room temperature and atmospheric pressure (Atkinson and Lloyd 1983). The reactions of alkoxy radicals with O_2 have received little direct attention, but recently Gutman et al. (1982) have determined a rate constant of 8×10^{-15} cm^3 $molecule^{-1}$ sec^{-1} at 296 K for the reaction

$$C_2H_5O + O_2 \rightarrow CH_3CHO + HO_2$$

Furthermore, from thermochemical considerations, Gutman et al. (1982) have derived rate constants at room temperature for the reaction of 1-alkoxy radicals with O_2 of $\sim 7 \times 10^{-15}$ cm^3 $molecule^{-1}$ sec^{-1}, with the 2-propoxy and 2-butoxy radicals reacting ~5 times faster. Hence, assuming a maximum of 2 ppm of NO_2 in these experiments (based on the total initial concentrations of nitrogen-containing species, e.g. NO and CH_3ONO, which can yield NO_2), and considering only the reactions of RO radicals with O_2 and NO_2, then a maximum yield of alkyl nitrate formation from the reaction of RO radicals with NO_2 of 2.0% can be calculated for 1-alkyl nitrates, with

yet lower maximum yields for the secondary alkyl nitrates. Since (a) all the initial nitrogenous species are not converted to NO_2 during NO_x-organic-air irradiations, (b) larger ($\geq C_4$) alkoxy radicals undergo significant decomposition and isomerization reactions (Gutman et al. 1982) and (c) the secondary alkoxy radicals undergo faster reaction with O_2, it may be concluded that <1% of the observed alkyl nitrate yields are due to the reaction of alkoxy radicals with NO_2 in the CH_3ONO-NO-n-alkane (propane through n-octane)-air irradiations carried out in this study. This is negligible for these n-alkanes.

The conclusion that alkyl nitrate yields from the RO + NO_2 reactions are minor is supported by the results of the experiment in which 1 ppm of NO_2 was also added to the initial CH_3ONO-NO-alkane-air mixture. The alkyl nitrate yields in this experiment were observed to be indistinguishable from those without added NO_2 (Tables II-8 and II-12). For the Cl atom-initiated systems (discussed in the following section), where NO_2 formation from CH_3ONO photolysis did not occur, alkyl nitrate formation from the RO + NO_2 reaction would be less significant still, and even for the ethane system would be $\leq$0.7%.

Thus it is clear that the major source of alkyl nitrates observed in the present experiments is from reaction (5), and that the observed alkyl nitrate yields should reflect the rate constant ratio $k_5/(k_5 + k_6) = \alpha$, since alkoxy radical formation (reaction 6) is the only significant process competing with reaction (5) in the alkane photooxidation chain. However, in order to derive α from the observed alkyl nitrate product yields, a correction must be made for the secondary reactions of the alkyl nitrates. This was carried out as indicated below.

We have shown above (Section II.B) that reaction with OH radicals is the major loss process for the alkyl nitrates and the alkanes under the conditions of these experiments. Therefore, the alkane and alkyl nitrate concentrations are governed by:

$$d[RH]/dt = -k_{10}[OH][RH] \qquad (IX)$$

$$d[RONO_2]/dt = \alpha\, k_{10}[OH][RH] - k_{14}[OH][RONO_2] \qquad (X)$$

where k_{10} and k_{14} are the rate constants for the reactions of OH radicals with the alkanes and the alkyl nitrates, respectively. Under conditions where the OH radical concentration is constant, these equations can be integrated to obtain:

$$[RH]_t = [RH]_o \, e^{-k_{10}[OH]t} \qquad (XI)$$

and

$$[RONO]_t = [RH]_o \, \frac{\alpha \, k_{10}}{(k_{10}-k_{14})} \left[e^{-k_{14}[OH]t} - e^{-k_{10}[OH]t} \right] \qquad (XII)$$

where $[RH]_o$ is the initial n-alkane concentration, [OH] is the constant hydroxyl radical concentration, and $[RH]_t$ and $[RONO_2]_t$ are the alkane and alkyl nitrate concentrations, respectively, at time t. Equations (XI) and (XII) can be combined to obtain

$$\alpha = F \left\{ \frac{[RONO_2]_t}{\Delta[RH]_t} \right\} \qquad (XIII)$$

where

$$F = \left(\frac{k_{10} - k_{14}}{k_{10}} \right) \left\{ \frac{1 - \left(\frac{[RH]_t}{[RH]_o} \right)}{\left(\frac{[RH]_t}{[RH]_o} \right)^{\frac{k_{14}}{k_{10}}} - \left(\frac{[RH]_t}{[RH]_o} \right)} \right\} \qquad (XIV)$$

and $\Delta[RH]_t = ([RH]_o - [RH]_t)$. Note that the correction factor F does not have any dependence on the OH radical concentration, and thus equation (XIV) might be expected to be valid even under conditions where [OH] is not constant throughout the experiment, as was the case for the irradiations carried out in this work. Computer simulations indeed showed that the use of these equations introduced a totally negligible error in accounting for the OH radical reactions with the alkyl nitrates.

Equations (XIII) and (XIV) were used to correct each of the data points for each alkyl nitrate isomer given in Tables II-7 through II-12. F was calculated using the experimentally observed amounts of n-alkanes

consumed and the values of k_{10} and k_{14} obtained from the kinetic studies described above (Section II.B). The largest correction corresponded to a value of F of 1.18 for the 2-octyl nitrate yield at 35% n-octane reacted (run 9-2A, Table II-12), and in most cases these corrections were relatively minor.

Plots of the total corrected alkyl nitrate yields against the amount of n-alkane reacted are shown in Figures II-10 and II-11 for the methyl nitrite photolysis runs. It can be seen that, consistent with our assumption that the alkyl nitrates are a primary product in the n-alkane photooxidations, in all cases straight line plots with zero intercepts (within one least square standard deviation) were obtained. Table II-14 lists the least squares slopes obtained from those plots, which can be identified with the fraction, α, of the n-alkane reacted yielding the observed alkyl nitrates.

Chlorine Photolysis System. The major reactions occurring in the Cl_2-NO-alkane-air irradiations can be represented as follows:

$$Cl_2 + h\nu \rightarrow 2\ Cl \tag{15}$$

$$Cl + NO_2 \rightarrow ClNO_2 \tag{16}$$

$$Cl + NO \underset{h\nu}{\overset{\rightarrow}{\leftarrow}} ClNO \tag{17}$$

$$Cl + RH \rightarrow HCl + R \tag{18}$$

$$OH + RH \rightarrow H_2O + R \tag{10}$$

$$R \xrightarrow{O_2,\ NO_x} \alpha'\ RONO_2 + (\text{oxygenated products}) + (1-\alpha')\ OH \tag{19}$$

$$RONO_2 + Cl \rightarrow \text{products} \tag{20}$$

$$RONO_2 + OH \rightarrow \text{products} \tag{14}$$

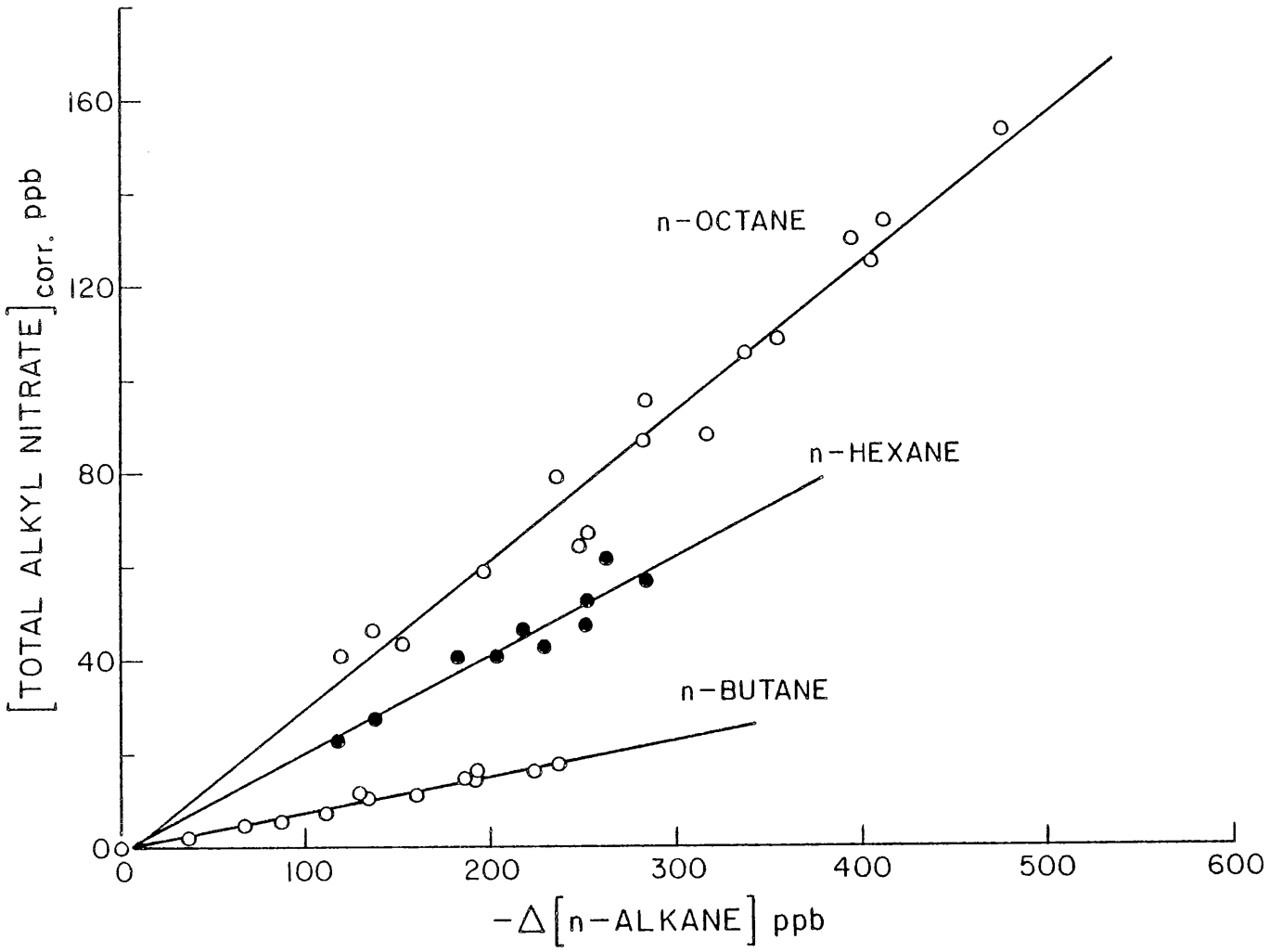

Figure II-10. Plots of Total Alkyl Nitrate Yields Observed in CH_3ONO-NO-n-Alkane-Air Irradiations, Corrected for Reaction with OH Radicals (See Text), Against the Amount of n-Alkane Consumed for n-Butane, n-Hexane and n-Octane.

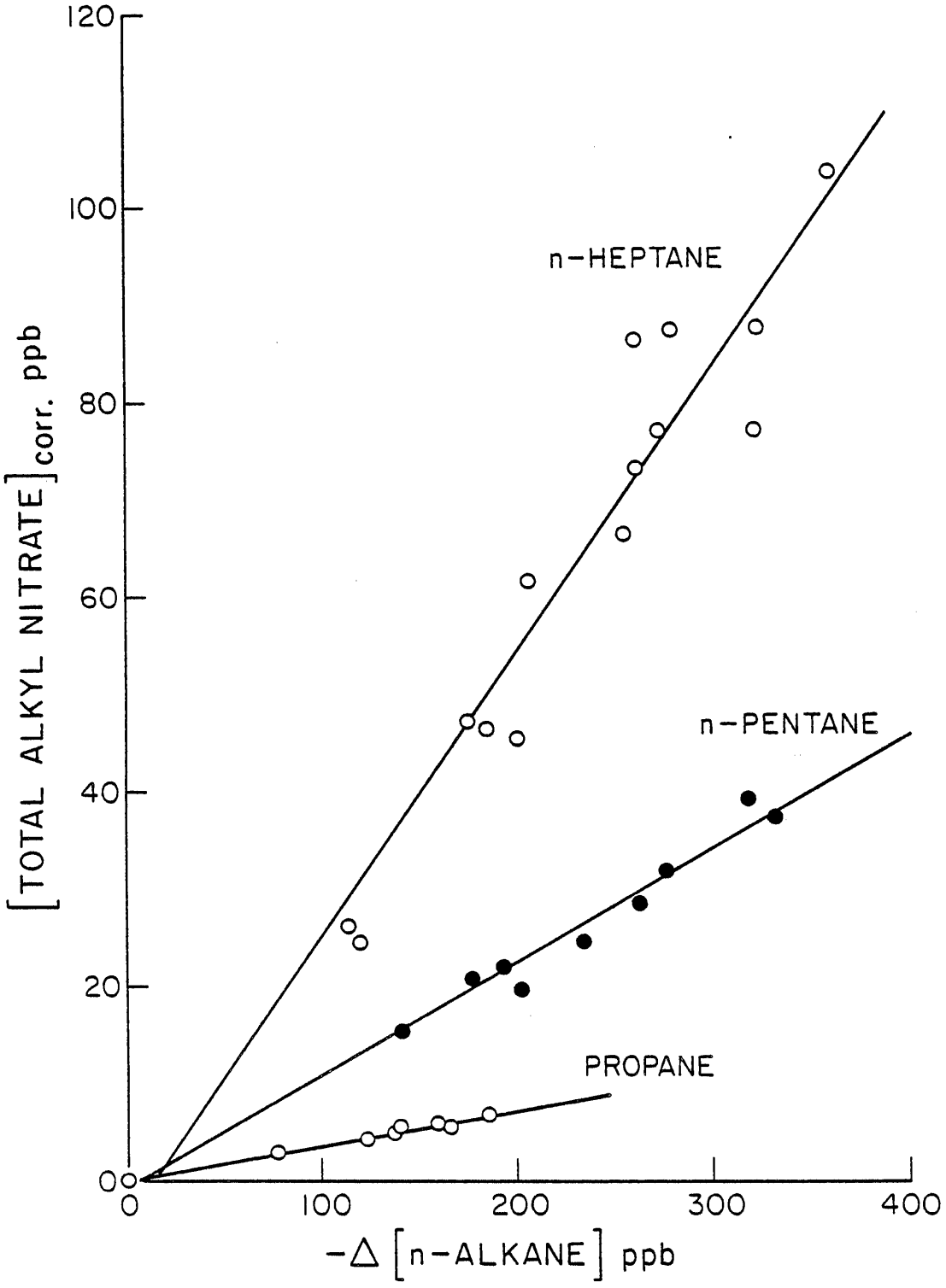

Figure II-11. Plots of Total Alkyl Nitrate Yields Observed in CH_3ONO-NO-n-Alkane-Air Irradiations, Corrected for Reaction with OH Radicals (for n-Pentane and n-Heptane, See Text), Against the Amount of n-Alkane Consumed for Propane, n-Pentane and n-Heptane.

Table II-14. Yields of Alkyl Nitrates, Relative to the n-Alkane Consumed in CH_3ONO-NO-n-Alkane-Air Irradiations

n-Alkane	$\frac{[\text{Total Alkyl Nitrate}]}{-\Delta[\text{n-Alkane}]}$ [a]
Propane	0.036 ± 0.005
n-Butane	0.077 ± 0.009
n-Pentane	0.117 ± 0.013, 0.129 ± 0.019 [b]
n-Hexane	0.208 ± 0.027, 0.223 ± 0.035 [b]
n-Heptane	0.293 ± 0.042, 0.309 ± 0.050 [b]
n-Octane	0.318 ± 0.027, 0.332 ± 0.034 [b]

[a] Obtained by least squares analyses of the data given in Tables II-7 through II-12 and shown in Figures II-10 and II-11. For n-pentane, n-hexane, n-heptane and n-octane, no gas chromatographic retention times were available for the 1-alkyl nitrates, hence the data for these n-alkanes are the sum of the yields of the 2-, 3- and, for n-heptane and n-octane, the 4-alkyl nitrates. The indicated error limits are two least squares standard deviations. Corrected for alkyl nitrate loss reaction with OH radicals (see text).

[b] Calculated to take into account 1-alkyl nitrate formation, based on the OH + n-alkane kinetic data described in Section II.B above. Error limits have been increased corresponding to a 50% uncertainty in these unobserved yields of 1-alkyl nitrate.

Note that OH radicals are generated in the NO_x-air photooxidation of the alkyl radicals formed by the reaction of Cl atoms with the alkanes, so the alkane is consumed by reaction with OH radicals as well as with Cl atoms. In reaction (19), α' represents the fractional alkyl nitrate yield in the Cl_2 photolysis system. Since, in general, a somewhat different ratio of the isomeric alkyl radicals is expected to be formed in reaction (18) than in reaction (10) (see following section), and it is possible that the different RO_2 isomers may have slightly different alkyl nitrate formation efficiencies, α' may not necessarily be the same as α, the fractional yield obtained when all of the alkane reacts with OH radicals.

Since the rate constants for the reaction of Cl atoms with alkyl nitrates are not known, and since the fraction of alkane or alkyl nitrate reaction with OH radicals versus Cl atoms is also not known, accurate

values of the correction factor to account for reactive loss processes of the alkyl nitrates cannot be calculated. However, an upper limit to this factor can be obtained by assuming that Cl atoms react with the alkyl nitrates no faster than they react with the parent alkanes. This assumption is likely to be valid, since the Cl atom reaction rates for the alkanes at room temperature are in the range $\sim 5 \times 10^{-11}$ cm^3 $molecule^{-1}$ sec^{-1} to $\sim 2 \times 10^{-10}$ cm^3 $molecule^{-1}$ sec^{-1} for the C_2 through C_4 alkanes (Lewis et al. 1980). With this assumption, and assuming no involvement of OH radicals, the correction factor would be 1.055 for 10% alkane reaction and 1.118 for 20% alkane reaction.

The total observed and corrected alkyl nitrate yields in the Cl_2-NO-n-alkane-air irradiations are listed for each data point in Table II-13 and plotted against the amount of n-alkane consumed in Figure II-12. The fractional alkyl nitrate yields from these systems, α', obtained from least squares slopes of the lines plotted in Figure II-12, are given in Table II-15. The corrected yield ratios for the observed alkyl nitrates in the Cl_2 photolysis experiments agreed with those in the CH_3ONO photolysis experiments to within ±15% for n-butane through n-hexane, and within ± 20% for propane. The Cl atom initiation system also enabled an upper limit to the alkyl nitrate yield to be obtained for the ethane system; this was not practical using CH_3ONO initiation since OH radicals react with ethane too slowly to yield an appreciable degree of reaction.

Isomeric Yield Ratios. Table II-16 gives the ratios of the isomeric yields of the alkyl nitrates observed in the CH_3ONO-NO-alkane-air irradiations, together with the expected ratios as calculated from the kinetic data described in Section II.B above, assuming the efficiency of alkyl nitrate formation is the same for each isomer formed from a given alkane. We showed in Section II.B above that the total OH radical rate constant for the n-alkanes propane through n-decane (at 299 ± 2 K) can be given by the sum of group rate constants (i.e., rate constants for each CH_3- group, for each -CH_2- bonded to two CH_3- groups, for each -CH_2- bonded to one -CH_3 and one -CH_2-, etc.), and the calculated ratios shown in Table II-16 are based on the reasonable assumption that these group rate constants actually reflect the rate of OH radical attack on the corresponding group.

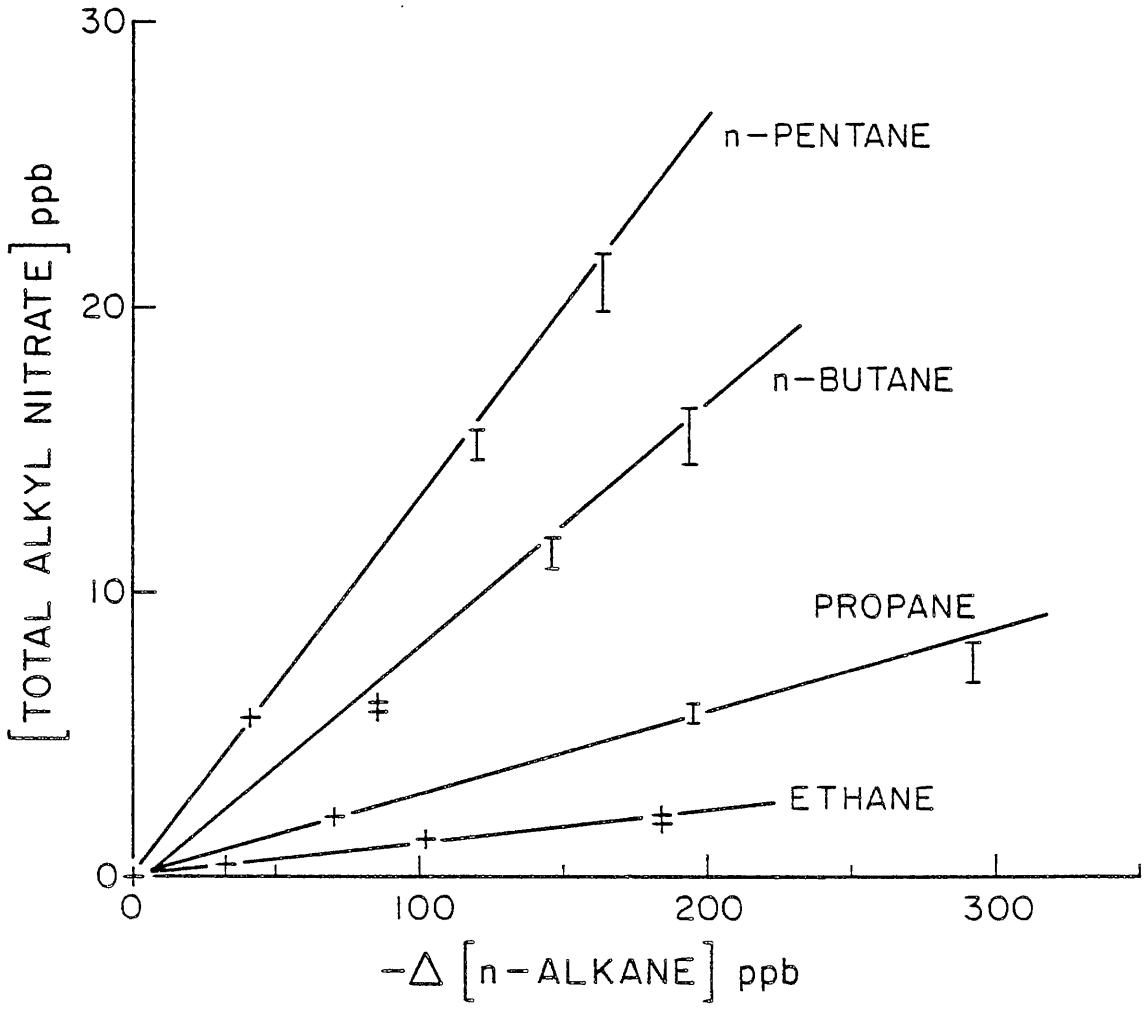

Figure II-12. Plots of Total Alkyl Nitrate Observed in Cl_2-NO-n-Alkane-Air Irradiations Against the Amount of n-Alkane Consumed for Ethane, Propane, n-Butane and n-Pentane. The Bottom Horizontal Bar of the Data Points is the Observed Yield, the Top Bar is that Assuming that the Alkyl Nitrates are Removed by Reaction with Rate Constants Equal to Those for Removal of the Parent n-Alkanes (See Text). The Lines Drawn are from the Least Squares Analyses of the Data Assuming that the Alkyl Nitrates React with Cl Atoms as Fast as do the Parent n-Alkanes.

Table II-15. Yields of Alkyl Nitrates Relative to the n-Alkane Consumed in Cl_2-NO-n-Alkane-Air Irradiations

n-Alkane	$\frac{[\text{Total Alkyl Nitrate}]}{-\Delta[\text{n-Alkane}]}$	
	Obs.[a]	Corr[b]
Ethane	0.010 ± 0.002	0.012 ± 0.002
Propane	0.024 ± 0.005	0.029 ± 0.003
n-Butane	0.075 ± 0.005	0.085 ± 0.009
n-Pentane	0.120 ± 0.005[c]	0.133 ± 0.004[c]
n-Hexane	0.171 ± 0.032[c]	0.193 ± 0.036[c]

[a]Based on observed yields.

[b]Ratio assuming that the alkyl nitrates are consumed as fast as are the n-alkanes in the experimental system employed.

[c]2- and 3-alkyl nitrates; due to unavailability of retention times for 1-alkyl nitrates, no data for these isomers obtained.

The observed isomeric alkyl nitrate ratios for the secondary alkyl nitrates in the CH_3ONO photolysis-initiated system are seen (Table II-16) to be in excellent agreement with those predicted from RO_2 formation yields from these n-alkane kinetic data (i.e., the alkyl nitrate ratios for the 2-, 3- and 4-alkyl nitrate isomers are in excellent agreement with the ratios of the 2-, 3- and 4- alkyl radical formation rates based on kinetic evidence). For propane and n-butane, however, the amounts of primary alkyl nitrate observed were approximately a factor of two lower than expected from kinetic results (though within the error limits for the butane system). This may reflect either a lower fraction of nitrate formation from RO_2 radicals for 1-alkyl peroxy radicals, as compared to 2-, 3- or 4- alkyl peroxy radicals, or a lower reactivity of primary C-H bonds towards OH radicals than presumed.

The data obtained in the Cl atom initiation system were not so extensive and were designed mainly for confirmation purposes. The alkyl nitrate isomeric ratios observed in this system are given in Table II-17. The [3-alkyl nitrate]/[2-alkyl nitrate] ratios observed for n-pentane and n-hexane are similar, though somewhat lower, than those in

Table II-16. Ratios of Alkyl Nitrate Isomers Formed During CH_3ONO-NO-n-Alkane-Air Irradiations, Compared with Ratios Calculated from Kinetic Data[a,b]

n-Alkane	[1-Alkyl Nitrate]/[2-Alkyl Nitrate] Observed[a]	[1-Alkyl Nitrate]/[2-Alkyl Nitrate] Calculated[b]	[3-Alkyl Nitrate]/[2-Alkyl Nitrate] Observed[a]	[3-Alkyl Nitrate]/[2-Alkyl Nitrate] Calculated[b]	[4-Alkyl Nitrate]/[2-Alkyl Nitrate] Observed[a]	[4-Alkyl Nitrate]/[2-Alkyl Nitrate] Calculated[b]
Propane	0.22 ± 0.10	0.45	-	-	-	-
n-Butane	0.07 ± 0.21	0.17	-	-	-	-
n-Pentane	c	0.17	0.67 ± 0.09	0.71	-	-
n-Hexane	c	0.17	1.34 ± 0.11	1.43	-	-
n-Heptane	c	0.17	1.35 ± 0.15	1.43	0.62 ± 0.10	0.71
n-Octane	c	0.17	1.41 ± 0.14	1.43	1.32 ± 0.18	1.43

[a]Observed alkyl nitrate yields corrected for reaction of alkyl nitrates with OH radicals (see text). Indicated error limits are two standard deviations.

[b]Calculated ratios from the kinetic data for the n-alkanes (Section II.B above).

[c]Not observed, no retention times available.

Table II-17. Ratios of Alkyl Nitrate Isomers Formed During Cl_2-NO-n-Alkane-Air Irradiations Compared with Ratios Calculated from Kinetic Data

n-Alkane	[1-Alkyl Nitrate]/[2-Alkyl Nitrate]		[3-Alkyl Nitrate]/[2-Alkyl Nitrate]
	Observed[a]	Calculated[b]	Observed[a]
Propane	0.36 ± 0.06	0.82	-
n-Butane	0.14 ± 0.13	0.40	-
n-Pentane	c	d	0.62 ± 0.02
n-Hexane	c	d	1.12 ± 0.12

[a]Indicated errors are two standard deviations.

[b]From Knox and Nelson (1959).

[c]Not observed.

[d]Not available.

the CH_3ONO photolysis systems, and are more nearly statistical. This is consistent with the fact that Cl atoms react much more rapidly with n-alkanes than do OH radicals and are thus less selective. These data, together with the corresponding isomeric ratios from the CH_3ONO system, indicate that for a given n-alkane all secondary alkyl peroxy radicals form the same fraction of secondary alkyl nitrates.

On the other hand, the 1-alkyl nitrate yields in the Cl_2 photolysis system are similar to those in the CH_3ONO system in that they are approximately a factor of two lower than expected on the basis of the relative amounts of alkyl, and hence alkyl peroxy, radicals initially formed (Knox and Nelson 1959). Although this could be due, at least in part, to a contribution to alkyl radical formation by OH radical reaction with the n-alkanes, these data further suggest that the fraction of 1-alkyl nitrates formed from primary alkyl peroxy radicals is indeed lower than the corresponding fraction of secondary alkyl nitrates from secondary alkyl peroxy radicals. Obviously, further work is needed to confirm and elucidate this observation.

Table II-18. Fractions of n-Alkanes Reacting to Form Alkyl Nitrates Via Reaction (5), i.e., the Rate Constant Ratio $k_5/(k_5 + k_6)$, Under Atmospheric Conditions, Together with Previous Literature Data

n-Alkane	$\alpha = k_5/(k_5 + k_6)$	
	This work	Literature
Ethane	≤ 0.014[a]	≤ 0.20[c]
Propane	0.036 ± 0.005[b]	0.04[d]
n-Butane	0.077 ± 0.009[b]	0.083 ± 0.02[e]; 0.086[d]
n-Pentane	0.129 ± 0.019[b]	0.14 ± 0.05[e]; 0.11[f]
n-Hexane	0.223 ± 0.035[b]	0.37 ± 0.08[e]; 0.15 ± 0.03[f]
n-Heptane	0.309 ± 0.050[b]	
n-Octane	0.332 ± 0.034[b]	

[a]From the Cl_2-NO-ethane-air irradiation.

[b]From CH_3ONO-NO-n-alkane-air irradiations. 1-Alkyl nitrate yields either monitored or calculated (see Table II-14). The rate constant ratios $k_5/(k_5 + k_6)$ for the 1-alkyl nitrates from 1-alkyl peroxy radicals are probably approximately a factor of two lower than these values. (1-Alkyl peroxy radicals formed account for 17% of all peroxy radicals for n-butane decreasing to 5% for n-octane, but account for 30% of the peroxy radicals from propane.)

[c]Plumb et al. (1982).

[d]Carter et al. (1979a).

[e]Darnall et al. (1976).

[f]Carter [re-analysis of the data in Darnall et al. (1976)].

Dependence of Alkyl Nitrate Yield on Carbon Number. The fraction of the n-alkanes which react to form alkyl nitrates under atmospheric conditions are given in Table II-18 and are plotted against carbon number in Figure II-13. These data were obtained for propane through n-octane from the CH_3ONO-NO-n-alkane-air irradiations together with the data for the Cl_2-NO-ethane-air irradiation. The experimental data for n-pentane through n-octane, which are for the secondary alkyl nitrates only, have been increased based on the kinetic data for the n-alkanes to allow for

1-alkyl nitrate formation (this correction is minor in all cases, decreasing from 10% for n-pentane to 4% for n-octane [Table II-18]). The datum for ethane is rigorously an upper limit since alkoxy radical combination with NO_2 could contribute a significant amount of the ethyl nitrate yields observed; this contribution is, as discussed above, minor for the other alkanes. These fractions α in Table II-18 and Figure II-13 are equated to the rate constant ratios $k_5/(k_5 + k_6)$.

It can be seen from Figure II-13 that the amount of reaction (5) proceeding via alkyl nitrate formation increases rapidly from $\lesssim$1% for ethane to ~30-33% for n-heptane and n-octane. The present data for propane through n-hexane are also compared with previous literature estimates in Table II-18, and can be seen to be, at least for propane and n-butane, in excellent agreement. Since these previous data (Darnall et al. 1976, Carter et al. 1979a) were obtained from product studies carried out in an ~5800-ℓ environmental chamber, versus the 75-ℓ chamber used here, surface or heterogeneous effects are unlikely to be involved in the observed alkyl nitrate formation.

Of further interest is the present observation of $\lesssim$1% $C_2H_5ONO_2$ formation from the reaction of ethoxy radicals with NO, indicating that the pathway

$$C_2H_5O_2 + NO \rightarrow C_2H_5O + NO_2$$

accounts for $\gtrsim$99% of the overall reaction. This is in accord with the recent data of Plumb et al. (1982) which show that $\gtrsim$80% of the reaction of $C_2H_5O_2$ radicals with NO produces NO_2.

The reaction pathway leading to alkyl nitrate formation, which is exothermic by ~57 kcal $mole^{-1}$ overall (Benson 1976), probably involves a three-member transition state. The available data are consistent with the following detailed mechanism:

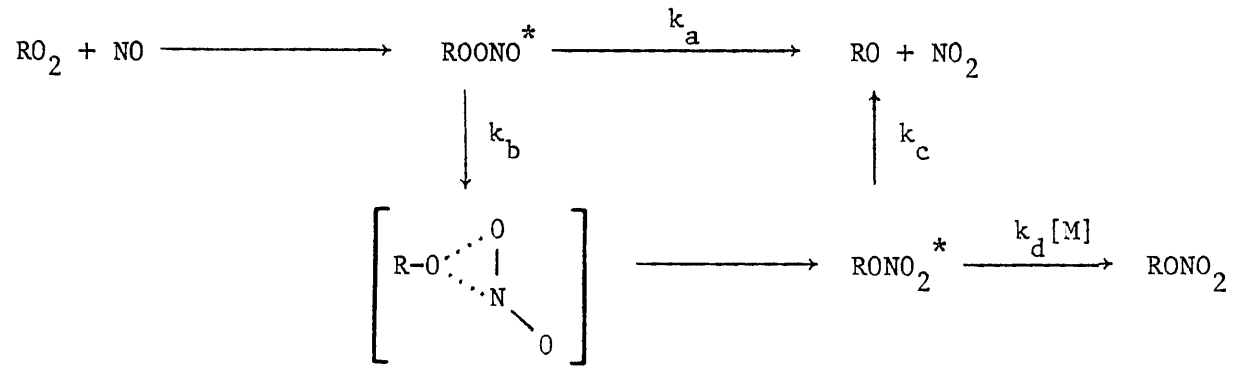

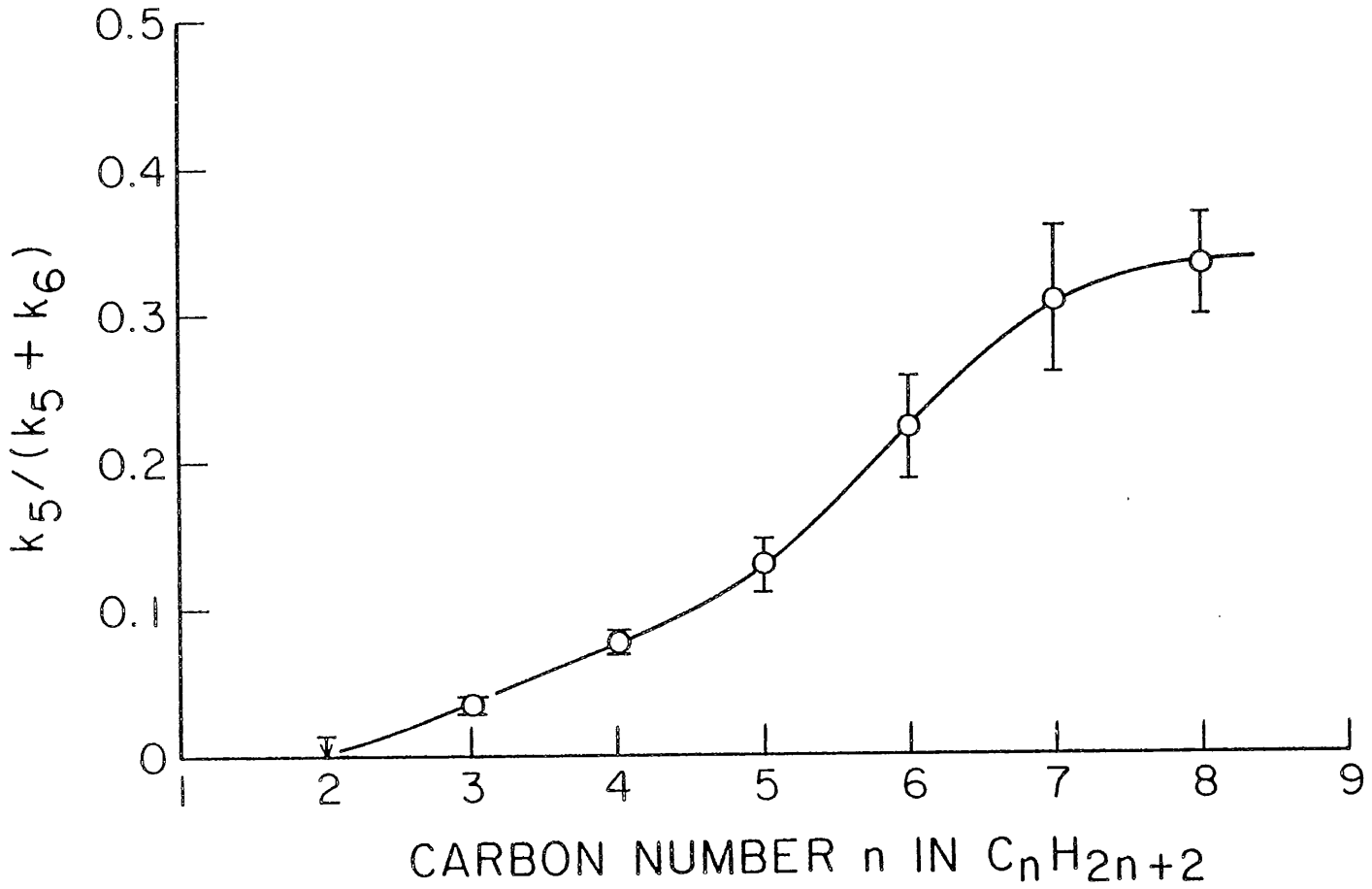

Figure II-13. Plot of $k_5/(k_5 + k_6)$ Against the n-Alkane Carbon Number. $k_5/(k_5 + k_6)$ is Set to be the Fractional Yield of Alkyl Nitrate Observed Under Atmospheric Conditions and Hence is an Average for the Isomeric Alkyl Nitrates Observed (See Text). The Datum for Ethane is from the Cl_2-NO-Ethane-Air Irradiation and is an Upper Limit. The Other Data are from CH_3ONO-NO-n-Alkane-Air Irradiations.

where * denotes vibrational excitation, k_a, k_b and k_c are overall rate constants for unimolecular decompositions or isomerizations of the vibrationally excited intermediates, and $k_d[M]$ is the overall rate of collisional stabilization of $RONO_2^*$. Thus the overall efficiency of alkyl nitrate production, α, is given by

$$\alpha = \left(\frac{k_b}{k_a + k_b}\right) \frac{k_d[M]}{(k_c + k_d[M])} \qquad \text{(XV)}$$

From the theory of unimolecular reactions (Robinson and Holbrook 1972), at a given total pressure decomposition of the vibrationally excited species is expected to become slower relative to collisional stabilization as the size of the molecule increases. Thus, from equation (XV), α is predicted to increase with the size of the molecule, consistent with the present experimental data. In addition, for sufficiently large molecules (or at sufficiently high pressures) where $k_d[M] \gg k_c$, equation (XV) yields

$$\alpha \rightarrow \alpha_\infty = k_b/(k_a + k_b)$$

and our data indicate that $\alpha_\infty \simeq 0.35$ based on the apparent limiting alkyl nitrate yield at high carbon number (Figure II-13). Although this mechanism is reasonable and consistent with the present data, further work regarding the effects of pressure and temperature on the alkyl nitrate yields is required to verify this mechanism. Such additional work has been carried out in these laboratories under separate funding (Atkinson et al. 1983b).

As indicated in the introduction, the formation of alkyl nitrates in hydrocarbon-NO_x-air irradiations is a sink for both oxides of nitrogen and radicals. Thus the observed increase of the alkyl nitrate yields with the size of the n-alkane means that the potential for contributing to photochemical air pollution (or at least some aspects of it) may be less for the larger ($\geq C_6$) n-alkanes than for the smaller ones.

D. NO_x-Air Photooxidations of C_6-C_8 n-Alkanes

In order to assess the photochemical reactivity of the longer-chain n-alkanes and to provide a data base for the development of detailed chemical kinetic computer models for this important class of organics, a series of NO_x-air irradiations of n-hexane, n-heptane and n-octane were carried out in the SAPRC 6400-ℓ all-Teflon environmental chamber. Because these alkane-NO_x-air photooxidation systems proved to be too unreactive for the maximum O_3 yields to be reached in reasonable amounts of time, a series of alkane-air irradiations, with added CH_3ONO present to supply both radicals and NO_x from its rapid photolysis, were also carried out in the 6400-ℓ all-Teflon chamber.

Experimental

The SAPRC all-Teflon indoor chamber consists of a replaceable ~6400-ℓ FEP Teflon bag, constructed from 50 μm-thick FEP Teflon film, which is attached to a semi-rigid framework (Figure II-14) and which can collapse as samples are withdrawn, thus avoiding dilution due to sampling. Irradiation is provided by two diametrically opposed banks of 40 Sylvania 40-W BL lamps, backed by arrays of Alzak-coated reflectors. The light intensity in the chamber is controlled by switching off sets of lights as previously described (Darnall et al. 1981), and the light intensities for the various levels of illumination are monitored by measuring the rate of photolysis of NO_2 in N_2 using the quartz tube, continuous flow technique of Zafonte et al. (1977). For the experiments reported here, the light intensity used was 70% of the maximum light intensity.

Before each experiment, the chamber was flushed with dry purified air (Doyle et al. 1977) for ~2 hr at a flow rate of ~12 cfm, and then with air at the desired relative humidity for ~1 hr. All starting materials (except methyl nitrite) were injected using gas-tight gas syringes and flushed into the chamber using dry ultra-high purity N_2. Commercially available tank NO (Matheson, CP grade, 99.0%) was used without further purification, and NO_2 was prepared by diluting this NO with dry, pure O_2 in a syringe. For methyl nitrite, which was prepared and stored as described above (Section II.B), a known partial pressure in an atmosphere of N_2 in an ~5-ℓ bulb was flushed into the chamber by a stream of ultra-high purity N_2.

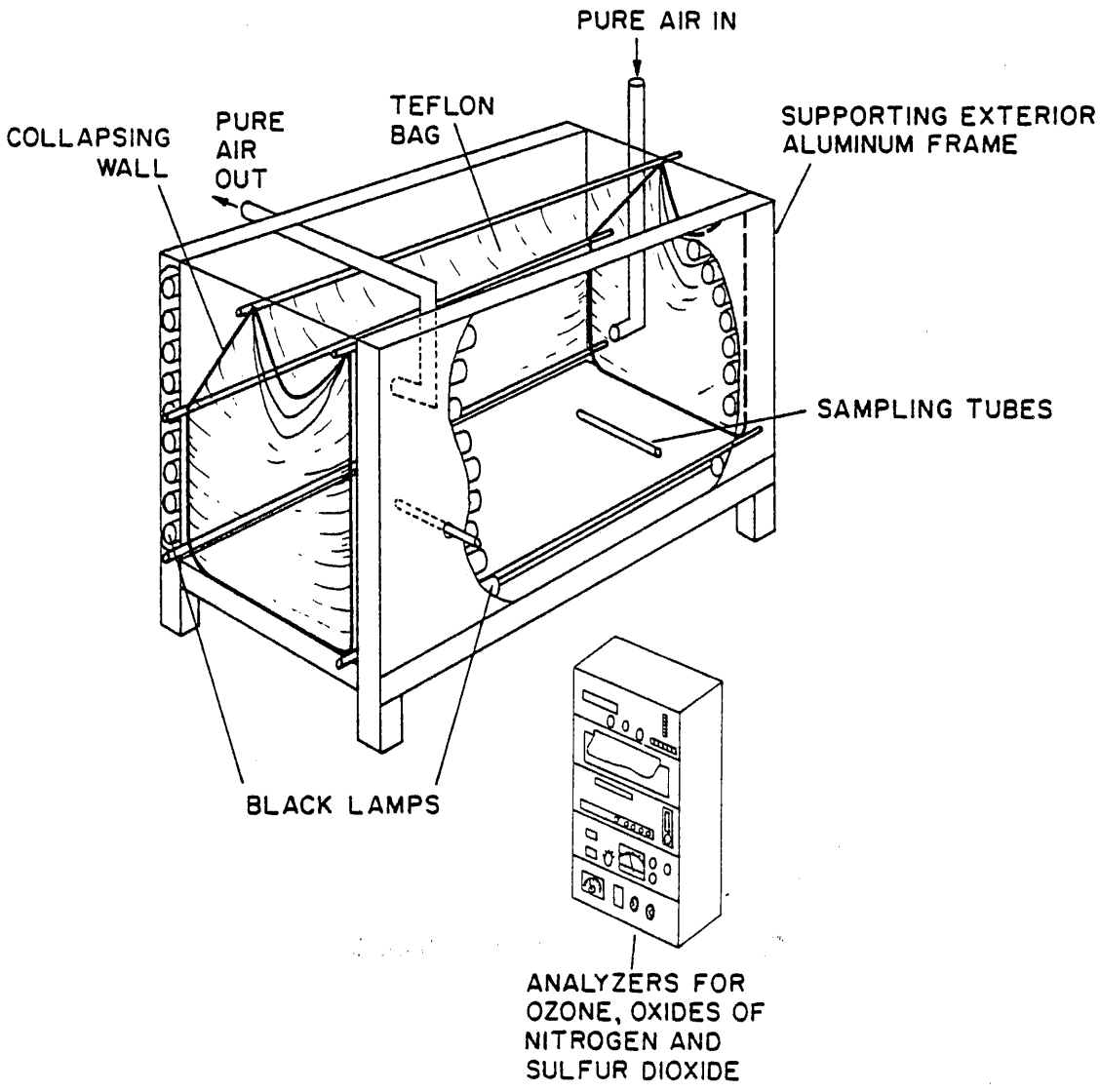

Figure II-14. SAPRC Indoor 6400-Liter All-Teflon Chamber.

Nitrogen oxides and NO_x were monitored using a chemiluminescence analyzer and O_3 was monitored by ultraviolet absorption. The n-alkanes were monitored by gas chromatography with flame ionization detection, using a 20-ft x 1/8-in SS column with 5% DC703/C20M on 100/120 mesh AW, DMCS Chromosorb G, operated at 333 K. Oxygenated products were analyzed using the 10-ft x 1/8-in SS column of 10% Carbowax 600, while alkyl nitrates were analyzed using a 5-ft x 1/8-in SS column of 5% Carbowax 600 on C-22 Firebrick, operated at 348 K. Peroxyacetyl nitrate (PAN) was analyzed by gas chromatography with electron capture detection using a 1/8-in x 1/8-in Teflon column of 5% Carbowax 400 on Chromosorb (80/100 mesh) operated at room temperature. Formaldehyde was monitored using an improved chromatropic acid technique (Pitts et al. 1979).

Results and Discussion

Alkane-NO_x-Air Irradiations. The detailed data sheets for these runs are given in Appendix A, and the initial concentrations and results are summarized in Table II-19. The photochemical reactivity in these runs was extremely low, even when hydrocarbon/NO_x ratios as high as ~400 were employed. In no case was an ozone maximum obtained with 6 hr of irradiation, and only in run ITC-540 was an apparent O_3 maximum observed during the irradiation (0.36 ppm in 6.25 hr). For the $\geq C_6$ alkanes, the major products observed were the expected $\geq C_6$ alkyl nitrates (see Section II.C), and no other organic products were observed in significant yields.

Although the fact that O_3 maxima were not obtained in most of these runs means that they cannot be used to compare the maximum O_3 formation potential of these alkanes, they can be used to compare their efficiency in oxidizing NO and causing O_3 formation. Ozone is formed in NO_x-air irradiations by the photolysis of NO_2,

$$NO_2 + h\nu \xrightarrow{O_2} O_3 + NO \qquad (21)$$

but in the absence of hydrocarbons, no net O_3 is formed because of its rapid reaction with NO,

Table II-19. Initial Concentrations and Selected Results on the Alkane-NO_x-Air Irradiations Conducted in the SAPRC ~6400-ℓ Indoor Teflon Chamber[a]

ITC Run Number		n-Butane 507	n-Butane 533	n-Hexane 559	n-Heptane 538	n-Heptane 540	n-Octane 552
Initial Conc. (ppm)	Alkane	3.75	2.96	46.57	8.62	43.65	53.60
	NO_x	0.09	0.12	0.13	0.12	0.11	0.13
Yield ppb[b] at Time = t	t (min)	360	360	300	360	390	360
	-Δ[alkane]	139	113	~1220	261	~2700	~1220
	$\Delta([O_3]-[NO])$	216	209	359	227	434	394
	2-RONO_2	9.5	6.7	17.1	24.5	63.0	19.1
	3-RONO_2	-	-	26.7	23.5	41.5	-[d]
	4-RONO_2	-	-	-	-[d]	-[d]	57.6
$\alpha \simeq \frac{\Delta([O_3]-[NO])}{-\Delta[alk]^{rct}}$	-Δ[alkane][b]	1.5 ± 0.1	1.8 ± 0.1	(<0.3)	0.8 ± 0.1	(<0.2)	(<0.3)
	2-RONO_2[c]	1.7 ± 0.1	2.2 ± 0.2	1.75 ± 0.2	0.95 ± 0.04	~0.65[e]	0.9 ± 0.2
	3-RONO_2[c]	-	-	1.6 ± 0.1	1.1 ± 0.1	~1.4[e]	~0.6[e]
	4-RONO_2[c]	-	-	-		-	0.7 ± 0.1

[a] $k_1 = 0.32\ min^{-1}$, 50% RH, 301 ± 2 K.

[b] -Δ[alkane] = alkane consumed, $\Delta([O_3]-[NO])$ = O_3 yield - change in NO (see text), 2-RONO_2 = 2-butyl, 2-hexyl, 2-heptyl or 2-octyl nitrate, depending on the initial alkane.

[c] Calculated using least squared regression of $\Delta([O_3]-[NO_3])$ against $-\Delta[alk]^{rct}$ for each time point where data for both available. "-Δ[alkane]" means $-\Delta[alkane]^{rct}$ used to derive α was taken directly from alkane data, "2-RONO_2" means $-\Delta[alkane]^{rct}$ was estimated from 2-alkyl nitrate yields and expected alkyl nitrate yields from the corresponding alkane given below (see Section II.B);

Alkane	Nitrate Yields: 2-RONO_2	3-RONO_2	4-RONO_2
n-Butane	0.074 ± 0.003	-	-
n-Hexane	0.087 ± 0.005	0.119 ± 0.005	-
n-Heptane	0.094 ± 0.005	0.129 ± 0.007	(not used)
n-Octane	0.084 ± 0.002	0.118 ± 0.003	0.111 ± 0.004

[d] Data not available.

[e] Based on single data point.

$$O_3 + NO \rightarrow O_2 + NO_2 \qquad (22)$$

However, in the presence of hydrocarbons such as the alkanes, NO is oxidized to NO_2 and nitrates by its reactions with the peroxy radicals formed, which tends to shift the photoequilibrium determined by reactions (21) and (22) towards higher O_3 levels.

In particular, the overall alkane photooxidation mechanism, discussed in detail in Section II.A, can be expressed as:

$$OH + \text{alkane} \rightarrow -\alpha\ NO + \beta\ NO_2 + \gamma\ OH + \text{products} \qquad (10)$$

and if reactions (21), (22) and (10) are assumed to be the major reactions influencing $[O_3]$ and [NO], then

$$\frac{d[O_3]}{dt} \cong k_{21}[NO_2] - k_{22}[O_3][NO]$$

$$\frac{d[NO]}{dt} = k_{21}[NO_2] - k_{22}[O_3][NO] - k_{10}\alpha[OH][\text{alkane}]$$

and thus

$$\frac{d([O_3]-[NO])}{dt} = k_{10}\alpha[OH][\text{alkane}] \qquad (XVI)$$

or

$$\Delta([O_3]-[NO])_t = \alpha k_{10} \int_o^t [OH]_\tau [\text{alkane}]_\tau d\tau$$

where k_{21}, k_{22} and k_{10} are the rate constants for reactions (21), (22) and (10), respectively (with k_{10} being the elementary OH + alkane rate constant), and $\Delta([O_3]-[NO])_t$ is (the change in $[O_3]$ - the change in [NO]) from the beginning of the irradiation until time t. The amount of alkane reacted with OH up to time t, $\Delta[\text{alkane}]_t^{rct}$, is given by

$$\Delta[\text{alkane}]_t^{rct} = k_{10} \int_o^t [OH]_\tau [\text{alkane}]_\tau d\tau \qquad \text{(XVII)}$$

and combining equations (I) and (II) yields:

$$\Delta([O_3]-[NO])_t = \alpha\Delta[\text{alkane}]_t^{rct} \qquad \text{(XVIII)}$$

If loss of the alkane is assumed to be due only to chemical reaction (as expected in a collapsible Teflon chamber where dilution should be negligible or minor), and since reaction with OH radicals is assumed to be the only significant chemical loss process for alkanes under these conditions, then one would expect

$$\Delta[\text{alkane}]_t^{rct} \simeq ([\text{alkane}]_o-[\text{alkane}]_t) = -\Delta[\text{alkane}]_t \qquad \text{(XIX)}$$

Thus a plot of $\Delta([O_3]-[NO])_t$ against $-\Delta[\text{alkane}]_t$ should yield a straight line with a slope of α, the efficiency of the alkane in oxidizing NO and thus causing O_3 formation.

Plots of $\Delta([O_3]-[NO])$ against $-\Delta[\text{alkane}]$ for the n-butane-NO_x-air run ITC-533, and for the n-heptane-NO_x-air run ITC-538 are shown in Figures II-15 and II-16, respectively. The slopes obtained for these and the other alkane-NO_x-air runs are summarized in Table II-19. It can be seen from Figures II-15 and II-16 (as well as from an analogous plot for run ITC-507, not shown) that for these runs good straight-line plots are obtained. This suggests that the approximations inherent in equations (XVIII) and (XIX) are reasonable, at least when the initial alkane level is less than ~9 ppm.

However, for the runs containing over 40 ppm of initial alkane, the observed alkane decay rates yielded unreasonably low values of α, and were much higher than expected based on the observed alkyl nitrate product yields (see Section II.C) or reasonable expectations of radical levels present in these runs (see Section IV). This suggests that a physical loss process for the alkanes may be non-negligible when such high alkane levels are present. An excess alkane decay rate of only ~0.5% hr^{-1} is all that is required to account for these results. This is not an unreasonably high rate for wall diffusion or heterogeneous removal of these species. Since the absolute amount of alkane removed by this non-chemical

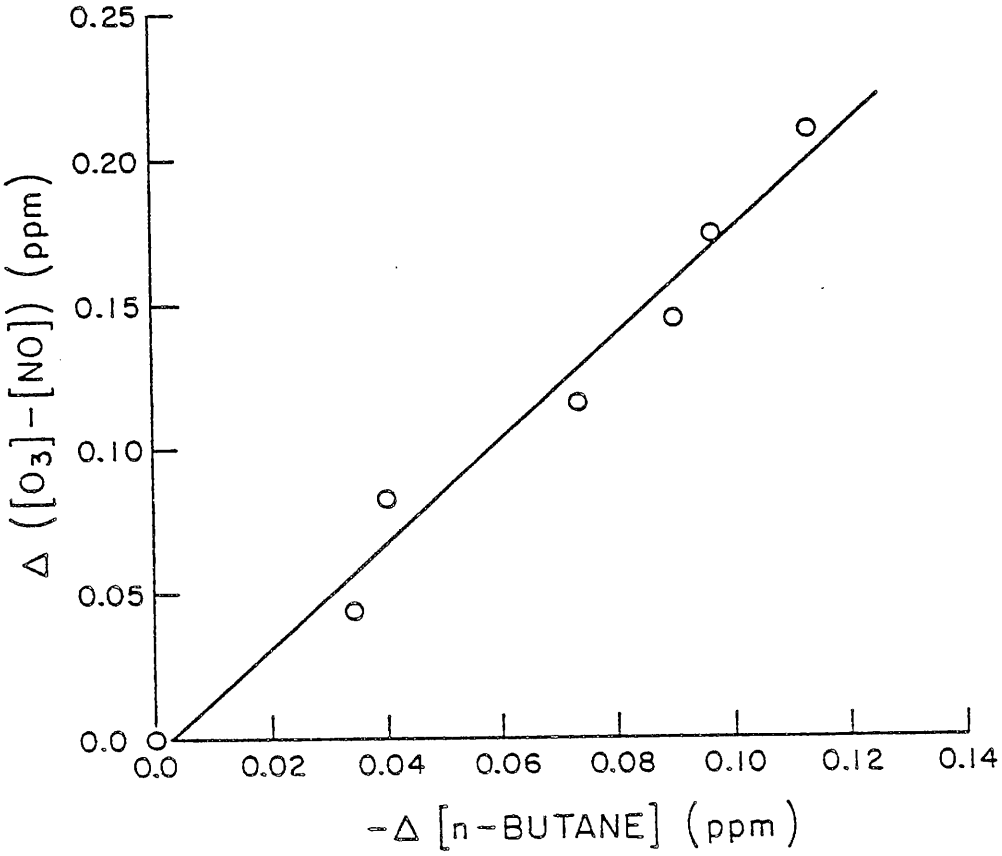

Figure II-15. Plot of $\Delta([O_3]-[NO])$ Against $-\Delta$[n-butane] for n-Butane-NO_x-Air Run ITC-533.

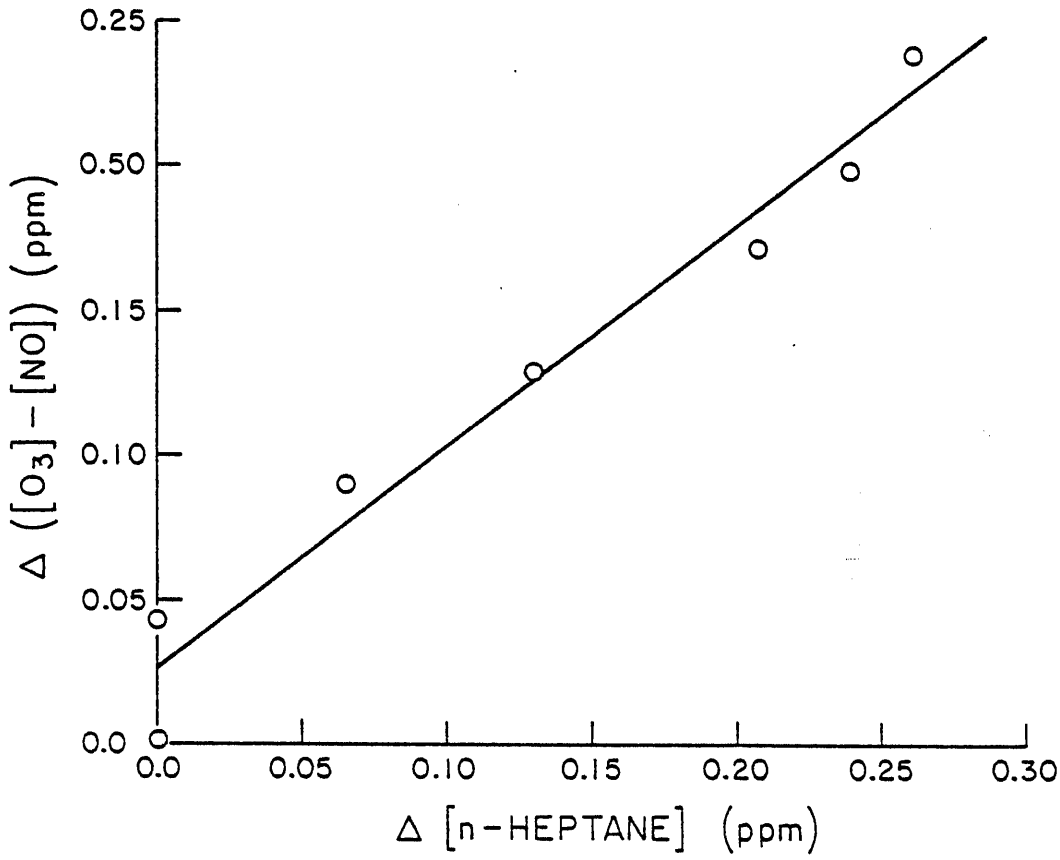

Figure II-16. Plot of $\Delta([O_3]-[NO])$ Against $-\Delta$[n-heptane] for n-Heptane-NO_x-Air Run ITC-538.

process, and thus the excess in the apparent amount of alkane reacted calculated by equation (XIX), is proportional to the amount of alkane present, this effect will be less important when the initial alkane levels are lower, but it is probably non-negligible for all the runs considered here.

An alternate technique to obtain α using equation (XVIII) which avoids problems caused by slow non-chemical loss processes of the alkanes is to derive $\Delta[\text{alkane}]^{rct}$ using the observed product yields, based on the known relationship between these yields and alkane reaction derived from separate experiments. In particular, as described in Section II.C, the relative alkyl nitrate yields from these and other alkanes have been measured with relatively high precision from CH_3ONO-alkane-NO irradiations (Section II.C). In this case, the effects of slow, non-chemical loss processes are minor, since the levels of these products are at least two orders of magnitude lower. Thus if δ_i is the known relative yield of product i from a given alkane and $[\text{product}_i]_t$ is its concentration at time t, we can write,

$$[\text{product}_i]_t \simeq \delta_i \Delta[\text{alkane}]^{rct} \qquad \text{(XX)}$$

and thus

$$\Delta([O_3]-[NO])_t \simeq \frac{\alpha}{\delta_i} [\text{product}_i]_t \qquad \text{(XXI)}$$

Equation (XX) and (XXI) thus neglect the effects of secondary reactions of the products. However, using the techniques described in Section II.C, the effect of secondary reactions of the alkyl nitrates are calculated to be negligible in these experiments.

An example of a plot of $\Delta([O_3]-[NO])$ against an alkyl nitrate yield is shown in Figure II-17, and the values of α calculated in this manner are summarized in Table II-17. In general, linear plots were obtained (i.e., no evidence of curvature), though it should be noted that due to significant H_2O interferences on the chromatographic analyses of the heptyl and octyl nitrates (which is not a problem in low humidity runs such as those discussed in Section II.C), the nitrate yield data from the heptane and octane runs, and thus the values of α derived from them, are somewhat more uncertain.

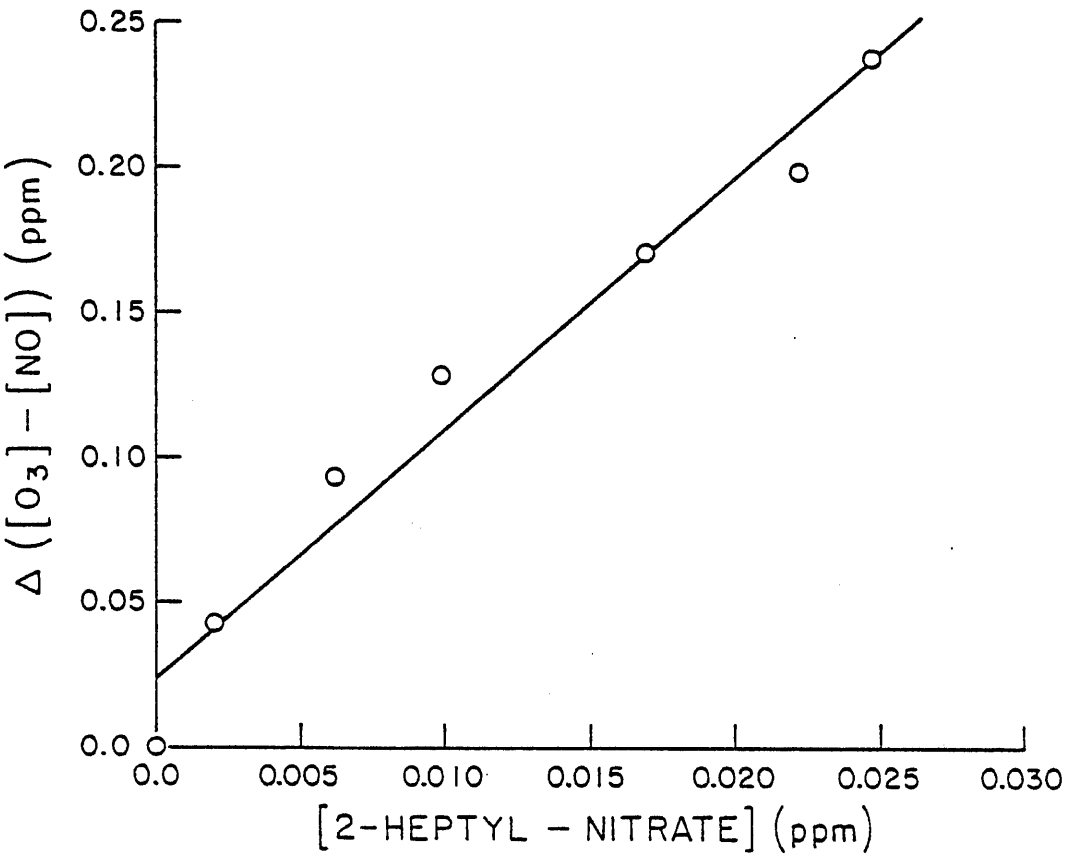

Figure II-17. Plot of $\Delta([O_3]-[NO])$ Against the 2-Heptyl Nitrate Yield for the n-Heptane-NO_x-Air Run ITC-538.

The results of these experiments indicate that α, the efficiency of the alkanes in oxidizing NO and causing O_3 formation, is 2.0, 1.7, 1.0 and 0.8 for n-butane, n-hexane, n-heptane and n-octane. Thus, it can be seen that the decrease in apparent efficiency of the alkanes in oxidizing NO is greater than the experimental uncertainties.

These experimental estimates of α can be compared with values predicted by our current mechanism for the photooxidation of the $\geq C_6$ n-alkanes discussed in Section II.A. Briefly, the major reactions affecting NO oxidation are summarized as follows:

$$RH + OH \xrightarrow{O_2} RO_2 + H_2O$$

$$RO_2 + NO \rightarrow \varepsilon\ RO\cdot + \varepsilon\ NO_2 + (1-\varepsilon)\ RONO_2$$

$$RO\cdot(\text{e.g. } R'\overset{\overset{\cdot}{O}}{\overset{|}{C}}-CH_2CH_2CH_2R'') \xrightarrow{O_2} HORO_2\cdot \text{ (e.g. } R'\overset{\overset{OH}{|}}{CH_2}CH_2CH_2\overset{\overset{OO\cdot}{|}}{CHR''})$$

$$HORO_2 + RO \rightarrow \varepsilon'\ HORO\cdot + \varepsilon\ NO_2\ (1-\varepsilon')\ HORONO_2$$

$$HORO\cdot \xrightarrow{O_2} HO_2 + HOR{=}O \text{ (e.g. } R'\overset{\overset{O}{\|}}{C}CH_2CH_2\overset{\overset{OH}{|}}{CH}R'')$$

$$HO_2 + NO \rightarrow OH + NO_2$$

or overall:

$$RH + OH \rightarrow -(1 + \varepsilon + \varepsilon\varepsilon')\ NO + (\varepsilon + 2\varepsilon\varepsilon')NO_2 + \varepsilon\varepsilon' OH + \text{products}$$

and thus:

$$\alpha = 1 + \varepsilon + \varepsilon\varepsilon';\ \beta = \varepsilon(1 + 2\varepsilon');\ \gamma = \varepsilon\varepsilon', \qquad \text{(XXII)}$$

where $(1-\varepsilon)$ is the alkyl nitrate formation efficiency from the reaction of the $\geq C_6$ peroxy radical with NO (which was measured for these and other alkanes as described in Section II.C) and $(1-\varepsilon')$ is the corresponding

efficiency for the reaction of NO with the postulated δ-hydroxy alkyl peroxy radical intermediate. The latter quantity is unknown, and it is assumed that $\varepsilon' = \varepsilon$. Therefore, based on measured values of $(1-\varepsilon)$ of 0.223, 0.309 and 0.332 for n-hexane, n-heptane and n-octane, respectively, we can derive values of α of, respectively, 2.4, 2.2 and 2.1, compared with the experimental values of 1.7 ± 0.2, 1.0 ± 0.3 and 0.8 ± 0.3. For n-butane, the above mechanism is not applicable, but our experimental value of $\alpha \cong 2.0$ for n-butane is in reasonable agreement with the theoretical value of $\alpha = 2.3$ derived by Atkinson et al. (1982b), based on our current understanding of the explicit n-butane-NO_x photooxidation mechanism (Carter et al. 1981, Atkinson and Lloyd 1983).

One possible cause for the discrepancies cited above, between the observed and predicted NO oxidation efficiencies for the higher alkanes, could be net conversion of NO_2 to NO by the process(es) which cause the chamber radical source. (See Section IV for a detailed discussion of this phenomenon.) Thus if the chamber radical source involves a process such as,

$$NO_2 \xrightarrow[-H_2O]{h\nu,\ wall} HONO$$

$$HONO + h\nu \rightarrow OH + NO$$

the overall process forming radicals would convert NO_2 to NO, and consequently tend to reduce the apparent overall oxidation efficiencies of the hydrocarbon(s) present. Indeed, experimental evidence for such "negative" NO oxidation involved in the radical source is given in Section IV. This is not a major consideration for organics such as the simple alkenes and the smaller alkanes which do not have significant radical sinks in their oxidation mechanisms (Carter et al. 1979a) or for organics, such as the aromatics (see Section III) which have significant radical sources, since in those cases the rate of consumption of the organic is significantly higher than the radical input rates. However, the photooxidation mechanism for the higher alkanes is characterized by significant radical sinks (caused by alkyl nitrate formation) and no significant radical sources,

which means that in order for the photooxidation to proceed, the radical removal in the alkane mechanism must occur with a similar rate as the radical source, and thus the rate of the radical source is not negligible compared to the rate of the alkane photooxidation reactions.

If it is assumed that in these alkane-NO_x-air irradiations the only significant radical source is the chamber radical source (as indicated by current model calculations [see, for example, Carter et al. 1979a]), and if it is assumed that the major radical sink is alkyl nitrate formation from the alkanes, then, in order that the OH production and destruction rates balance, we can combine the overall radical initiation process

$$NO_2 \xrightarrow[-H_2O]{\text{wall, } h\nu} \rightarrow NO + OH$$

with the overall alkane oxidation process

$$OH + \text{alkane} \rightarrow -\alpha\ NO + \beta\ NO_2 + \gamma\ OH + \text{products} \qquad (10)$$

Hence, we obtain the following net process:

$$\text{alkane} \rightarrow -(\alpha + \gamma - 1)\ NO + (\beta + \gamma - 1)\ NO_2 + \text{products}$$

and thus:

$$-\frac{d([O_3]-[NO])}{dt} \simeq \alpha + \gamma - 1 \qquad \text{(XXIII)}$$

This ignores radical termination due to

$$OH + NO_2 \rightarrow HNO_3 \qquad (23)$$

but, for most of our experiments, the alkane level is sufficiently high that $(1-\gamma)k_{10}[\text{alkane}] \gg k_{23}[NO_2]$, so this is a reasonably good approximation. Combining equations (XXII) and (XXIII), we obtain,

$$-\frac{d([O_3]-[NO])}{dt} \simeq \varepsilon + 2\ \varepsilon\varepsilon' \qquad \text{(XXIV)}$$

and, assuming that $\varepsilon \cong \varepsilon'$, the current mechanism would predict NO oxidation efficiencies of 2.0, 1.6 and 1.6 for n-heptane, n-octane and n-heptane, respectively. These are still significantly higher than the observed values. However, if we take the experimental measurements of the NO oxidation rate and use equation (XXIV) to derive ε', we obtain $\varepsilon' =$ 0.6, 0.1 and 0.1 from n-hexane, n-heptane and n-octane, respectively, which correspond to respective alkyl nitrate formation efficiencies, $(1-\varepsilon')$, of 0.4, 0.8 and 0.9. Thus, these results suggest that alkyl nitrate formation from the reaction of NO with species such as

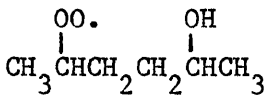

is far more efficient than nitrate formation from the corresponding non-hydroxy-substituted alkyl peroxy radicals. This means that the photooxidation mechanisms of the larger alkane involve radical and NO_x sinks of higher magnitude than previously believed.

It should be noted, however, that the nature of the chamber radical source, including its effects on overall NO conversion rates, remains highly uncertain, and, until it is better understood, the above analysis must be considered to be primarily speculative in nature. In particular, the chamber radical input rate has been found to be quite valuable in the indoor Teflon chamber (see Section IV). Thus the effects of the alkanes on the radical levels cannot be determined unambiguously from these experiments, especially since model simulations have shown the results of these experiments to be extremely sensitive to the chamber radical source, even when it is allowed to vary only within the ranges determined by the associated tracer-NO_x-air chamber characterization experiments. In addition, as indicated previously, the reactivities of these runs were too low for maximum O_3 yields to be determined in reasonable amounts of time. Thus other types of experiments are required to obtain data more useful for assessing these aspects of alkane reactivity.

Alkane-CH_3ONO-Air Irradiations. In order to obtain data concerning ozone formation from the NO_x-air photooxidations of alkanes under conditions where the bulk of the radicals are supplied by known, reproducible chemical processes (as opposed to the chamber radical source which is the

dominant radical source in the alkane-NO_x-air irradiations), and where the reactivity is sufficiently high so maximum O_3 yields can be determined, a series of n-hexane, n-heptane and n-octane-air irradiations were carried out where both the radicals and the NO_x are produced by the photolysis of methyl nitrite:

$$CH_3ONO + h\nu \xrightarrow{O_2} HCHO + NO_2 + OH$$

(See Section II.C for a discussion of the CH_3ONO photolysis system.) The conditions and results of these experiments are summarized in Table II-20, and the detailed data tabulations are given in Appendix A.

From Table II-20 it can be seen that the addition of 1-9 ppm of n-hexane, n-heptane or n-octane to a CH_3ONO (0.4-0.5 ppm)-air irradiation causes the final O_3 yield to increase from 0.4 ppm to 1.0-1.3 ppm; but the final O_3 yields in these alkane-CH_3ONO-air irradiations appear to be remarkably insensitive to the amount of alkane present or even to the identity of the alkane added. However, the data do suggest that under similar conditions, n-hexane may form slightly more O_3 than n-heptane, and n-heptane may form slightly more O_3 than n-octane. This trend in reactivity is the opposite of what one would expect on the basis of their respective rate constants for reaction with an OH radical, but is in line with (a) the increasing NO_x and radical removal caused by the increased alkyl nitrate yields from the higher alkanes (Section II.C), and (b) the apparent reduction in the NO oxidation efficiency with size of the alkane discussed in the previous section.

In order to determine the extent to which these data are consistent with the currently assumed mechanism for NO_x-air photooxidations of long-chain alkanes, computer model simulations of these experiments were conducted. The alkanes and the alkyl nitrates were assumed to react with OH radicals with the rate constants derived in this program (Section II.B), and the alkyl nitrate yields discussed in Section II.C were also assumed. The alkane photooxidation mechanism employed was based on that discussed in Section II.A and earlier in this section. For simplicity, 100% isomerization of the $\geq C_6$ alkoxy radicals was assumed, the alkyl nitrate formation efficiency from the reaction of NO with the δ-hydroxy

Table II-20. Initial Conditions and Observed and Calculated Maximum O_3 Yields and Alkane Consumed in the CH_3ONO-Air and the CH_3ONO-Alkane-Air Irradiations Carried Out in the SAPRC ~6400-ℓ Indoor Teflon Chamber[a]

ITC Run Number	Alkane Studied	Initial Conc. (ppm)		O_3 Yield (ppm)		Alkane Consumed (ppm)	
		Alkane	CH_3ONO[b]	Exp't[c]	Model[d]	Exp't[c]	Model[d]
556	n-Hexane	0.92	0.48	1.4	1.08	0.33	0.41
555	n-Hexane	4.69	0.47	1.20	1.34	0.69	0.70
554	n-Hexane	9.25	0.42	1.15	1.31	0.81	0.71
545	n-Heptane	0.91	0.47	0.98	1.03	0.35	0.42
544	n-Heptane	4.29	0.46	1.11	1.17	0.61	0.66
541	n-Heptane	8.17	0.45	1.10	1.17	0.70	0.69
549	n-Octane	0.96	0.45	0.92	1.00	0.38	0.44
548	n-Octane	4.75	0.46	0.99	1.13	1.18	0.65
547	n-Octane	8.21	0.48	1.10	1.18	0.76	0.75
542	-	0	0.44	0.39	0.39	-	-
546	-	0	0.49	0.33	0.42	-	-
553	_	0	0.42	0.39	0.38	-	-

[a] $T = 301 \pm 1$ K, <5% RH, $k_1 = 0.32$ min^{-1}.

[b] Initial CH_3ONO based on increase in total NO_x measurement after CH_3ONO injected, based on assuming 100% interference of alkyl nitrites on commercial chemiluminescent NO_x detectors (Winer et al. 1974).

[c] After 240 min of irradiation.

[d] Detailed model calculation. See text.

peroxy radicals so formed was assumed to be the same as from the corresponding reaction of NO with the unsubstituted $\geq C_6$ peroxy radicals, and, although these alkane models are quite insensitive to the assumed mechanism for the products, the δ-keto alcohol products were assumed to react in a manner analogous to that of equal mixtures of methylethyl ketone and n-propyl alcohol. The inorganic mechanism employed was that of Atkinson

and Lloyd (1983), and appropriate provisions for chamber effects were included, though these calculations were also not very sensitive to these effects.

The calculated O_3 yields and calculated amounts of alkane consumed are shown in Table II-20, where they can be compared with experimental results. In general, excellent fits to the O_3 yields and to the O_3 concentration-time profiles were obtained with all calculations. The calculated amount of alkane reacted was generally slightly overpredicted in the 1 ppm alkane runs and slightly underpredicted in 8-9 ppm alkane runs. The underprediction at higher alkane levels may be due to some loss of alkanes resulting from dilution or other non-chemical processes (as observed in the 40-50 ppm alkane-NO_x runs discussed earlier), but the overprediction at low alkane levels suggests a possible problem with the mechanism. However, in general the fits of these calculations to the data were quite good, although this may reflect more the insensitivity of this experimental system to variations in reactivity parameters than the accuracy of this model, especially since, as discussed in the previous section, this model did not correctly predict the observed NO oxidation efficiencies of these alkanes.

E. Summary and Conclusions

As a result of studies conducted under this SAPRC-ARB program, we believe significant progress has been made in our quantitative understanding of the atmospheric chemistry of the higher n-alkanes. The primary homogeneous consumption pathway for these compounds in the atmosphere is reaction with the hydroxyl radical, and very precise relative determinations of these rate constants have been made for the C_3-C_{10} n-alkanes. The kinetic data obtained fit a very simple formula based on the number of $-CH_2-$ groups bonded to a $-CH_2-$ and a $-CH_3$ group or to two $-CH_2-$ groups, which allows the prediction, with a reasonable degree of confidence, not only of the total OH radical rate constant for the $\geq C_{11}$ n-alkanes (for which kinetic data are not currently available) and for a number of branched alkanes, but also of the relative probability of OH attack on the various isomeric positions within the molecule.

The major known atmospheric photooxidation products of the n-alkanes are the corresponding alkyl nitrates and (to a lesser extent) aldehydes

and ketones, and the rate constants for the reactions of OH radicals with representative alkyl nitrates, and with several representative ketones have been determined. Although ketones probably undergo photodecomposition to some extent, reaction with OH radicals is also the major atmospheric sink for these molecules. The kinetic data for these products could also be predicted to some extent by simple group additivity type formulae as applied to the parent alkanes, though in this case (especially for the ketones) the fit is not quite as good. However, the results of this study are sufficient to allow the OH radical rate constants with other alkyl nitrates and ketones to be estimated to within ±50% or better, and also give us an indication of the relative contributions of OH attack on the various isomeric positions.

Alkyl nitrate formation has been known for several years to be an important aspect of the photooxidation mechanism for the n-alkanes, but until this study, the data concerning the effect of chain length on alkyl nitrate yields have been limited to C_3-C_6 alkanes (and were rather imprecise). In this study, alkyl nitrate yields were determined, with good precision, for the C_2-C_8 n-alkanes, allowing the effect of size of the molecule to be more clearly demonstrated. The alkyl nitrate yields increased monotonically from $\lesssim$1% for ethane to ~33% for n-octane, with the yields apparently leveling off for higher alkanes at around 35%. This is an important input to computer models for the atmospheric reactions of these alkanes.

Although as a result of our kinetic and product yield studies we now have a much more precise knowledge of several important aspects of alkane photooxidation mechanisms, the results of the limited number of environmental chamber studies performed under this program indicate that much additional work is required before predictive computer models for the NO_x-air photooxidations of the $\gtrsim C_6$ n-alkanes can be considered to be validated. One major problem is that of obtaining environmental chamber data suitable for unambiguous model validation, since alkane-NO_x-air irradiations are extremely unreactive, and they are so sensitive to radical initiation from the chamber radical source that this is the single most important input parameter in the models even if it is allowed to vary only within the range experimentally measured in tracer-NO_x-air irradiations (see Section IV). Furthermore, when CH_3ONO is added to provide a more

reproducible and more precisely defined radical source, the results of the irradiation appear to be highly insensitive to mechanistic and reactivity parameters used in the major simulations, making these runs also not particularly suitable for model validation, since even a grossly incorrect model can fit the data.

However, although our environmental chamber data were inadequate for comprehensive model validation and testing, the results of the alkane-NO_x-air irradiations could be used to make some estimates of efficiencies of n-butane and of n-hexane through n-octane in oxidizing NO, and thus causing O_3 formation. Evidence was obtained that the efficiency decreased significantly as the size of the molecule increased, ranging from the expected two molecules of NO oxidized per molecule of n-butane consumed, down to a corresponding ratio of only ~1.0 to ~0.8 for n-heptane and n-octane. The low NO oxidation ratios for n-heptane and n-octane are in significant disagreement with the mechanism generally assumed, which predicts ratios of at least two even for n-octane, though this may be due in part to conversion of NO_2 to NO by whatever process causes the chamber radical source. Clearly, additional work is required on the photooxidation mechanims of n-alkanes, especially including development of more sensitive and suitable types of experiments for comprehensive model validation and fundamental studies of the mechanism and the products formed following alkoxy radical isomerization.

III. AN INVESTIGATION OF THE ATMOSPHERIC CHEMISTRY OF SELECTED AROMATICS, HYDROCARBONS AND AROMATIC PHOTOOXIDATION PRODUCTS

A. Introduction and Background

Significant advances have been made in recent years concerning the atmospheric chemistry of aromatic hydrocarbons which are constituents of unleaded gasoline and other fuels currently in use. From both laboratory and smog chamber studies, it has been known since the early 1970s that the only important chemical loss process for the aromatic hydrocarbons under atmospheric conditions is via reaction with the OH radical. Data are now available concerning both the overall OH radical rate constants and the relative amounts of OH radical addition and H-atom abstraction for most aromatics, including benzene (Atkinson et al. 1979). For substituted benzenes such as toluene, two reaction pathways occur (Atkinson et al. 1979): OH radical addition to the ring and H-atom abstraction from the substituent groups.

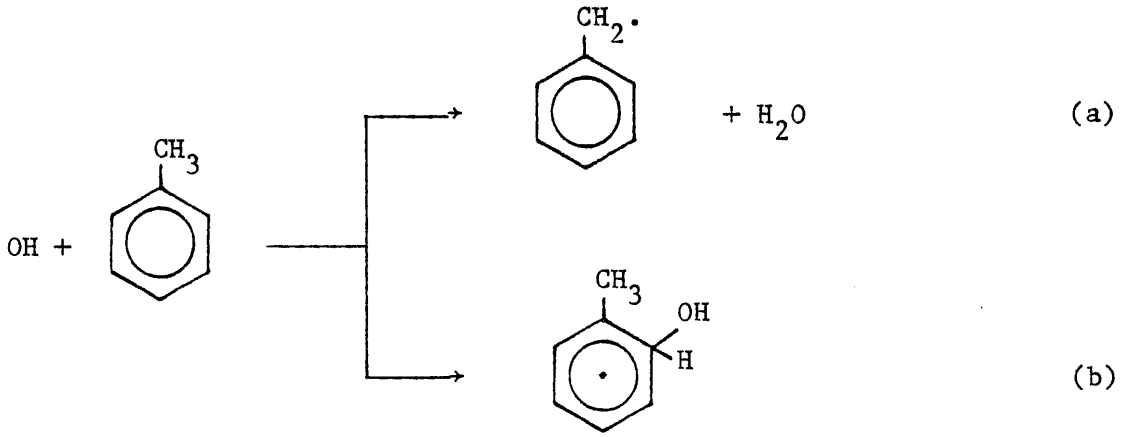

(A)

For toluene, the most studied aromatic, $k_a/(k_a + k_b)$ ≈0.08 (Atkinson et al. 1983a).

Under atmospheric conditions, the benzyl radical will react to form benzaldehyde and benzyl nitrate. These reaction pathways have been

discussed in detail previously (Atkinson et al. 1980) and are analogous to the relatively well known alkyl radical reactions.

The uncertainties in the aromatic-NO_x photooxidation mechanisms lie in the fate of the addition adducts (A). Both experimentally and theoretically, the situation is unclear, but some data are available which allow a reasonable mechanism to be postulated (Atkinson et al. 1980, 1983a).

The OH-aromatic adducts can react with O_2 via two pathways: H-atom abstraction to form cresols, or reversible O_2 addition to the adduct (Atkinson et al. 1979, 1980):

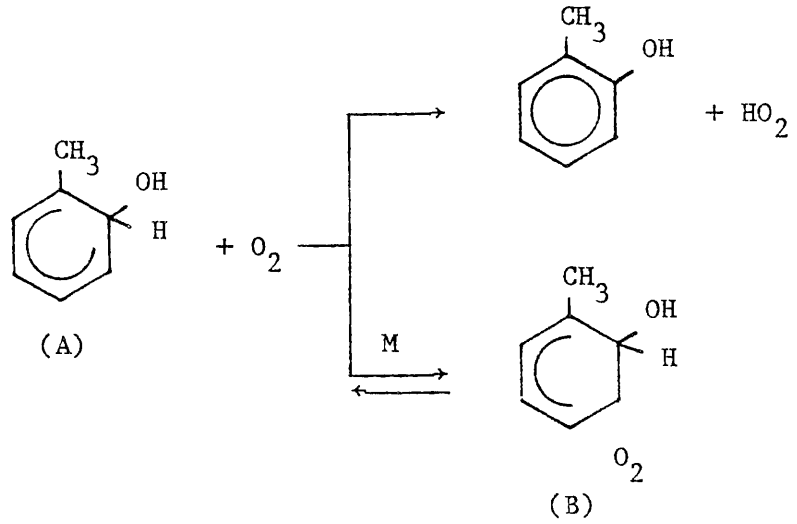

Recent work from these laboratories (Atkinson et al. 1983a) has shown that the o-cresol yield from toluene is 13 ± 7%, independent of pressure over the range ~60-740 torr.

The prompt formation of biacetyl and other α-dicarbonyls in the NO_x photooxidation of o-xylene (Darnall et al. 1979, Takagi et al. 1980) and the observation of 1,4-unsaturated dicarbonyls from toluene (Besemer 1982) and 1,2,4-triethylbenzene (Takagi et al. 1982) indicates that the only plausible reaction pathway occurs via the formation of bicyclic radicals of the form

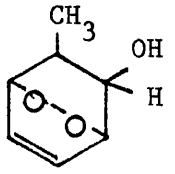

(C)

These bicyclic radicals must presumably then add O_2 and react with NO similar to alkyl radicals:

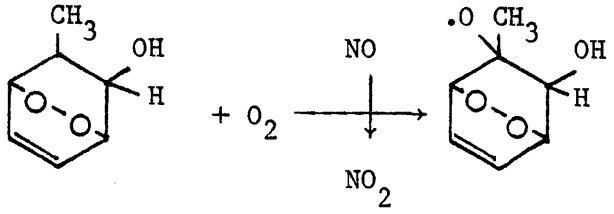

followed by spontaneous decomposition of the resulting bicyclic oxy radicals, yielding, in the case of toluene, methylglyoxal and cis-2,4-butenedial, for initial attack of the OH radical at the ortho position.

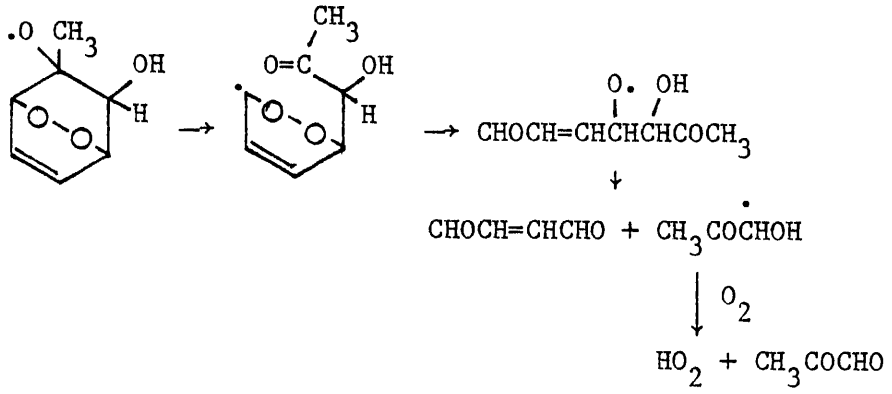

OH radical addition at the meta and para positions will, by analogous reaction pathways, yield glyoxal instead of methylglyoxal as the α-dicarbonyl.

Extension of the toluene mechanism to other aromatics is relatively straightforward. In the case of benzene, H-atom abstraction from the aromatic ring is essentially negligible (Atkinson et al. 1979, Tully et

al. 1981), and so OH radical addition is the sole process. By analogous reaction schemes to those shown above for toluene, the products expected are phenol and, from ring cleavage, the dicarbonyls, glyoxal [$(CHO)_2$] and 2-butene-1,4-dial [CHOCH=CHCHO]. Glyoxal apparently does not photolyze in the actinic region to yield radicals (Calvert and Pitts 1966, Osamura et al. 1981), but rather photodissociates to formaldehyde and carbon monoxide.

$$(CHO)_2 + h\nu \rightarrow HCHO + CO$$

It is of interest to note that this postulated reaction scheme predicts that benzene, unlike toluene and the xylenes (Pitts et al. 1979), should have low photochemical reactivity since (a) it has a comparatively low OH radical reaction rate constant of 1.2×10^{-12} cm^3 $molecule^{-1}$ sec^{-1} at 298 K (Atkinson et al. 1979, Tully et al. 1981) and (b) its major product, glyoxal, apparently does not photodissociate to form radicals (as do the analogous α-dicarbonyls methylglyoxal and biacetyl, formed from toluene and the xylenes).

Although this mechanism appears to be consistent with the available data, much more experimental data are needed before the same level of understanding is achieved as is the case presently for the alkanes or alkenes. In particular, the yields of the α-dicarbonyls and of phenolic compounds from the aromatics are of great importance, and the photolysis rates and OH radical reaction rate constants for the α-dicarbonyls are needed in order to develop accurate detailed chemical computer models for this class of organics. In addition, it is of interest to experimentally verify whether benzene is indeed relatively unreactive in NO_x-air irradiations, as predicted by this mechanism.

During this ARB-funded program, we have carried out the following exploratory studies dealing mainly with benzene and α-dicarbonyls:

- The yields of glyoxal from benzene and glyoxal and methylglyoxal from toluene during their CH_3ONO-NO-air photooxidations have been determined using differential optical absorption spectroscopy to monitor the dicarbonyls.
- The yield of phenol from benzene during these irradiations has been determined using gas chromatography.

- The OH radical rate constants and the photolysis rates in the SAPRC 5800-ℓ evacuable chamber of the α-dicarbonyls glyoxal, methylglyoxal and biacetyl have been determined.
- A series of NO_x-air photooxidations of benzene in the SAPRC 6400-ℓ all-Teflon chamber has been carried out.

These studies, and the data obtained, are described in the following sections.

B. Hydroxyl Radical Rate Constants and Photolysis Rates of α-Dicarbonyls

Rate constants for the reactions of OH radicals with glyoxal and methylglyoxal were determined at 298 ± 2 K, relative to the rate constant for the reaction of OH radicals with cyclohexane, and the photolysis rates of glyoxal, methylgyoxal and biacetyl were obtained in 1 atm of air in an environmental chamber. In addition, upper limits to the rate constants for the reaction of O_3 with glyoxal and methylglyoxal were determined at 298 ± 2 K.

Experimental

Photolysis and OH Radical Reactions. The technique for the determination of relative OH radical rate constants and of photolysis rates was essentially identical to those described in Section II.B above. Hydroxyl radicals were generated by the photolysis of methyl nitrite in air at ≳290 nm, at part-per-million concentrations:

$$CH_3ONO + h\nu \rightarrow CH_3O + NO$$

$$CH_3O + O_2 \rightarrow HCHO + HO_2$$

$$HO_2 + NO \rightarrow OH + NO_2$$

In order to minimize the formation of O_3 during these irradiations, NO was included in the reaction mixtures. In the presence of an α-dicarbonyl and a reference organic (cyclohexane in this case), the OH radicals can, besides reacting with CH_3ONO, NO, NO_2 and the organic reaction products, react with these organics:

$$OH + \text{dicarbonyls} \rightarrow \text{products} \quad (1)$$

$$OH + \text{cyclohexane} \rightarrow \text{products} \quad (2)$$

Additionally, the α-dicarbonyls also photolyze:

$$\text{dicarbonyl} + h\nu \rightarrow \text{products} \quad (3)$$

Under the experimental conditions employed, reactions of the dicarbonyls and cyclohexane with $O(^3P)$ atoms and O_3 were negligible, and since dilution due to sampling was also negligible (<0.2%), then

$$\frac{-d[\text{dicarbonyl}]}{dt} = k_1[OH][\text{dicarbonyl}] + k_3[\text{dicarbonyl}] \quad (I)$$

$$\frac{-d[\text{cyclohexane}]}{dt} = k_2[OH][\text{cyclohexane}] \quad (II)$$

and hence

$$\ln\left(\frac{[\text{dicarbonyl}]_{t_o}}{[\text{dicarbonyl}]_t}\right) = k_1 \int_{t_o}^{t} [OH]dt + k_3(t-t_o) \quad (III)$$

and

$$\ln\left(\frac{[\text{cyclohexane}]_{t_o}}{[\text{cyclohexane}]_t}\right) = k_2 \int_{t_o}^{t} [OH]dt \quad (IV)$$

where k_1, k_2 and k_3 are the rate constants for reactions (1), (2) and (3), respectively, $[\text{dicarbonyl}]_{t_o}$ and $[\text{cyclohexane}]_{t_o}$ are the concentrations of the α-dicarbonyl and cyclohexane, respectively, at time t_o, and $[\text{dicarbonyl}]_t$ and $[\text{cyclohexane}]_t$ are the corresponding concentrations at time t. Eliminating the integrated OH radical concentrations from equations (III) and (IV) yields

$$\frac{1}{(t-t_o)} \ln\left\{\frac{[\text{dicarbonyl}]_{t_o}}{[\text{dicarbonyl}]_t}\right\} = k_3 + \frac{k_1}{k_2(t-t_o)} \ln\left\{\frac{[\text{cyclohexane}]_{t_o}}{[\text{cyclohexane}]_t}\right\} \quad (V)$$

Hence plots of $(t-t_o)^{-1}$ ln ($[dicarbonyl]_{t_o}/[dicarbonyl]_t$) against $(t-t_o)^{-1}$ ln ($[cyclohexane]_{t_o}/[cyclohexane]_t$) should yield straight lines of slope k_1/k_2 and intercept k_3. The OH radical concentrations during the irradiations were varied by changing the initial CH_3ONO concentrations, and irradiations were also carried out in the absence of CH_3ONO to minimize the OH radical concentrations.

Irradiations of CH_3ONO-dicarbonyl-cyclohexane-NO-air and dicarbonyl-cyclohexane-air mixtures were carried out in the SAPRC 5800-ℓ Teflon-coated, evacuable, thermostatted environmental chamber, equipped with a 25-KW xenon arc solar simulator. The radiation from this solar simulator, which approximates that of the deep-space solar spectrum in the ultraviolet and visible regions (Winer et al. 1980), was filtered by passage through a 0.64-cm Pyrex pane in order to eliminate radiation below ~300 nm. The resulting spectral distribution, which approximates that of the lower tropospheric solar spectrum, measured at the time of the present experiments is shown in Figure III-1. The absolute light intensity, monitored as the photolysis rate of NO_2 in N_2 (Winer et al. 1980), was 1.40×10^{-3} sec^{-1}, with an estimated uncertainty of ~ ±10%.

Cyclohexane was quantitatively monitored prior to and during the irradiations by gas chromatography with flame ionization detection using a 20-ft x 1/8-in stainless steel column with 5% DC703/C20 M on 100/120 mesh AW, DMCS Chromosorb G, operated at 333 K. The α-dicarbonyls were monitored prior to and during the irradiations by differential optical absorption spectroscopy (DOAS) with a multi-pass optical system (3.77-m focal length White system) arranged along the longitudinal axis of the chamber using typically 32 passes, corresponding to a 120.6-m pathlength. The wavelength regions used to monitor these α-dicarbonyls were from 430-460 nm (Coveleskie and Yardley 1975).

For glyoxal and methylglyoxal, irradiations of α-dicarbonyl-cyclohexane-air and α-dicarbonyl-CH_3ONO-NO-cyclohexane-air irradiations were carried out. The initial concentrations were: glyoxal, $\sim 1.2 \times 10^{14}$ molecule cm^{-3} or methylglyoxal, $\sim 2.4 \times 10^{14}$ molecule cm^{-3}; CH_3ONO (when present), $\sim(3\text{-}20) \times 10^{13}$ molecule cm^{-3}; NO (when present), $\sim(2\text{-}3) \times 10^{13}$ molecule cm^{-3} and cyclohexane, $\sim 2.4 \times 10^{13}$ molecule cm^{-3}. It should be noted that since photolysis of these α-dicarbonyls can, in the presence of NO, yield OH radicals and since glyoxal and methylglyoxal react rapidly

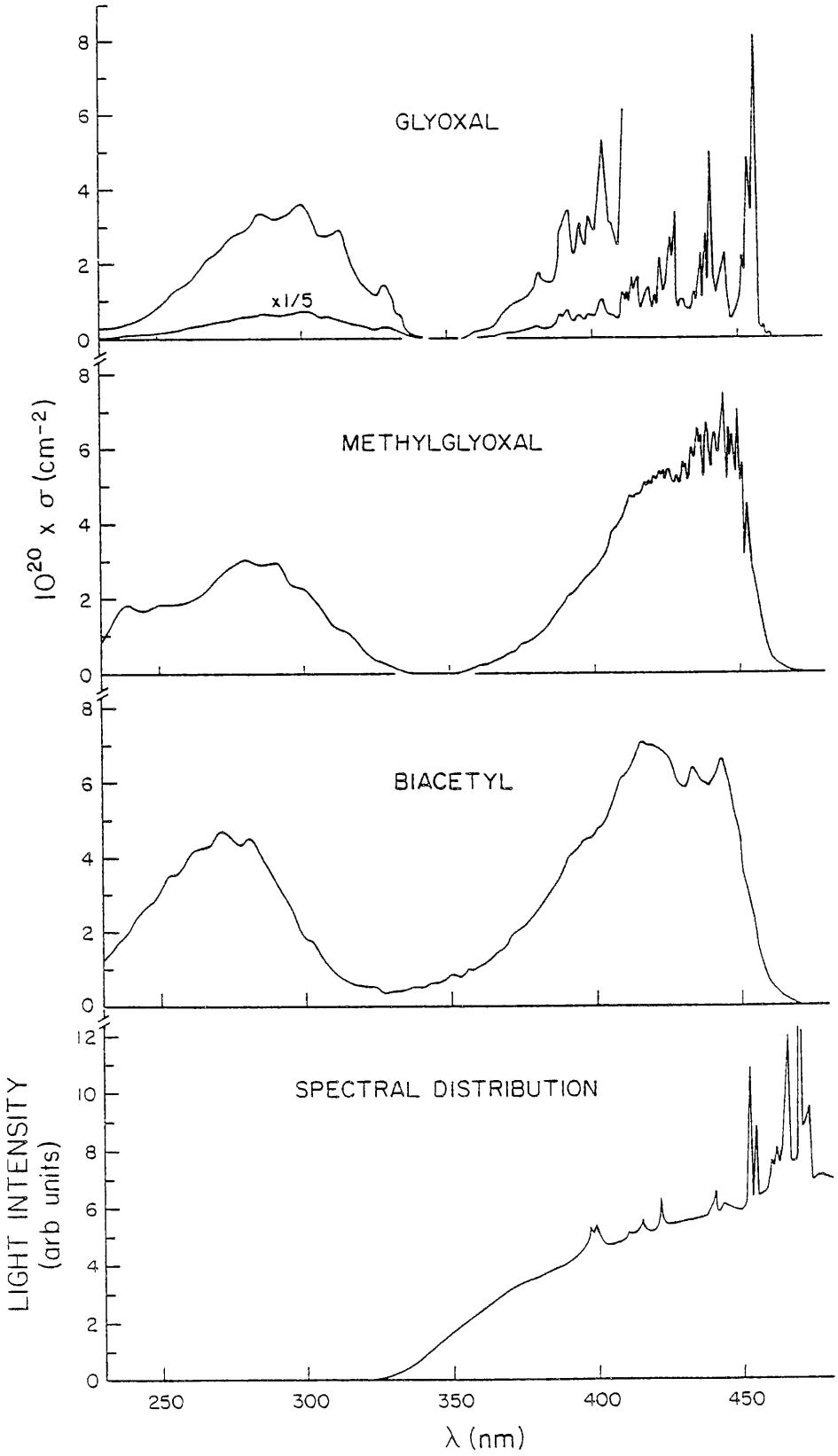

Figure III-1. Gas Phase Absorption Spectra Determined for Glyoxal, Methylglyoxal and Biacetyl, Together with the Relative Spectral Distribution Used in This Study.

with OH radicals, the observed glyoxal and methylglyoxal decay rates in the α-dicarbonyl-air irradiations are expected to be higher than the actual photolysis rates. For biacetyl, only a biacetyl-air photolysis was carried out, at an initial concentration of biacetyl of ~2.7 x 10^{14} molecule cm^{-3}, since the reaction of OH radicals with biacetyl is very slow (Darnall et al. 1979) and the observed biacetyl decay rate corresponds to its photolysis rate.

Ozone Reactions. The technique used for the determination of the ozone reaction rate constants was based on observing the rate of ozone decay in the presence of a known excess of a reactive compound (Atkinson et al. 1981b, 1983c). In the presence of such a reactant, the processes removing O_3 are:

$$O_3 + \text{wall} \rightarrow \text{loss of } O_3 \qquad (4)$$

$$O_3 + \text{dicarbonyl} \rightarrow \text{products} \qquad (5)$$

and hence

$$\frac{-d[O_3]}{dt} = (k_4 + k_5)[\text{dicarbonyl}](O_3) \qquad (VI)$$

where k_4 and k_5 are the rate constants for reactions (4) and (5). With the dicarbonyl concentration being in large excess over the initial O_3 concentration ($[\text{dicarbonyl}]/[O_3]_{\text{initial}} \geq 100$), the dicarbonyl concentration remained essentially constant throughout the reaction, and equation (VI) may be rearranged to yield:

$$\frac{-d\ln[O_3]}{dt} = k_4 + k_5[\text{dicarbonyl}] \qquad (VII)$$

Thus, with a knowledge of k_4, the background ozone decay rate, the rate constant k_5, or an upper limit thereof, can be readily obtained.

As described previously (Atkinson et al. 1981b, 1983c), reactions were carried out in a ~175-ℓ volume Teflon bag constructed out of a 2-mil thick, 180 x 140-cm FEP Teflon sheet, heat-sealed around the edges and fitted with Teflon injection and sampling ports at each end of the bag. The reaction bag was initially divided into two subchambers, with O_3 being

injected into one subchamber and the dicarbonyl into the other. The reactions were initiated by removing the bag divider and rapidly mixing the contents of the bag by pushing down on alternate sides of the entire bag for ~1 min. Initial O_3 concentrations after mixing were ~2 x 10^{13} molecule cm^{-3} and, after mixing of the reactants, the O_3 concentrations were monitored as a function of time by a Monitor Labs Model 8410 chemiluminescence ozone analyzer.

Absorption Cross-Sections. For the purpose of calculating effective quantum yields (see below), the absorption cross-sections for glyoxal, methylglyoxal and biacetyl were determined using a Cary 17-D spectrophotometer and known pressures (~3-13 torr as measured with an MKS Baratron capacitance manometer) of the α-dicarbonyls.

Materials. Glyoxal and methylglyoxal were prepared by first evaporating a commercially available glyoxal-water or methylglyoxal-water solution to dryness under vacuum. Then, after adding P_2O_5 to the resulting crystalline- or polymer-like material and mixing, the α-dicarbonyl was distilled off under vacuum and collected at 77 K. Biacetyl and cyclohexane were obtained from the Aldrich Chemical Company.

Results

Photolysis and OH Radical Reactions of Glyoxal and Methylglyoxal. Irradiations of glyoxal or methylglyoxal-cyclohexane-air and glyoxal or methylglyoxal-CH_3ONO-NO-cyclohexane-air mixtures were carried out, with cyclohexane serving as the reference organic. The data from these irradiations, plotted in the form of equation (V), are shown in Figures III-2 and III-3 for glyoxal and methylglyoxal, respectively. It can be seen from these figures that the data yield good straight line plots, in accordance with equation (V), and the slopes (yielding the rate constant ratios k_1/k_2) and the intercepts (the glyoxal or methylglyoxal photolysis rates k_3) are given in Table IV-1. The OH radical concentrations, as derived from the cyclohexane decay rates via equation (II), were higher by a factor of ~30-100 and 3-9 for the glyoxal and methylglyoxal systems, respectively, when CH_3ONO was included in the initial reactant mixture, compared to when CH_3ONO was absent.

During the irradiation of the glyoxal-cyclohexane-air mixture, formaldehyde, a potential photolysis product (Osamura et al. 1981), was

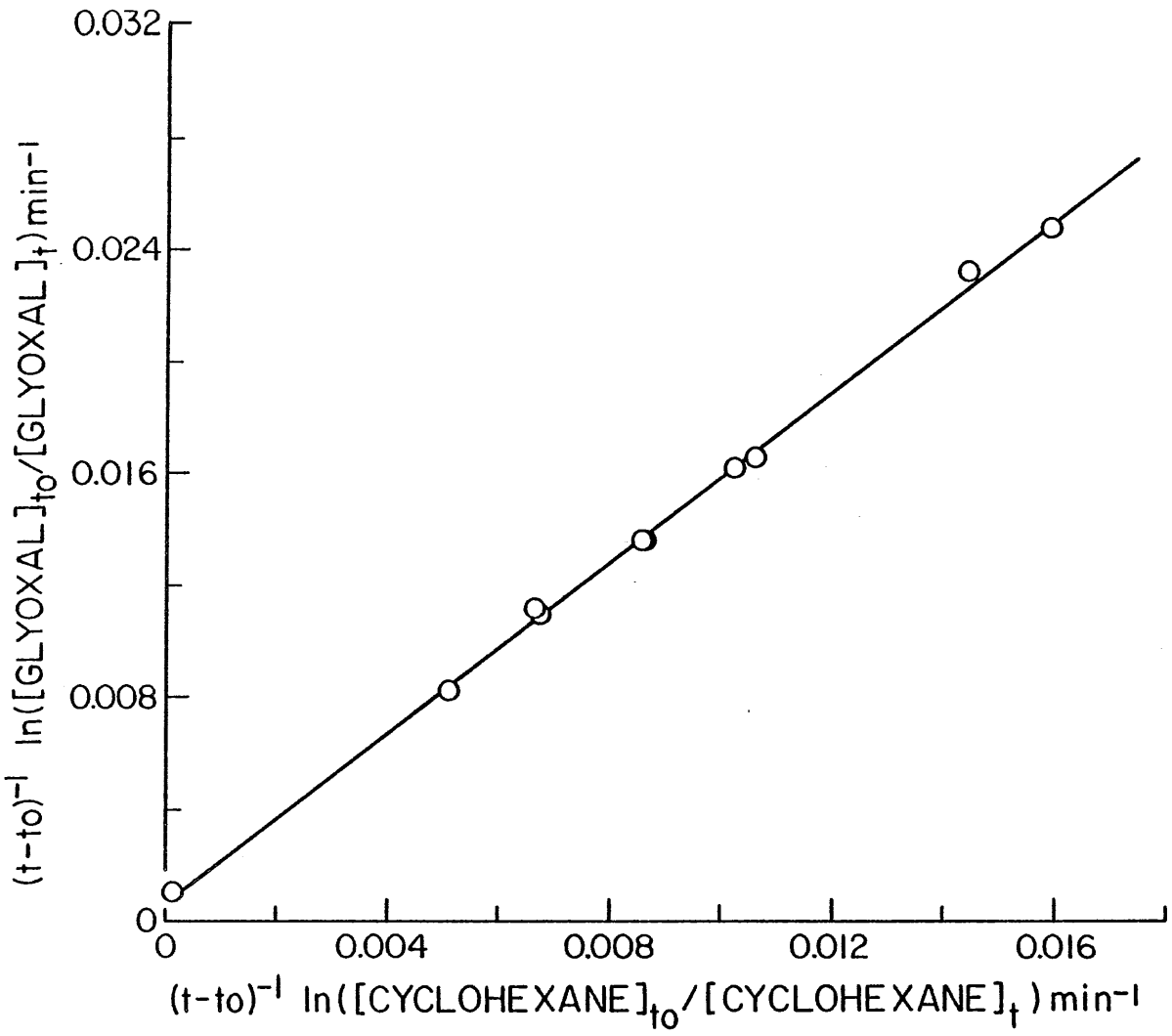

Figure III-2. Plot of Equation (V) for Glyoxal.

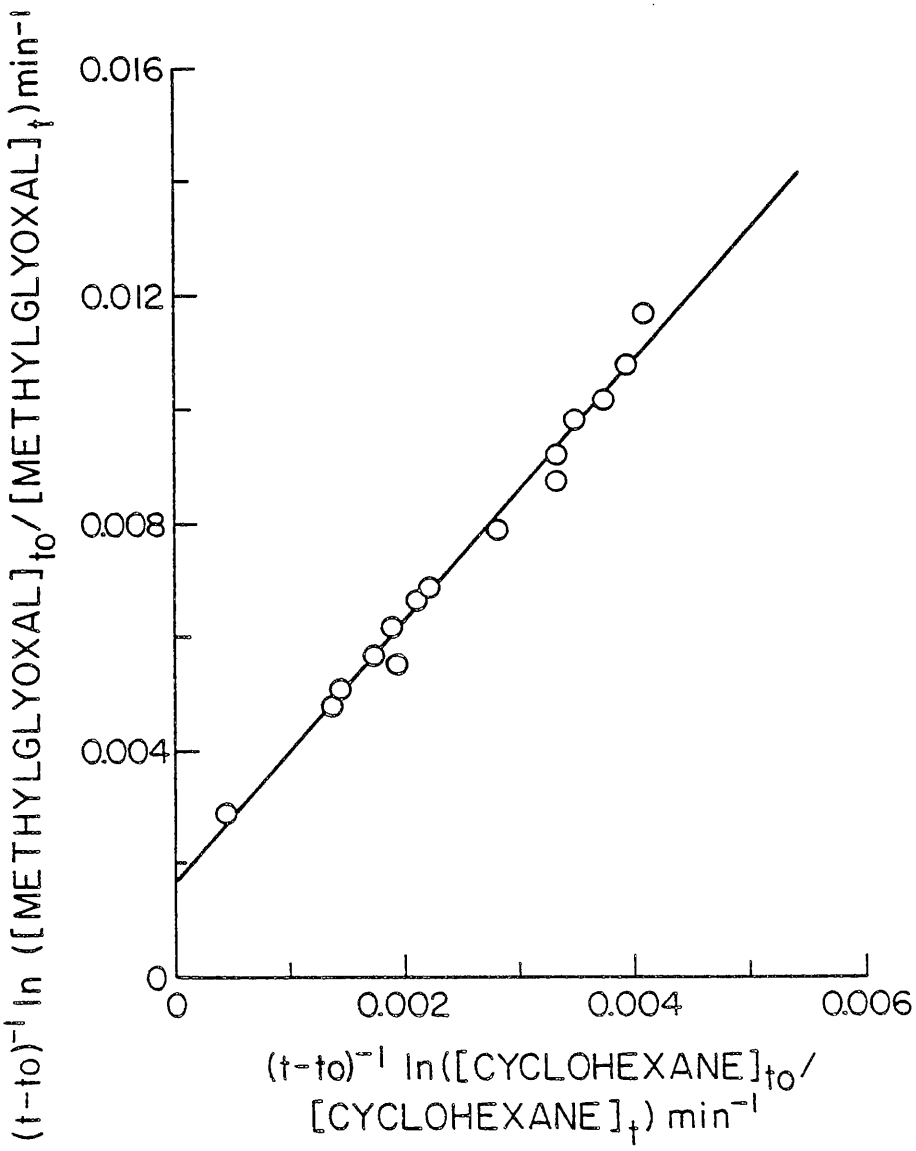

Figure III-3. Plot of Equation (V) for Methylglyoxal.

Table III-1. Photolysis Rates k_3 and OH Radical Reaction Rate Constant Ratios k_1/k_2 and Rate Constants k_1 for the α-Dicarbonyls Studied

α-Dicarbonyl	k_1/k_2[a]	$10^{11} \times k_1$ (cm^3 $molecule^{-1}sec^{-1}$)[a,b]	$10^5 \times k_3$ (sec^{-1})[a,c]
Glyoxal	1.52 ± 0.05	1.15 ± 0.04	1.1 ± 0.7
Methylglyoxal	2.29 ± 0.16	1.73 ± 0.13	2.7 ± 0.7
Biacetyl	d	d	5.0 ± 0.3

[a]Indicated error limits are two least squares standard deviations.

[b]Placed on an absolute basis using a rate constant of $k_2 = (7.57 \pm 0.05) \times 10^{-12}$ cm^3 $molecule^{-1}$ sec^{-1}, which in turn is based on a rate constant for the reaction of OH radicals with n-butane of 2.58×10^{-12} cm^3 $molecule^{-1}$ sec^{-1} (Atkinson et al. 1982a).

[c]At an NO_2 photolysis rate constant of 1.4×10^{-3} sec^{-1}.

[d]See text.

detected by DOAS at the end of the irradiation at a concentration of 9.0×10^{11} molecule cm^{-3}, which corresponds to a yield of ~13% of the glyxoal photolyzed.

Photolysis of Biacetyl. Since reaction of biacetyl with OH radicals is slow [$k_2 = 2.4^{+0.8}_{-0.6} \times 10^{-13}$ cm^3 $molecule^{-1}$ sec^{-1} (Darnall et al. 1979)], the photolysis rate for biacetyl was obtained directly from the exponential biacetyl disappearance in an irradiated biacetyl-air mixture. This photolysis rate is also given in Table III-1.

Ozone Reactions. The O_3 decay rates obtained in the presence of $\sim 3 \times 10^{15}$ molecule cm^{-3} of glyoxal and methylglyoxal were 7×10^{-6} sec^{-1} and 1.8×10^{-5} sec^{-1}, respectively. These ozone decay rates in the presence of added glyoxal or methylglyoxal were indistinguishable from the background O_3 decay rates observed in the absence of reactants, which typically range from $\sim(5\text{-}30) \times 10^{-6}$ sec^{-1} in this system. Thus, from these data, upper limits to the rate constants k_5 of

$$k_5(\text{glyoxal}) < 3 \times 10^{-21} \text{ cm}^3 \text{ molecule}^{-1} \text{ sec}^{-1}$$

and $k_5(\text{methylglyoxal}) < 6 \times 10^{-21}$ cm^3 molecule^{-1} sec^{-1}

can be derived.

Discussion

Reaction with OH Radicals and O_3. The present rate constant for reaction of OH radicals with methylglyoxal of $k_1 = (1.73 \pm 0.13) \times 10^{-11}$ cm^3 molecule^{-1} sec^{-1} at 298 ± 2 K is a factor of 2.4 higher than the recent absolute value obtained using the flash photolysis-resonance fluorescence technique (Kleindienst et al. 1982). The reason for this discrepancy is not known at the present time, but the rate constants k_1 for glyoxal and methylglyoxal determined here are very similar to those at room temperature for formaldehyde ($k_1 = 1.0 \times 10^{-11}$ cm^3 molecule^{-1} sec^{-1} (Atkinson and Pitts 1978, Stief et al. 1980) and acetaldehyde ($k_1 = 1.6 \times 10^{-11}$ cm^3 molecule^{-1} sec^{-1} (Atkinson and Pitts 1978), respectively, indicating that the extra >C=O group has little effect on these reactions. These OH radical rate constants are expected to be essentially independent of temperature over a small temperature range centered at ~300 K, and lead to 1/e atmospheric lifetimes due to reaction with OH radicals of ~24 hr and ~16 hr for glyoxal and methylglyoxal, respectively, assuming an OH radical concentration of 1×10^6 cm^{-3}.

The upper limits for the rate constant for reaction of O_3 with methylglyoxal of $k_5 < 6 \times 10^{-21}$ cm^3 molecule^{-1} sec^{-1} determined in this work is totally consistent with the previous room temperature data from these laboratories (Pate et al. 1976, Atkinson et al. 1981b) which yielded values of $k_5 = (1.1 \pm 0.5) \times 10^{-21}$ cm^3 molecule^{-1} sec^{-1} (Pate et al. 1976) and $k_5 < 7 \times 10^{-20}$ cm^3 molecule^{-1} sec^{-1} (Atkinson et al. 1981b). Thus, these data show that, as expected, reaction with O_3 is negligible for these α-dicarbonyls under atmospheric conditions.

Photolysis. The photolysis rates for the α-dicarbonyls given in Table III-1 are only strictly applicable for the light intensity and spectral distribution employed in these irradiations. However, these data can be normalized for differences in the light intensity by dividing the observed α-dicarbonyl photolysis rates by the observed NO_2 photodissociation rate constant of 1.4×10^{-3} sec^{-1} measured under the same experimental conditions, and the resulting photolysis rate ratios are given in

Table III-2. The present ratio of the biacetyl and NO_2 photolysis rates of 0.036 ± 0.004 is in excellent agreement with the ratio of 0.032-0.040 obtained previously by Darnall et al. (1979) in the same environmental chamber at a higher light intensity.

The ratio of the rate constants for the photolysis of the α-dicarbonyls, k_3, relative to that for NO_2, k_{NO_2}, can be related to the absorption cross-sections, σ_λ, of the α-dicarbonyls and the relative spectral distribution, J_λ^{rel}, of the radiation according to the expression

$$\frac{k_3}{k_{NO_2}} = \frac{\int_{\lambda_{min}}^{\lambda_{max}} J_\lambda^{rel}\ \sigma_\lambda\ \phi_\lambda d\lambda}{\int_{\lambda_{min}}^{\lambda_{max}} J_\lambda^{rel}\ \sigma_\lambda^{NO_2}\ \phi_\lambda^{NO_2}\ d\lambda} \qquad \text{(VIII)}$$

where ϕ_λ is the quantum yield for photodissociation of the α-dicarbonyl, $\sigma_\lambda^{NO_2}$ and $\phi_\lambda^{NO_2}$ are the known (NASA 1982, Atkinson and Lloyd 1983) NO_2 absorption cross-sections and photodissociation quantum yields, respectively, and λ_{min} and λ_{max} are the minimum (~290 nm) and maximum (~470 nm for the α-dicarbonyls, 420 nm for NO_2) wavelengths for which photodissociation occurs in the present experimental system. The measured absorption cross-sections for glyoxal, methylglyoxal and biacetyl are plotted as a function of wavelength in Figure III-1, which also shows the relative spectral distribution used in this study.

Thus the only unknown quantity in equation (VIII) is the quantum yield for the photodissociation of the α-dicarbonyls. However, since these quantum yields cannot exceed unity, equation (VIII) allows the maximum photolysis rate ratios k_3/k_{NO_2} to be calculated by setting $\phi_\lambda = 1$ at all wavelengths, and these calculated maximum photolysis rate ratios are given in Table III-2, along with the experimentally determined ratios. Also given in Table III-2 are the photolysis rate ratios calculated on the assumption that photodissociation only occurs from the lower wavelength absorption band, i.e.

$$\phi_\lambda = 1 \text{ for } \lambda \leq 340 \text{ nm}$$

Table III-2. Observed and Calculated Photolysis Rate Ratios k_3/k_{NO_2} for Glyoxal, Methylglyoxal and Biacetyl, and Calculated α-Dicarbonyls Effective Quantum Yields

	k_3/k_{NO_2}			
		Calc		Effective
α-Dicarbonyl	Obs[a]	$\phi_\lambda = 1$	$\phi_\lambda = 1, \lambda \leq 340$ nm $\phi_\lambda = 0, \lambda > 340$ nm	Quantum Yield ϕ[b]
Glyoxal	0.008 ± 0.005	0.29	0.00038	0.029 ± 0.018
Methylglyoxal	0.019 ± 0.005	0.18	0.00003	0.107 ± 0.030
Biacetyl	0.036 ± 0.004	0.23	0.00007	0.158 ± 0.024

[a]The indicated error limits include two standard deviations of the α-dicarbonyl photolysis rates (Table III-1) together with a 10% uncertainty in k_{NO_2}.

[b]Effective quantum yield = $[k_3/k_{NO_2}(\text{obs})]/[k_3/k_{NO_2}(\text{calc}, \phi_\lambda = 1)]$.

$$\phi_\lambda = 0 \text{ for } \lambda > 340 \text{ nm}$$

It can be seen from Table III-2 that the observed photolysis rate ratios are significantly less than the calculated maximum values. However, it is also clear from Table III-2 that the α-dicarbonyl photodissociation quantum yields at $\lambda > 340$ nm must be non-negligible, since the use of $\phi_\lambda = 1$ ($\lambda \leq 340$ nm), $\phi_\lambda = 0$ ($\lambda > 340$ nm) leads to calculated photolysis rate ratios much lower than the observed values. Thus these data show that for glyoxal $\gtrsim$ 95%, and for methylglyoxal and biacetyl >99%, of the presently observed α-dicarbonyl photodissociation occurs from the 340-470 nm absorption band, and that relaxation processes such as fluorescence or relaxation to the ground state compete significantly with photodecomposition in this wavelength region.

The "effective" quantum yields for the photodissociation of the α-dicarbonyls studied here, obtained by dividing the observed photolysis rate ratios by those calculated assuming $\phi_\lambda = 1$, are given in Table III-2 and are 0.03 for glyoxal, 0.11 for methylglyoxal and 0.16 for biacetyl. Since, in general, it is expected that ϕ_λ will vary with wavelength, these "effective" quantum yields are valid only for the particular spectral

distribution used in this study. However, since the spectral distribution of the filtered solar simulator used is similar to that of sunlight in the lower troposphere (Winer et al. 1980), then the photolysis rate ratios k_3/k_{NO_2} observed here can be used with the NO_2 photodissociation rate constants k_{NO_2} to estimate the atmospheric α-dicarbonyl photolysis rates k_3.

These estimated atmospheric photodecomposition lifetimes for glyoxal, methylglyoxal and biacetyl are compared in Table III-3 with the estimated lifetimes for removal of these species by reaction with OH radicals and with O_3. It can be seen that, despite the relatively low "effective" photodissociation quantum yields, the photodissociation lifetimes are appreciably shorter than the lifetimes due to reaction with OH radicals or O_3 (the latter reaction being essentially negligible). Photolysis of these α-dicarbonyls is thus clearly their major tropospheric loss process.

The formation of peroxyacetyl nitrate (PAN) was observed during the irradiation of methylglyoxal-NO_x-air and biacetyl-NO_x-air mixtures, showing that in both cases, photodissociation yields, at least partially, CH_3CO radicals:

$$CH_3COCHO + h\nu \rightarrow CH_3CO + CHO$$

$$CH_3COCOCH_3 + h\nu \rightarrow 2\ CH_3CO$$

followed by (Atkinson and Lloyd 1983)

$$CH_3CO + O_2 \rightarrow CH_3CO_3$$

$$CH_3CO_3 + NO_2 \rightleftarrows CH_3C(=O)OONO_2 \quad \text{(PAN)}$$

However, the magnitude of these and other photodissociation pathways was not determined in this work.

For glyoxal, the observation of formaldehyde shows that the process

$$(CHO)_2 + h\nu \rightarrow HCHO + CO$$

occurs, with the formaldehyde yield corresponding to approximately 13% of

Table III-3. Atmospheric Lifetimes of Glyoxal, Methylglyoxal and Biacetyl Due to Photolysis, Reaction with OH Radicals and Reaction with O_3

α-Dicarbonyl	$\tau_{Photolysis}$[a] (hrs)	τ_{OH}[b] (hrs)	τ_{O_3}[c] (hrs)
Glyoxal	5	24	$>9 \times 10^4$
Methylglyoxal	2	16	$>4 \times 10^4$
Biacetyl	1	>900	$\gtrsim 4 \times 10^{4}$[d]

[a]At a zenith angle of 0°.

[b]At an OH radical concentration of 1×10^6 cm^{-3}.

[c]At an O_3 concentration of 1×10^{12} cm^{-3} (40 ppb).

[d]Estimated by analogy with glyoxal and methylglyoxal.

the glyoxal photolyzing via this pathway. (Loss of formaldehyde by photolysis and reaction with OH radicals was minor under the irradiation conditions employed.) Hence the major photodissociation pathway of glyoxal is probably

$$(CHO)_2 + h\nu \rightarrow 2\ CO + H_2$$

as has been discussed recently (Osamura et al. 1981).

Conclusion

While obviously further work is needed concerning the photodissociation pathways and wavelength-dependent quantum yields for the region λ >290 nm, the present data are important and necessary inputs to chemical kinetic computer modeling studies of the aromatic hydrocarbons and of isoprene. In particular, this work indicates that the photolysis rate of methylglyoxal, a critical parameter in NO_x-air photooxidation chemical computer models for toluene and other aromatics, is significantly lower than has been previously assumed (thus the present photolysis rate ratio of $k_3/k_{NO_2} = 0.019 \pm 0.005$ can be compared to the previously assumed ratios of ~0.045 (Killus and Whitten 1982) and 0.15 (Atkinson et al.

1980). Thus, it is obvious that all present chemical computer models of the aromatic-NO_x-air systems need to be re-evaluated in light of these present data.

C. Determination of Product Yields from the NO_x Photooxidation of Benzene and Toluene

The yields of selected products (glyoxal and phenol from benzene, and glyoxal and methylglyoxal from toluene) were determined during irradiations of CH_3ONO-NO-aromatic-air mixtures. From a knowledge of the OH radical reactivities of these products, their yields, corrected for secondary reaction, could be derived. The data obtained are detailed below.

Experimental

Irradiations of CH_3ONO-NO-benzene-air and CH_3ONO-NO-toluene-air mixtures were carried out in the 5800-ℓ evacuable Teflon-coated chamber. The characteristics and operating procedures of the 5800-ℓ evacuable chamber-solar simulator facility have been described in detail previously (Winer et al. 1980), and only the pertinent details will be briefly discussed here.

The solar simulator, employing a 25 KW point source xenon arc, provides a well-collimated light beam which, to a large extent, does not illuminate the chamber walls, thus minimizing wall photochemistry. In all experiments reported here, a 0.64 cm Pyrex pane was used to obtain a spectral distribution applicable to that in the lower troposphere. The light intensity within the chamber was monitored by measuring the rate of photolysis of NO_2 in N_2 (k_1) by the method described by Holmes et al. (1973) with updated rate constants (Hampson and Garvin 1978).

Between irradiations the chamber was evacuated overnight to $\lesssim 2 \times 10^{-5}$ torr (Winer et al. 1980). For these experiments, the chamber was initially filled to ~10 torr with dry N_2, and then NO and CH_3ONO were flushed into the chamber from an ~5-ℓ Pyrex bulb attached to a vacuum line by a stream of ultra-high purity nitrogen. The NO was purified by passage through a trap containing activated Linde Molecule Sieve 13X. After these injections, the chamber was filled to ~740 torr with purified matrix air (Doyle et al. 1977, Winer et al. 1980), and the aromatic was injected by flushing the contents of an ~1-ℓ Pyrex bulb dosed with the desired amount

of aromatic into the chamber with N_2. The α-dicarbonyls were monitored by differential optical absorption spectroscopy (Section III.B) with an optical pathlength of 150.8 m. The aromatic hydrocarbons were monitored prior to and during the irradiations by gas chromatography with flame ionization detection (GC-FID), using a 10-ft x 1/8-in stainless steel column of 10% Carbowax 600 on C-22 Firebrick (100/120 mesh), operated at 348 K.

Phenol was monitored by GC-FID using a 6-ft x 0.25-in glass column packed with 80/100 Carbopack C/0.1% SP-1000, temperature programmed from 423-523 K at 20 K min^{-1}. Gas samples from the chamber of ~1-ℓ volume were drawn through 0.25-in x 3.25-in glass traps packed with Tenax GC 50/80 mesh. These samples were then transferred by the carrier gas at 523 K from this trap to the column head which was at 423 K, followed by the temperature programming of the column as noted above.

Because of the time involved in sampling via the Tenax packed traps (~10-15 min), three to five 10- to 20-min irradiations of the same mixture were carried out during each experiment, with GC and DOAS analyses being conducted at the end of each irradiation period.

Results and Discussion

Irradiations of CH_3ONO-NO-benzene-air and CH_3ONO-NO-toluene-air mixtures were carried out at ~303 K and 740 torr total pressure. The initial reactant concentrations and the observed amounts of aromatic hydrocarbons consumed and product species formed, as measured at various times during the irradiations, are given in Tables III-4 and III-5.

Since phenol, glyoxal and methylglyoxal react with OH radicals more rapidly than do benzene or toluene, corrections must be made for these secondary reactions in order to derive the fraction of the OH radical reaction with the aromatics yielding phenol, glyoxal and methylglyoxal. These corrections were made as described below.

Under the experimental conditions employed in the present study, the predominant loss process for phenol and the two α-dicarbonyls was via reaction with the OH radical. In particular, based on the results given in the previous section (III.B) and the measured light intensity during the irradiation, loss of the α-dicarbonyls due to photolysis was calculated to be minor. Since these products from the NO_x photooxidation of toluene are formed and lost via OH radical reactions, then

$$-d[\text{aromatic}]/dt = k_6[OH][\text{aromatic}] \quad \text{(VIII)}$$

and

$$d[\text{product}]/dt = \alpha k_6[OH][\text{aromatic}] - k_7[OH][\text{product}] \quad \text{(IX)}$$

where α is the fraction of the OH radical reaction with aromatic yielding the product under consideration, k_6 is the overall rate constant for the reaction of OH radicals with the aromatic hydrocarbon and k_7 is the rate constant for the reaction of OH radicals with the product

$$OH + \left\{ \begin{array}{l} \text{phenol} \\ \text{glyoxal} \\ \text{methylglyoxal} \end{array} \right\} \rightarrow \text{loss of product} \quad (7)$$

Under conditions where the OH radical concentration is constant, these equations can be integrated to obtain:

$$[\text{aromatic}]_t = [\text{aromatic}]_{t_o} e^{-k_6[OH]t} \quad \text{(X)}$$

and

$$[\text{product}]_t = [\text{aromatic}]_{t_o} \frac{k_6}{(k_6-k_7)} \left[e^{-k_7[OH]t} - e^{-k_6[OH]t} \right] \quad \text{(XI)}$$

where $[\text{aromatic}]_{t_o}$ is the initial aromatic hydrocarbon concentration, [OH] is the constant hydroxyl radical concentration and $[\text{aromatic}]_t$ and $[\text{product}]_t$ are the aromatic hydrocarbon and product concentrations, respectively, at time t. Equations (X) and (XI) can be combined to obtain

$$\alpha = F \left\{ \frac{[\text{product}]_t}{\Delta[\text{aromatic}]_t} \right\} \quad \text{(XII)}$$

where $\Delta[\text{aromatic}]_t$ is the amount of toluene consumed at time t, and F is

Table III-4. Experimental Data for the Benzene-CH_3ONO-NO-Air Irradiations

Run No.	Initial Concentration (ppb)			ΔBenzene (ppb)	Phenol (ppb)		Glyoxal (ppb)	
	Benzene	CH_3ONO	NO		Obs[a]	Corr[b,c]	Obs	Corr[b]
735	8681	10100	5050	515	73.9	104-139	d	
				664	94.1	166-204	d	
				760	109.7	220-264	d	
746	9958	10200	5080	292	54.1	49-74	d	
				470	89.0	116-147	d	
				663	95.8	154-190	d	
				797	127.9	245-150	125-287	180-215

[a]Peak at the same retention time observed in the pre-irradiation analyses, corresponding to 18 ± 1 ppb phenol.

[b]Corrected as discussed in text for secondary reactions.

[c]Range of values depends on whether pre-irradiation value subtracted or not.

[d]Not detected by DOAS. (Detection limit ≅ 100-150 ppb.)

Table III-5. Experimental Data for the Toluene-CH_3ONO-NO-Air Irradiation EC-747

Initial Concentration (ppb)				Glyoxal (ppb)		Methylglyoxal (ppb)	
Toluene	CH_3ONO	NO	-Δ[toluene] (ppb)	Obs	Corr[a]	Obs	Corr[a]
9400	10,000	5140	785	193	208	400	448
			1209	305	345	650	780
			1573	387	457	875	1120
			1828	466	569	b	-
			2350	497	646	b	-

[a]Corrected as discussed in text for secondary reactions.

[b]No measurement obtained.

the correction factor which takes into account the reaction of the product with the OH radical:

$$F = \left(\frac{k_6 - k_7}{k_6}\right)\left\{\frac{1 - \left(\frac{[\text{aromatic}]_t}{[\text{aromatic}]_{t_o}}\right)}{\left(\frac{k_7}{k_6}\right) - \left(\frac{[\text{aromatic}]_t}{[\text{aromatic}]_{t_o}}\right)}\right\}\left(\frac{[\text{aromatic}]_t}{[\text{aromatic}]_{t_o}}\right) \qquad \text{(XIII)}$$

Equation (XIII), which has been shown to be applicable even when the OH radical concentrations vary with time (Atkinson et al. 1982), was used to correct each of the product data points in Tables III-4 and III-5. F was calculated using the experimentally observed amounts of toluene consumed and the rate constant ratios, k_6/k_7, of 22.5 for phenol (Zetzsch 1982), 1.8 for glyoxal and 2.7 for methylglyoxal (Atkinson et al. 1979 and

Section III.B above). These correction factors were relatively minor for glyoxal and methylglyoxal ($F \leq 1.47$) but were much larger for phenol, with F being as high as 2.4 for the highest benzene conversion employed.

For benzene the sole observed glyoxal concentration corresponds to an ~25% yield of glyoxal. It should be noted that because benzene reacts so slowly with OH radicals (with a rate constant of 1.2×10^{-12} cm^3 $molecule^{-1}$ sec^{-1} [Atkinson et al. 1979]) it was difficult to achieve a high enough conversion of benzene to detect glyoxal using the DOAS system. The observed phenol yields, corrected for secondary reactions, indicate that the reaction of OH radicals with benzene yields phenol ~28 ± 8% of the time. The scatter in the data may be due, at least partially, to the difficulty of analyzing phenol and to uncertainties in the OH radical rate constant for phenol. Obviously, further work is necessary before the yields of these and other products are known with any degree of confidence.

For toluene, the glyoxal yield, after correction for secondary reactions, is plotted against the amount of toluene consumed in Figure III-4, and from a least squares analysis, the glyoxal yield is 29 ± 3%, where the indicated error is two least squares standard deviations. The methylglyoxal data correspond to an ~64% yield (Table III-5). Since the benzaldehyde and o-cresol yields have been determined (Atkinson et al. 1983a) to be 7.3 ± 2.2% and 13.1 ± 7.2%, respectively, the major expected reaction pathways thus give a reasonable (though somewhat high) overall balance, since the benzyl nitrate and the m- and p-cresol yields are expected (Atkinson et al. 1983a) to be minor (<5% combined). This scheme gives an overall product yield of ~115-120% (uncertain to at least ±20%), indicating that the major reaction pathways have indeed been monitored.

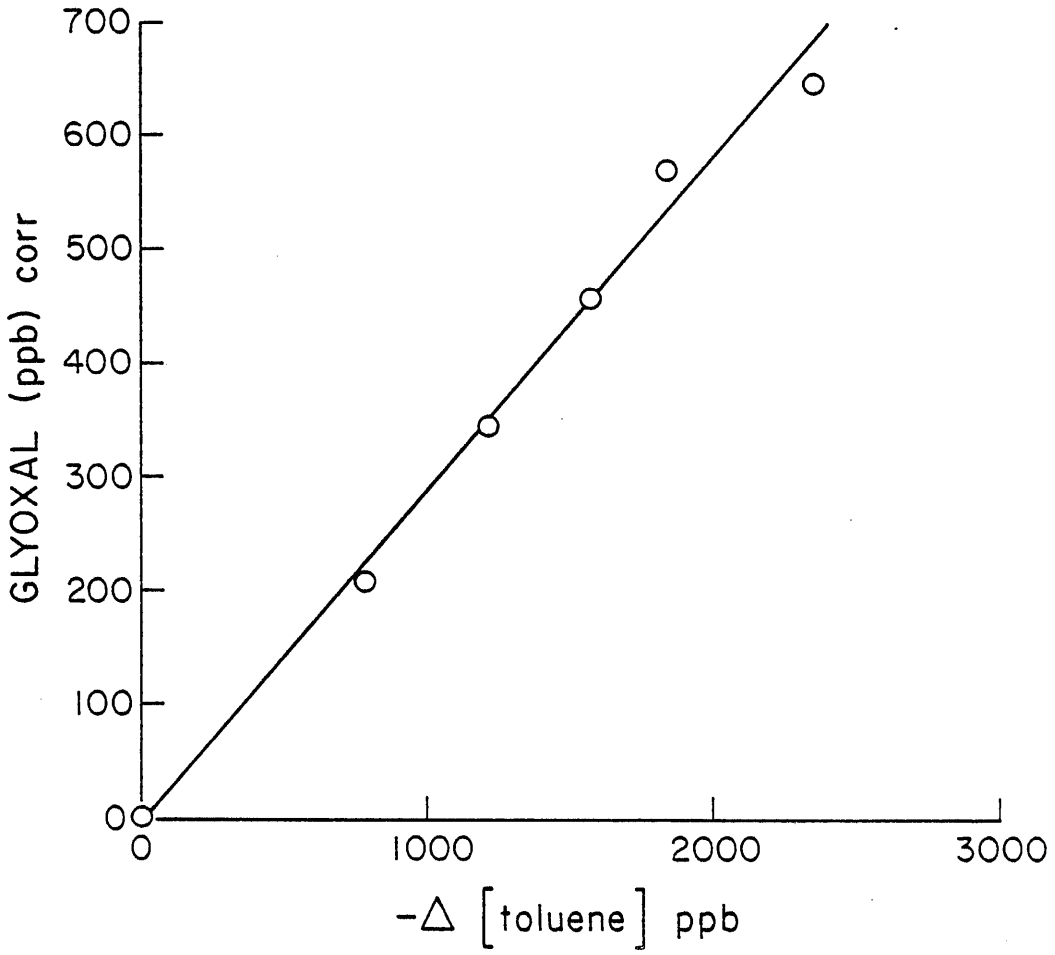

Figure III-4. Plot of the Glyoxal Yield, Corrected for Secondary Reactions (See Text) Against the Amount of Toluene Consumed.

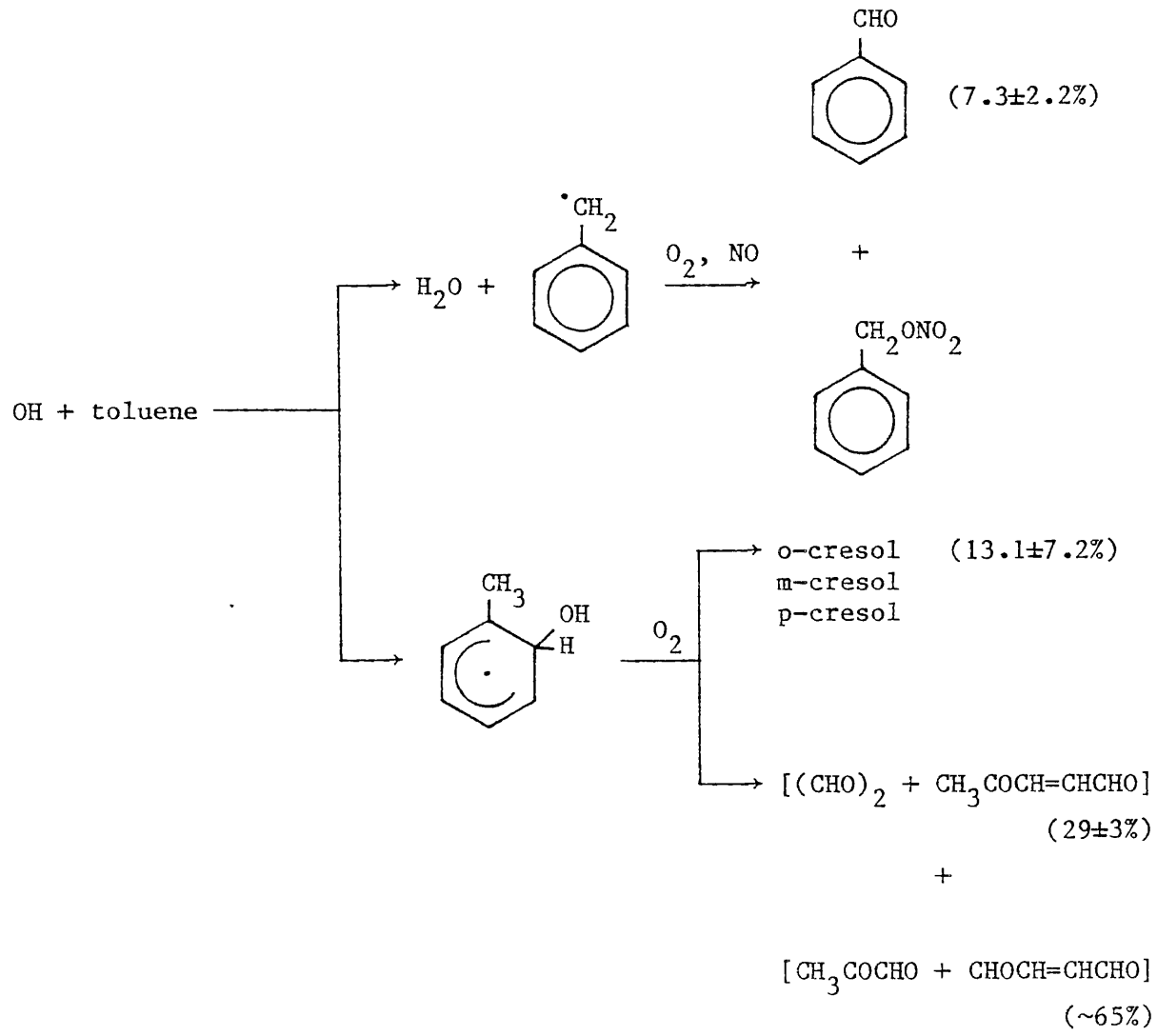

D. NO_x-Air Photooxidation of Benzene

In order to investigate the photochemical reactivity of benzene and to provide a data base for the development of detailed chemical computer models for this aromatic hydrocarbon, a series of benzene-NO_x-air photooxidations were carried out.

Experimental

The irradiations were carried out in the ~6400-ℓ all-Teflon chamber, and the techniques and procedures were as described in Section II.D for

the n-alkane-NO_x-air irradiations. Nitric oxide and NO_x were monitored by chemiluminescence, O_3 by ultraviolet absorption (Dasibi 1003AH) and formaldehyde by an improved chromotropic acid technique (Pitts et al. 1979). Benzene was analyzed by GC-FID using the 10-ft x 1/8-in 10% Carbowax C-600 column and PAN by GC-ECD as described in Section II.D.

Results and Discussion

A summary of the initial conditions and results of the three benzene-NO_x-air irradiations are shown in Table III-6, and plots of the concentration-time data for the major measured species are shown in Figures III-5 through III-7. Detailed tabulations of the data are given in Appendix A.

It is immediately apparent from these results that benzene is much more photoreactive than the $\geq C_6$ n-alkanes, despite the fact that it has a lower rate constant for reaction with OH radicals. In particular, even when the hydrocarbon/NO_x ratio is as high as ~400, n-hexane-NO_x-air irradiations do not attain an O_3 maximum within 6 hr, while a corresponding benzene-NO_x-air run gave an O_3 maximum in less than 2 hr, and a benzene-NO_x run with a hydrocarbon/NO_x ratio as low as ~25 gave an O_3 maximum in less than 5 hr.

As is believed to be the case for toluene (see, for example, Atkinson et al. 1980), it is probable that the relatively high reactivity of benzene is due to secondary reactions of the products and not to reactions of benzene itself. This is evident from examining the total NO_x concentration-time profiles shown in Figures III-5 through III-7, and the benzene profiles in Figures III-6 and III-7, where an apparent induction period in the decay of these species is evident. This induction period indicates radical initiation and NO_x removal processes occurring at much more rapid rates later in the irradiation than initially.

In order to assess to what extent current aromatic photooxidation mechanisms are consistent with these data, a limited computer modeling study was carried out, and the results of the model calculations are compared with the experimental data in Figures III-5 through III-7. Curve "A" was calculated using a mechanism based entirely on strict analogy to the toluene mechanism given by Atkinson et al. (1980, 1982b), with no adjustment or parameters other than adjusting the chamber radical source (see Section IV) to fit the initial NO consumption rate. The inorganic

Table III-6. Initial Conditions and Selected Results of the Benzene-NO_x-Air Irradiations Carried Out in the SAPRC ~6400-ℓ All-Teflon Chamber[a]

ITC Run Number		560	561	562
Initial Conc.:	Benzene	55.38	13.19	13.96
(ppm)	NO	0.079	0.082	0.434
	NO_2	0.037	0.032	0.125
	NO_x	0.115	0.113	0.553
Maximum O_3	(ppm)	0.323	0.273	0.412
	(hours)	1.5	1.75	4.75
Maximum NO_2	(ppm)	0.078	0.084	0.373
	(hours)	0.5	0.5	2.75
Initial $\frac{-d([O_3]-[NO])}{dt}$	(ppb min^{-1})	~3	~2	~1

[a] T = 301 ± 1 K, ~50% RH, k_1 = 0.32 min^{-1}.

reaction mechanism and rate constants and the reactions and rate constants of most of the products used in this calculation were the same as employed by Atkinson et al. (1980, 1982b) (other than updating the rates of glyoxal photolysis and reaction with OH radicals, based on the results discussed in Section III.B of this report), so they need not be discussed here. The benzene and phenol reactions employed are totally analogous to the mechanism assumed by Atkinson et al. (1980, 1982b) for toluene and o-cresol, respectively, and are indicated below.

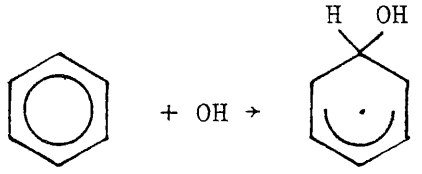

$$+ OH \rightarrow \quad (k_1 = 1.2 \times 10^{-12}\ cm^3\ molecule^{-1}\ sec^{-1}) \quad (6)$$

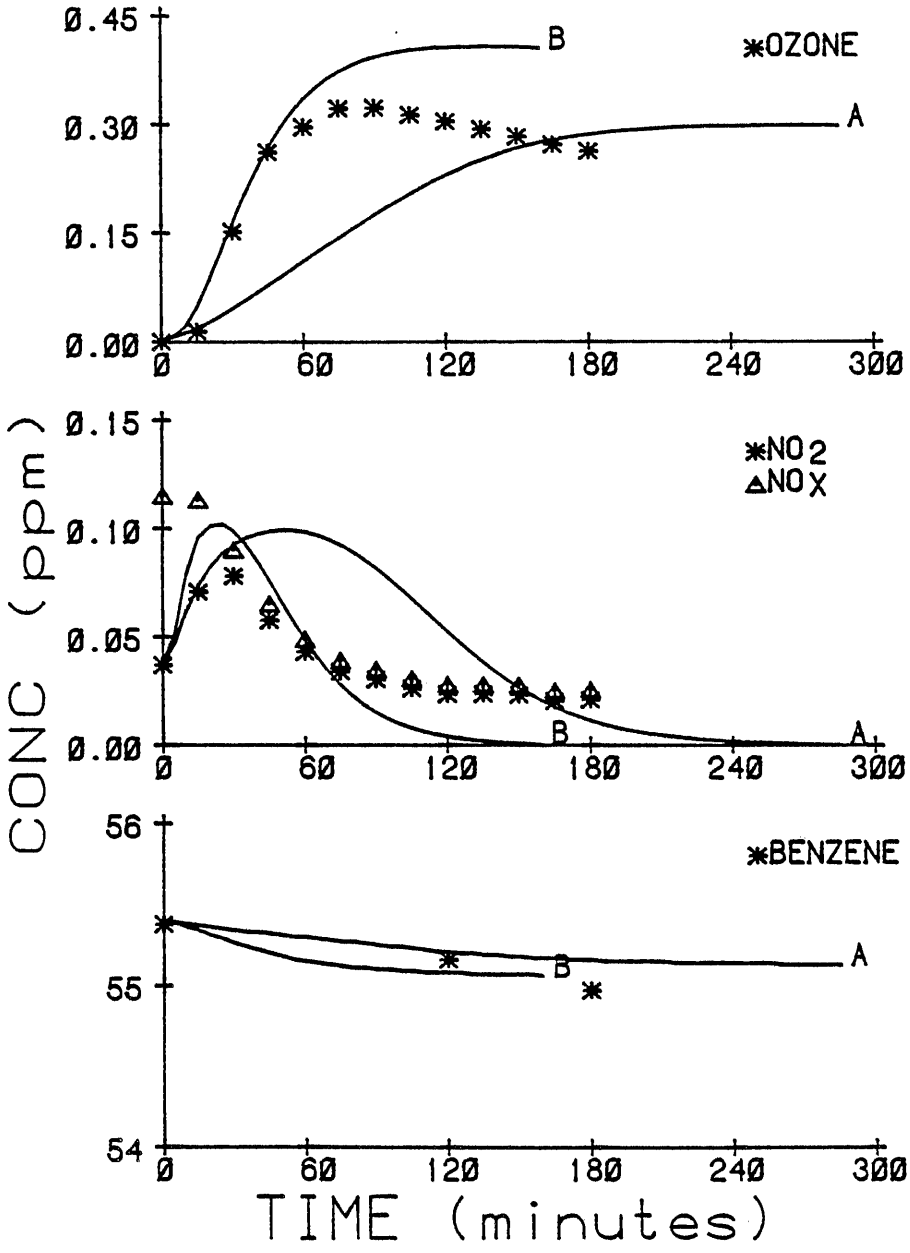

Figure III-5. Observed and Calculated Concentration-Time Profiles for Selected Species in Benzene-NO_x-Air Run ITC-560. *, Δ = Experimental Data. A = Model Calculation, Unadjusted Model. B = Model Calculation, k_{16} = 0.03 min^{-1}.

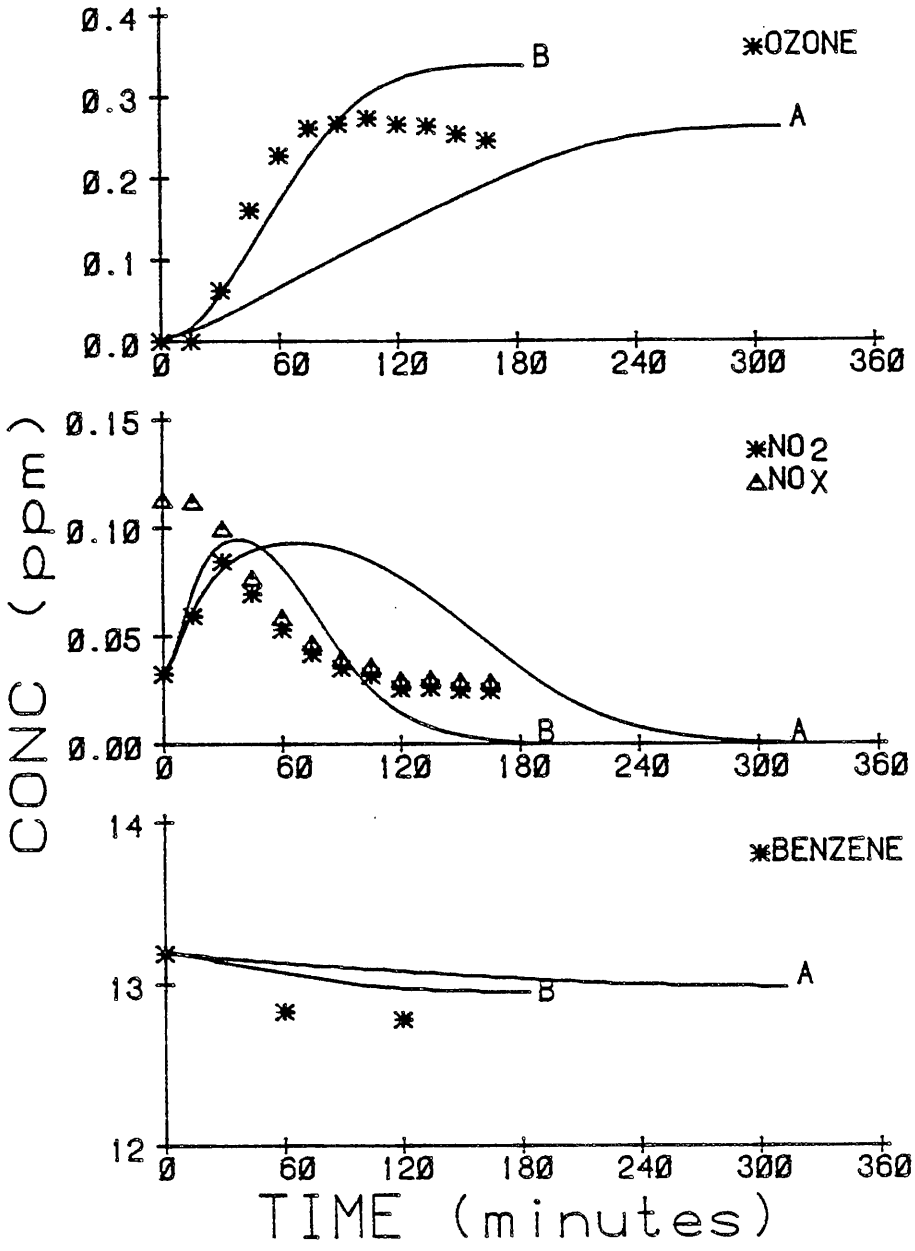

Figure III-6. Observed and Calculated Concentration-Time Profiles for Selected Species in Benzene-NO_x-Air Run ITC-561. *, Δ = Experimental Data. A = Model Calculation, Unadjusted Model. B = Model Calculation, k_{16} = 0.03 min^{-1}.

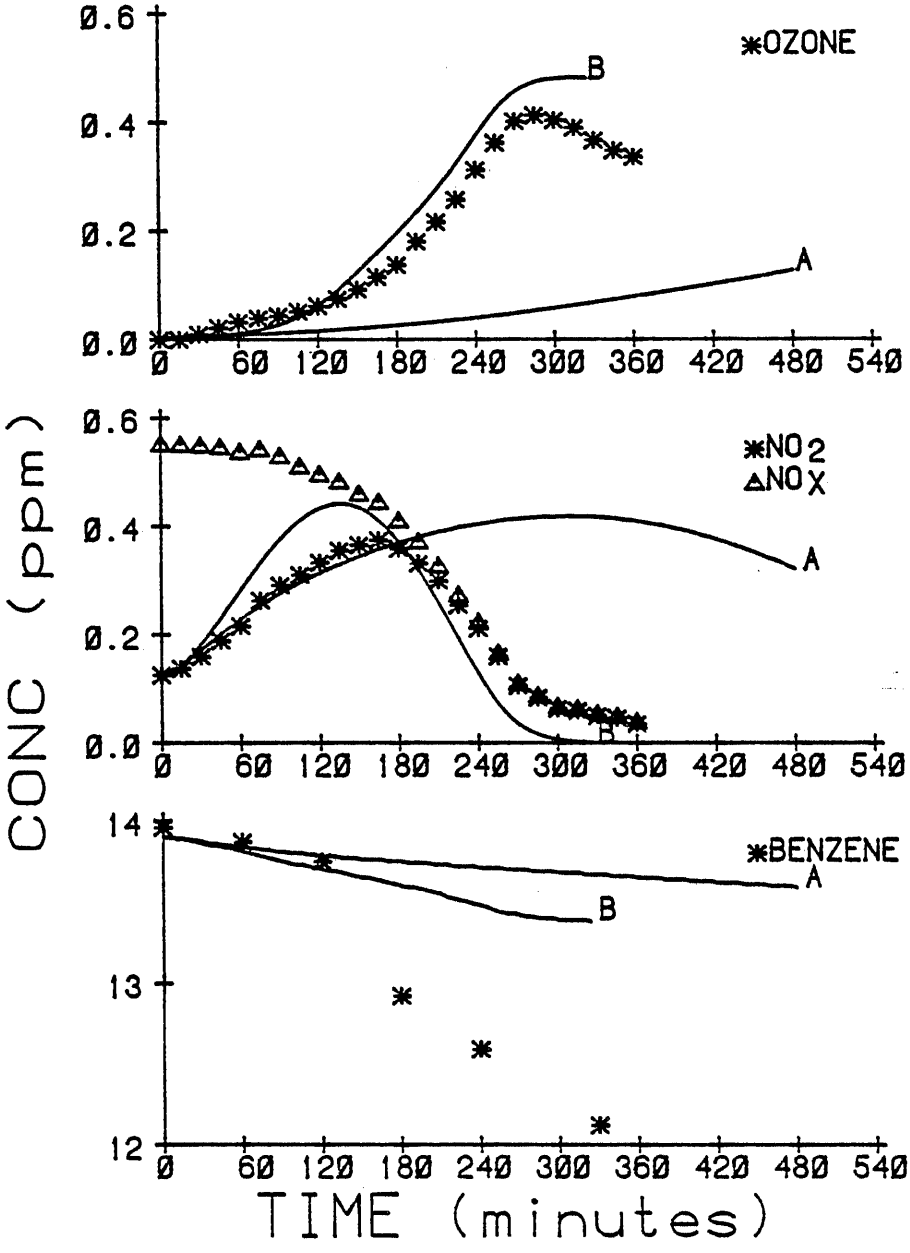

Figure III-7. Observed and Calculated Concentration-Time Profiles for Selected Species in Benzene-NO_x-Air Run ITC-562. *, Δ = Experimental Data. A = Model Calculation, Unadjusted Model. B = Model Calculation, k_{16} = 0.03 min^{-1}.

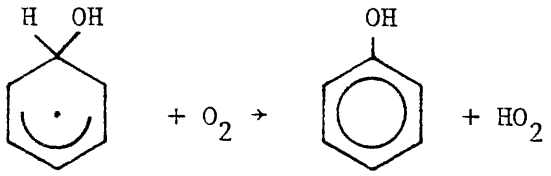

(8)

with $\frac{k_8}{k_9} \sim 0.4$

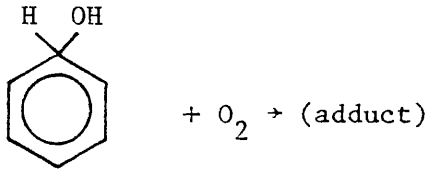

(9)

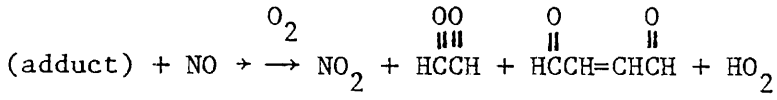

(10)

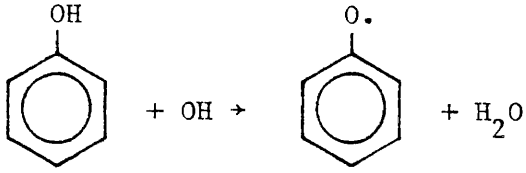

(11)

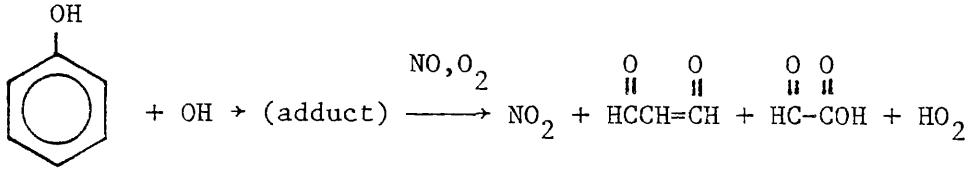

(12)

with $k_{11} + k_{12} \simeq 2 \times 10^{-11}$ cm^3 molecule^{-1} sec^{-1}

and $k_{11}/k_{12} = 0.09$

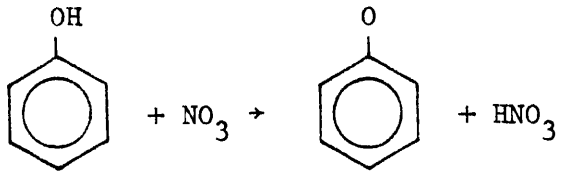

(13)

$$k_{13} = 2 \times 10^{-12} \text{ cm}^3 \text{ molecule}^{-1} \text{ sec}^{-1}$$

Here k_6 and k_{13} are based on measured values (Atkinson et al. 1979, Carter et al. 1981, respectively), k_8/k_9 is based on results of studies described in Section III.C, and k_{11} and k_{12} are estimated based on known reactions of cresols (Atkinson and Lloyd 1983).

It can be seen from Figure III-5 through III-7 that the mechanism used to calculate curves "A" does not successfully predict the high reactivity of this system which occurs after the induction period. This suggests a serious problem in the mechanisms of Atkinson et al. (1980, 1982b), and Killus and Whitten (1982), since the high reactivity of toluene was attributed entirely to the rapid photolysis of methylglyoxal, which obviously cannot be formed from benzene. (The photodecomposition of glyoxal is not believed to produce radicals; see Section III.C.) However, the relatively low quantum yield for methylglyoxal photodecomposition measured in this program (Section III.C) already indicated that the current mechanisms have problems, since the photolysis rates of methylglyoxal required to fit the toluene-NO_x chamber data (Atkinson et al. 1980, Killus and Whitten 1982) are inconsistent with these new quantum yields. Thus, there clearly must be another radical source in the aromatic photooxidation mechanisms, one that is formed in both the benzene and the toluene systems.

One postulated photooxidation product of unknown reactivity characteristics believed to form in both the benzene and the toluene systems is 2-butene-1,4-dial, and reactions of this product might possibly account for the excess reactivity in both systems. In order to explore this possibility, calculations were conducted with the same mechanism employed to generate curves "A", except that one of the following reactions, with varying rate constants, were included:

$$HCCH{=}CHCH + O_3 \rightarrow HCCH + CO + CO_2 + 2\ HO_2 \quad (14)$$

$$HCCH{=}CHCH + NO_3 \rightarrow \text{product} + HO_2 \quad (15)$$

$$HCCH{=}CHCH + h\nu \rightarrow \text{product} + 2\ HO_2 \quad (16)$$

It was found that no matter what rate constant was employed, the inclusion of reactions (14) and (15) would not fit the data, since they predicted the wrong concentration-time profiles. If a relatively low rate constant was employed, the calculated induction period was too low, while higher rate constants predicted much more rapid rates of O_3 formation or NO_x removal following the induction period than was observed. On the other hand, assuming that 2-butene-1,4-dial undergoes photolysis to form radicals at a rate of ~0.03 min^{-1} (i.e, ~10% that of NO_2), reaction (16) gave a relatively good fit to the O_3 and NO_x profiles in all runs, as shown on curves "B" in Figures III-5 through III-7.

This reasonably good fit to the data obtained by assuming that 2-butene-1,4-dial undergoes rapid photodecompositon does not necessarily imply that this is indeed the extra radical source in the aromatic mechanisms. However, the fact that assuming rapid product + O_3 or product + NO_3 reactions give poor fits, while using rapid photolysis gives good fits strongly suggests photolysis of some product must be important in forming radicals in these systems. Work is clearly required to more unambiguously identify the specific product, or group of products, responsible.

It should also be noted from Figures III-6 and III-7 that even the "best fit" mechanism (curves "B") does not successfully predict the rapid rate of decline of benzene following the induction period. It is obvious that if the radical initiation rates were somehow adjusted to give OH levels sufficient to account for the benzene decay rates, then this mechanism would predict rates of O_3 formation and NO_x removal which are much

higher than experimentally observed. However, it is known that benzene does not react significantly with O_3 (Pate et al. 1976) and NO_3 (Japar and Niki 1975), and it is not likely to react significantly with HO_2 radicals (Graham et al. 1979), nor should it photolyze under these conditions (Calvert and Pitts 1966). Thus, it is unclear what the sink process for benzene may be. It should be noted, however, that toluene does not show any analogous rapid decay following an induction period, so perhaps this result for benzene reflects some experimental artifact. It is obvious that more work is required before this system is adequately understood.

E. Summary and Conclusions

As a result of this SAPRC-ARB program, much more is now known about the photooxidation mechanisms of aromatic hydrocarbons and their known oxidation products than was previously the case. The rates of reaction of the α-dicarbonyls, known to be important oxidation products of the aromatics, with OH radicals and with O_3 (i.e., upper limits) have been determined. In addition, the atmospheric photodecomposition rates of the α-dicarbonyls have been measured for the first time. The yields of the α-dicarbonyls glyoxal and methylglyoxal from toluene and of glyoxal and phenol from benzene have also been determined, and environmental chamber studies of the atmospheric photochemical reactivity of benzene have been conducted. Most of the information obtained in these studies has not been available previously, and these results constitute important and necessary inputs into the development of computer models for atmospheric reactions of the aromatic hydrocarbons.

However, the results of these studies have indicated the existence of significant problems in the currently assumed aromatic photooxidation mechanisms, and thus, on the whole, these studies tended to raise at least as many questions as they resolved. The relatively high reactivity of toluene in NO_x-air photooxidations had been thought to be due primarily to rapid photodecompositon of methylglyoxal, and on the basis of this it was predicted that benzene would be relatively unreactive photochemically. However, the methylglyoxal photolysis rate measured in this study was significantly lower than required to supply the radicals necessary for the models to fit results of experimental toluene-NO_x-air irradiations, and in addition benzene was found to be far more reactive in NO_x-air irradiations

than expected. Both these results could possibly be explained by assuming relatively rapid photolyses of 2-butene-1,4-dial, postulated to be formed as a product in both systems, but this product has not been directly observed and its atmospheric reactions are unknown.

In addition, our current theories of aromatic-NO_x-air photodecomposition mechanisms predicts only two overall pathways following the reaction of OH radicals with benzene; one leading to formation of phenol, the other forming glyoxal + 2-butene-1,4-dial. However, the yields of phenol + glyoxal observed in this study account for only ~50% of the benzene reacted. Finally, the rate of benzene consumption observed in the later stages of the benzene-NO_x-air irradiations conducted under this study is far higher than predicted by the models, even when rapid photolysis of the products is assumed. Thus the aromatic photooxidation mechanism appears to be more complex and more poorly understood than had previously been thought, and clearly more work is required before our knowledge of this system is sufficient for the development of reliable, predictive photochemical models.